UNDERSTANDING THE ROLE OF CARDIOLIPIN IN HELICOBACTER PYLORI FLAGELLAR SYNTHESIS

by

JOSHUA CHU

(Under the Direction of Timothy Hoover)

ABSTRACT

Helicobacter pylori is an Epsilonproteobacteria that colonizes the human stomach mucosa and a causative agent of peptic ulcers and gastric cancer. *H. pylori* uses a cluster of polar, sheathed flagella for motility, which is required for host colonization. As part of my dissertation studies, I found the glycerophospholipid cardiolipin (CL) has a role in flagellum biogenesis. Inactivating a cardiolipin synthase gene (*clsC*) in *H. pylori* G27, but not *H. pylori* B128, abolished flagellum biosynthesis. Analysis of glycerophospholipids in the two *clsC* mutants revealed that both were similarly deficient in CL. Motile variants of the G27 *clsC* mutant were obtained following transformation with genomic DNA from the B128 *clsC* mutant. Resequencing the genomes of seven motile G27 *clsC* recipients showed that all possessed the *flgI* (encodes flagellar P ring protein) allele from B128. The G27 and B128 FlgI proteins differ at five amino acid positions. Introducing the B128 *flgI* allele into the G27 *clsC* mutant rescued flagellum biosynthesis. Cryo-electron tomography (cryo-ET) of the G27 *clsC* mutant showed flagellum assembly was arrested at a step that preceded formation of the P ring. Taken together, these results suggest G27 FlgI, but not B128 FlgI, fails to form the P ring in the absence of wild-type CL levels. In related studies, I discovered CL appears to be a major component of the *H. pylori* flagellar sheath, a membrane that

surrounds the flagellum and is contiguous with the outer membrane. Using a comparative genomics approach, I identified several genes that are present in *Helicobacter* species that possess a sheath but are absent in *Helicobacter* species that lack a sheath. Interestingly, one of these genes is *clsC*. Four other sheath-specific genes (HP1486-HP1489) encode a predicted efflux system that I targeted for mutagenesis. Disrupting the HP1488 homolog in B128 inhibited flagellum biosynthesis. Cryo-ET revealed that the B128 mutant was missing part of a cage-like structure that surrounds the flagellar motor. I hypothesize the cage-like structure is an efflux system encoded by HP1486-HP1489 that transports CL to the outer membrane where it is incorporated into the flagellar sheath.

INDEX WORDS: *Helicobacter pylori*, flagella, ClsC, RpoD, RpoN, FliA, FlgI

UNDERSTANDING THE ROLE OF CARDIOLIPIN IN HELICOBACTER PYLORI FLAGELLAR SYNTHESIS

by

JOSHUA CHU

B.S., Auburn University, 2013

A Dissertation Submitted to the Graduate Faculty of The University of Georgia in Partial Fulfillment of the Requirements for the Degree

DOCTOR OF PHILOSOPHY

ATHENS, GEORGIA

2019

UNDERSTANDING THE ROLE OF CARDIOLIPIN IN HELICOBACTER PYLORI FLAGELLAR SYNTHESIS

by

JOSHUA CHU

Major Professor:	Timothy R. Hoover
Committee:	Anna C. Glasgow Karls
	Robert J. Maier
	Vincent J. Starai

Electronic Version Approved:

Suzanne Barbour
Dean of the Graduate School
The University of Georgia
August 2019

DEDICATION

This work is dedicated to Jim and Kay Dommel, two people who saw more than a simple farmhand and knew I was destined for greater things long before I knew I was capable. In one of my greatest times of personal hardship, they supported me without question and continuously challenged me to do better. I also dedicate this work to my loving wife, who makes me want to be a better person, and because of you I am. I would not be the man I am today without you.

ACKNOWLEDGEMENTS

I would like to thank my committee members, Dr. Timothy Hoover, Dr. Anna Karls, Dr. Rob Maier, and Dr. Vincent Starai for their guidance and feedback. In particularly would like to thank Dr. Timothy Hoover for his support and guidance as my advisor. I would like to thank all the past and present members of the Hoover lab. I would especially like to thank Dr. Stéphane Benoit for professional and personal guidance throughout my graduate school training. I would like to thank the Trent lab for their continuous support during the experimental and analysis stages of my projects. I also want to thank Abigail Courtney from the Lewis lab for her assistance analyzing my NGS data. I would like to acknowledge funding sources from the National Science Foundation, the National Institutes of Health, University of Georgia, and the Office of the Dean of the Franklin College of Arts and Sciences.

TABLE OF CONTENTS

Page

LIST OF TABLES

Page

LIST OF FIGURES

Page

CHAPTER 1

INTRODUCTION AND LITERATURE REVIEW

Background and Significance

Helicobacter pylori is an Epsilonproteobacterium found in the stomach of over 50% of the world's population (1, 2). Individuals infected with *H. pylori* typically do not develop clinical symptoms, but the infection can progress to serious diseases such as peptic ulcers and chronic gastritis. If infections are left untreated, a small subset of individuals can develop gastric cancer or mucosa-associated lymphoid tissue (MALT) lymphoma, which has led to *H. pylori* becoming the only bacterium to be classified as a class I carcinogen (3-8). Although infection rates vary according to geographical location, the highest rates of infection are usually observed in developing countries, primarily due to limited treatment options, socioeconomic status, and poor hygiene (9, 10).

Gastric cancer is the third most common cause of cancer-related death worldwide, and *H. pylori* related gastric cancer accounts for more than 90% of these deaths (11). For decades, treatment focused on a triple therapy approach that included clarithromycin, metronidazole or amoxicillin, and a proton-pump inhibitor (12). The rise of *H. pylori* strains that are resistant to these key antibiotics is diminishing the efficacy of this treatment and making treating infections increasingly difficult (12-14). The observed resistances are likely due to overuse of antibiotics and treatment of other infectious diseases. Interestingly, this can be illustrated by comparing different regions of Europe. Countries in northern Europe, which have stricter policies that

regulate antibiotic use, observe clarithromycin resistance in less than 5% of *H. pylori* clinical isolates, while some countries in southern Europe that do not practice the same policies experience clarithromycin resistance rates in clinical isolates of *H. pylori* as high as 20% (15-17).

Since the discovery of *H. pylori* as the causative agent of peptic ulcer disease by Barry Marshall and Robin Warren, the spectrum of diseases associated with *H. pylori* is remarkable (18). Approximately 90-95% of duodenal ulcers and 70-75% of gastric ulcers can be credited to *H. pylori*; a small proportion of individuals may develop gastric adenocarcinoma in response to long-term infections (19, 20). Within the past 20 years, *H. pylori* infections have been linked to neurologic, dermatologic, hematologic, metabolic and allergic diseases (21-28). Interestingly, the presence of specific genetic markers in *H. pylori*, such as *cagA*, appear to inversely influence the development of diseases such as heart disease, rosacea, and asthma (23, 29-33). While the breadth of diseases associated with *H. pylori* infections continue to grow, demonstrating causation remains elusive.

The mode of transmission utilized by *H. pylori* is poorly understood. The proposed mechanisms include fecal-oral, oral-oral, gastric-oral, or unidentified common environmental sources, such as contaminated water (34). The likely route of transmission is person-to-person, with the acquisition of the bacterium occurring at a very young age (35-37). Studies show household members that test negative for *H. pylori* are at a 4.8-fold increased risk of acquiring the bacterium from a household member that is positive, indicating that familial transmission plays a significant role in distributing *H. pylori* (37). While humans are the primary reservoir for *H. pylori*, strains have been isolated from other primates, but this is not likely a significant contributor to infecting humans since interactions between humans and other primates are limited (9). Several

studies examined contaminated water as a source of transmission, but the results are inconsistent and requires further evaluation (38).

The overall role *H. pylori* has on human health is complicated. In 2007, Linz *et al*. reported the association between *H. pylori* and humans can be traced to the migration of humans from the African continent, suggesting a relationship existing for more than 55,000 years (39). Some reports claim *H. pylori* has a protective role for humans, preventing diseases like acid reflux and asthma, and the treatment *H. pylori* infections will likely lead to an increase in serious diseases like gastric cancer (40, 41). But the relationship between this bacterium and humans is unclear, and whether *H. pylori* has a collective positive impact on human health has yet to be definitively established.

Characteristics of *Helicobacter pylori*

H. pylori is an Epsilonproteobacterium that is characteristically spiral shaped. It is generally two to four microns in length and ~0.5 microns in width. Each cell typically possesses two to six polar, sheathed flagella. *H. pylori* has a second morphology, changing from spiral to coccoidal following prolonged *in vitro* incubation, and this coccoidal form is termed viable but non-culturable (VBNC) (42, 43). Studies of stomach biopsies using scanning electron microscopy to investigate the morphological states of *H. pylori* discovered both morphological states co-exist (44-46). Numerous attempts have been made to develop a method to resuscitate the VBNC state. In 2011, Richards *et al*. reported a successful formulation to convert VBNC cells to culturable cells that included broth supplemented with trace minerals, serum and lysed erythrocytes (47). This discovery was a critical step in allowing researchers to identify the mechanisms that control the conversion between the two cell states.

H. pylori is a fastidious organism, generally requiring a growth medium that is supplemented with serum, blood or beta-cyclodextrin, and requiring low concentrations of oxygen (48, 49). The microaerophilic atmosphere typically used to grow cells is 2-5% O_2, 5-10% CO_2, and 0-10% H_2, although H_2 is not a requirement for growth (50). Additionally, the media should be a neutral pH since *H. pylori* grows best between pH 5.0 and 8.0.

The genome size of *H. pylori* is approximately 1.7 Mbp, which is less than 40% of the genome size of most *E. coli* strains (51). The genetic diversity observed in *H. pylori* is immense, which results from its natural transformability, elevated mutation rate and high recombination rate (51, 52). In addition to these genetic features, *H. pylori* strains often harbor multiple cryptic plasmids whose functions are currently unknown, although these plasmids have been modified to genetically manipulate the bacterium in a laboratory setting (53, 54).

Flagellar Gene Regulation and Flagellum Assembly

Flagellum biosynthesis is a highly ordered process that involves coordinating the expression of structural and regulatory genes with the assembly of the nascent flagellum. The *H. pylori* flagellum is comprised of three major components: the basal body, the hook, and the filament (55). The basal body consists of several distinct structures, including the cytoplasmic ring (C ring), the export apparatus, the flagellum motor, the rod, and the rings (P and L rings) that anchor the flagellum to the cell. The C ring in *H. pylori* is made of four different proteins, FliG, FliM, FliN and FliY, and has roles in shuttling proteins to the flagellar export apparatus and controlling the rotational direction of the flagellum (56). The flagellar export apparatus is a Type III secretion system (flagellar T3SS; fT3SS) that consists of six different membrane proteins, FlhA, FlhB, FliO, FliP, FliQ and FliR, and three cytoplasmic proteins, FliH, FliI, and FliJ, and is

responsible for transporting axial components of the flagellum (i.e. proteins that make up the rod, hook and filament) across the cell membrane (57). The rod proteins are the first to be secreted by the fT3SS, followed by the hook protein and hook-associated proteins. The hook is a curved-like structure that transmits torque from the rod to the filament. After the hook is completed, the filament protein subunits, referred to as flagellins, are assembled into the filament, which is a long tail-like structure extending from the body of the bacterial cell.

H. pylori has three different sigma factors for RNA polymerase, RpoD (σ^{80}), RpoN (σ^{54}), and FliA (σ^{28}), each of which is required for transcription of a specific set of flagellar genes (55). Although many bacteria, such as *Vibrio cholerae* and *Pseudomonas aeruginosa*, have a master regulator that initiates a transcriptional hierarchy that controls the expression of flagellar genes so that their products are synthesized as they are needed for flagellum assembly, a master regulator has yet to be identified in *H. pylori* (58). Gene products required during early flagellum assembly and some regulatory proteins rely on RpoD for their transcription (59). The transcription of genes whose products are required midway in flagellum assembly (e.g. *flgE* and *flgK*, which encode the hook protein and hook-associated protein 1, respectively) requires RpoN and a two-component system consisting of the sensor kinase FlgS and the response regulator FlgR (60, 61). FlgS is a cytoplasmic protein that recognizes an assembly checkpoint associated with the fT3SS and is essential in initiating the signaling cascade that results in the transcriptional activation of RpoN-dependent genes (55, 58, 59, 62, 63). Transcription of the late flagellar genes requires FliA and is negatively regulated by the anti-sigma factor FlgM (64, 65). In contrast to *Salmonella enterica* serovar Typhimurium, the FlgM protein is not exported by the fT3SS in *H. pylori*, but rather, its inhibition is thought to be relieved by binding to FlhA (66, 67).

Glycerophospholipids

E. coli served as the model organism to investigate bacterial membrane lipids for decades, but phospholipid research investigating other bacterial species has shown lipid biochemistry cannot be represented by a single organism (68, 69). Gram-positive organisms are characterized by the presence of a single membrane bilayer, while Gram-negatives possess two distinct membranes, the inner and outer membranes. The membrane of Gram-positive and inner membrane of Gram-negative cells are similar to each other, distinguished as a lipid bilayer composed of different phospholipids, although the phospholipid composition can differ dramatically between the two cell types (70-72). The outer membrane of Gram-negative bacteria is asymmetrical, with the inner leaflet composed of phospholipids and the outer leaflet of lipid A. The predominant phospholipids in *E. coli* are phosphatidylethanolamine (PE; ~75%), phosphatidylglycerol (PG; ~20%), and cardiolipin (CL; ~5%) (69, 72). *E. coli* initiates phospholipid biosynthesis utilizing the metabolite cytidine diphosphate-diacylglycerol (CDP-DAG), which diverges into two separate pathways. In one pathway, PE is synthesized in two steps using phosphatidylserine synthase (Pss) to add L-serine to CDP-DAG generating phosphatidylserine, which is subsequently converted to PE upon the removal of CO_2 by phosphatidylserine decarboxylase (Psd) (69). The second pathway synthesizes PG using phosphatidylglycerolphosphate synthase (PgsA) to catalyze the condensation of glycerol-3-phosphate (G3P) to form PG phosphate (PGP). The anionic phospholipid PG is synthesized by one of three phosphatases (PgpA, PgpB, PgpC), which dephosphorylate PGP. Three cardiolipin synthases (ClsA, ClsB, ClsC) catalyze the formation of the anionic phospholipid CL, although the phospholipid substrates of these enzymes differ. ClsA and ClsB transfer phosphatidic acid from one PG molecule to a second PG molecule to produce CL and glycerol. In contrast, ClsC transfers

phosphatidic acid from a PE molecule to PG to produce CL and ethanolamine (73-76). While the information collected from studying *E. coli* has progressed the understanding of lipid metabolism, many organisms are missing one or more of these phospholipids and synthesize different lipids, indicating that *E. coli* membrane chemistry cannot be applied to all bacteria (69, 77, 78).

Phospholipases refer to a group of enzymes sharing the ability to catalyze the hydrolysis of a glycerophospholipid ester linkage. An enzyme is assigned to one of four classes (A, B, C, or D) according to the specific bond targeted within the phospholipid (Figure 1.2) (79). Phospholipase A enzymes are split into A_1 and A_2, where phospholipase A_1 enzymes hydrolyze fatty acyl ester bonds at the *sn*-1 position, while the fatty ester bonds at the *sn*-2 positions are hydrolyzed by phospholipase A_2 enzymes (80). Phospholipase B enzymes possess both phospholipase A_1 and phospholipase A_2 enzymatic activities (81). The phospholipase C enzyme cleaves the phosphodiester bond before the phosphate, which releases a diacylglycerol with a phosphate head group (79). Finally, the phospholipase D (PLD) enzymes cleave the phosphodiester bond after the phosphate, yielding a phosphatidic acid and an alcohol (82).

The PLD superfamily includes enzymes that are involved in phospholipid metabolism, members of which cleave phosphodiester bonds (82). Historically, enzymes categorized as a PLD enzyme hydrolyzed phosphatidylcholine, releasing choline and the messenger signaling lipid phosphatidic acid (83). Sequence analysis revealed a large subset of PLD enzymes that share a conserved $HxKxxxxDx_6GSxN$ motif (HKD), with the histidine residue critical for catalytic activity (83-85). Enzymes classified in this superfamily typically share little sequence and structural similarity outside of the catalytic site (82, 86). Cardiolipin synthases are PLD enzymes that catalyze the formation of CL from either two PG molecules or a PG and a PE molecule (74, 87-89). The structure of CL is unlike that of other phospholipids as it has a small hydrophilic head

consisting of two phosphates connected by a glycerol backbone and a large hydrophobic tail consisting of four large acyl chains. These features impart a conical shape to the CL molecule that facilitates the enrichment of CL at the cell poles and septa (90-93). Some proteins preferentially interact with CL, and polar enrichment allows these proteins to discriminate between cellular features and properly localize in the absence of scaffold or landmark proteins (94). Depleting the cell of CL may affect important physiological processes, such as ATP synthesis, DNA replication, protein translocation, cell division, DNA repair and osmo-regulation (95-97).

Cardiolipin in the Membrane

Mitochondria play an important role in the generation of energy for eukaryotic cells through oxidative phosphorylation (98, 99). Cardiolipin adopts a conical structure and segregates to regions of high-negative curvature in the inner membrane of mitochondria. A large proportion of the mitochondrial inner membrane contains CL and is responsible for the generation of the mitochondrial cristae (98, 100). The respiratory chain proteins are significantly enriched in the cristae and require cardiolipin for structural stability and enzymatic activity (98, 101). Mitochondrial morphology is essential for normal function and plays an important role in development, aging and cell death (98). Mitochondria that are deficient in CL have an increase in cell size and the cristae are disorganized, which can lead to multiple cardiovascular diseases such as Barth syndrome, cardiomyopathy, atherosclerosis, and heart failure (102).

Similar to the mitochondrial cristae, bacteria use CL microdomains to localize proteins to areas of the cell possessing a high-degree of negative curvature (103). Cardiolipin enrichment at the cell pole of bacterial cells were demonstrated by comparing the total phospholipid composition between wild-type *E. coli* and minicells (90). The proteins ProP, from *E. coli*, and IcsA, from

Shigella flexneri, have also been demonstrated to require CL to polarly localize (96, 104, 105). Disruption of CL production or preventing the accumulation of CL at the cell pole interferes with cell shape maintenance or the inhibition of the respiratory chain, indicating CL is required for a variety of cell processes (103).

Flagellar Sheath Biosynthesis

Early investigations suggested the flagellum was an appendage "peeling" away from the membrane and naturally occurred as bacteria move across different surfaces (106, 107). We now know the flagellum is a complex assembly, requiring gene expression and protein assembly to be synchronized at the highest precision. Since the late 1940s, scientists have investigated the sheath that surrounds the flagellum filament in a small group of bacteria, such as multiple *Vibrio* species, *Pseudomonas* species, *H. pylori*, *Bdellovibrio bacteriovorus*, and *Azospirillum brasilense* (108-111). In contrast to unsheathed flagella, the sheathed filament must have an additional mechanism to coordinate filament polymerization and sheath biogenesis. The flagellar sheath is enigmatic, and raises questions such as: are the outer membrane and sheath discontinuous lipid bilayers, is sheath biogenesis independent of flagellar synthesis, and what physiological roles does the sheath play?

The flagellar sheath was initially described as an extension of the outer membrane in the early 1950s, and it was suggested that the filament and sheath rotate simultaneously (112). In order for the filament and sheath to rotate together, the intersection of the base of the flagellum and outer membrane must be discontinuous to enable the sheath to rotate with the filament (113). This would suggest the sheath is "floating" and may remain in place through hydrophobic interactions with the core filaments, generating a rigid membrane structure. Alternatively, another

model proposes that only the flagellar filament rotates within a flexible sheath (113). In this model the filament rotates freely within the sheath, indicating the membrane must be flexible enough to allow distortion by the rotational forces induced by the filament, but robust enough to remain associated with the cell body. Costerton and Thompson investigated the membrane plasticity of a marine pseudomonad and determined both inner and outer membranes have a "plastic" physical nature, supporting the malleability of the outer membrane (114). Carson and Eagon found that the peptidoglycan layer is not the sole contributor to cell shape in *P. aeruginosa*, and the outer membrane significantly contributes to the rigidity of the cell (115). Both studies support the plasticity and rigidity requirements that the membrane must possess to withstand the perturbations produced by rotational forces.

Addressing the continuity between the outer membrane and flagellar sheath has been difficult. If the sheath is discontinuous, there must be an underlying mechanism dedicated to the movement of lipid and protein components from the outer membrane to the growing filament and organize these components around the protein subunits. Alternatively, if there is continuity, does the membrane reorganize around the growing filament, or are protein and lipid components transported to the distal end and assembled as the flagellum grows? Early investigations demonstrated antibodies directed against LPS reacted strongly with the outer surface of the cell but not with the flagellar sheath (116). Investigators also reported antibodies directed against crude sheath preparations did react strongly with a component in the cell surface and flagellar sheath, indicating the lipid composition between the outer membrane and the sheath is more complex (116). While this result argues against LPS being a component of the flagellar sheath and supports the discontinuity model, what the antibodies detected was unclear. In later studies, Fuerst and Perry used immunogold-labeling to demonstrate LPS could be detected in the outer membrane and

flagellar sheath (117). Additional evidence for LPS in the flagellar sheath was found in *H. pylori* when phospholipid fatty acids and LPS-specific fatty acids were detected in highly purified flagellar sheaths (118). Collectively, there is strong evidence showing the contiguous model is correct, but the coordination of sheath biogenesis and the growing filament remains a mystery.

With the considerable evidence supporting the continuity model, researchers wanted to understand the mechanisms involved in the synchronization between the growing filament and remodeling of the outer membrane. Bacterial species that do not synthesize a flagellar sheath were speculated to use the L ring as a boundary that prevents the outer membrane from remodeling and developing into the sheath (119). But if the L ring was the primary component that influences the formation of the flagellar sheath, one would not expect the flagellum to possess both components. Arguing against this hypothesis, the L ring and flagellar sheath can be identified in *V. cholerae*, indicating there is an alternative mechanism that supports sheath biogenesis (120). One of the major challenges in investigating sheath biogenesis is the isolation of a mutant that is motile and lacks a sheath, or a non-motile variant that produces a core-less sheath. Richardson *et al*. utilized transposon mutagenesis and isolated non-motile mutants in the *V. cholerae* classical strain that synthesized a non-polar, core-less sheath (121). The failure to properly localize the sheath indicates the filament or basal body assembly is required to be position correctly, but more importantly, this observation indicates sheath biogenesis may occur independently of flagellar synthesis in *V. cholerae*. This study was the first to demonstrate that the two processes can be uncoupled. Recently, Qin *et al*. used cryoelectron tomography (cryo-ET) to visualize the basal body of *H. pylori* and observed major remodeling of the outer membrane surrounding the filament (122). The observations by Qin and colleagues contradicts the observation by Richardson *et al*., indicating sheath biogenesis is tightly coupled with filament growth. But there is a possibility the

two bacterial species synthesize the sheath by different mechanisms, suggesting sheath biogenesis evolved independently in different bacterial species.

The physiological role of the flagellar sheath and the reason the sheath is restricted to a small subset of bacteria is unknown. A study investigating the sheath of *B. bacteriovorous* identified the lipid domain is distinct from the outer membrane, containing more phospholipid (~57%) and less protein (~26%) than described for the outer membrane (123). Consistent with this result, Geis *et al*. reported there are no fatty acids typical of the flagellar sheath, but the fatty acid profile for phospholipids and LPS in the sheath is different when compared to whole cells (118, 124). As a result, the higher percentage of phospholipids may increase the fluidity of the sheath compared to the outer membrane. Brennan *et al*. demonstrated that both *Vibrio fischeri* and *V. cholerae* release LPS from their sheathed flagella as they rotate, and proposed that the release of LPS plays a role in the *Vibrio*-squid symbiosis by triggering the host immune response (125). Whether or not the release of LPS from the flagellar sheath has a role in host-symbiont interactions, the observation by Brennan *et al.* are consistent with the proposed fluidity of the flagellar sheath and supports the model of the filament freely rotating within the sheath. But whether the release of LPS is a consequence of the fluidity of the membranous sheath or a survival strategy requires further examination. Investigators have also proposed the sheath prevents detection by the innate immunity, while others suggest it prevents the protein filament from depolymerizing in acidic conditions (126). The sheath may also be required for the localization of adhesions responsible for bacterial cells to attach to the intestinal tissue (117). The mechanism by which specific proteins localize to the flagellar sheath is not known, but it might involve recognition of certain phospholipids, which would be consistent with the differences in fatty acid content observed between the sheath and outer membrane.

Research Summary

The overall aim of my research is to investigate the role of CL in *H. pylori* flagellar biosynthesis. CL is found in both Gram-positive and Gram-negative bacteria, and several studies have identified this phospholipid as a key component for localization of proteins and important physiological processes like DNA replication and ATP synthesis in both cell types (96, 97, 101, 127). Our motivation to investigate CL originated from the reports that protein localization was affected in the absence of CL or other anionic phospholipids. The absence or depletion of specific phospholipids has not been implicated previously as a factor in motility, so I wished to determine if flagellum assembly in *H. pylori* would progress in the absence of CL. Our lab identified a putative cardiolipin synthase gene in *H. pylori*. Bacteria often possess multiple cardiolipin synthase genes that are expressed at different stages and conditions of growth (76, 128). The gene identified in *H. pylori* is predicted to encode an enzyme that shares 32% amino acid identity with ClsC from *E. coli*. The *clsC* homolog in *H. pylori* G27 was interrupted by introducing a chloramphenicol acetyltransferase (*cat*) gene that resulted in a non-motile phenotype. Transmission electron microscopy indicated that the *clsC* mutant cells were aflagellated, and subsequent cryo-ET revealed that flagellum assembly did not progress past the periplasm. Differential gene expression was evaluated for the *H. pylori* G27 *clsC* mutant and wild-type strains using RNA-seq, which determined that genes required midway through flagellar biosynthesis were upregulated in the *clsC* mutant. This is consistent with cryo-ET results and indicate genes are properly transcribed, but the gene products are not localized or assembled.

Disrupting the *clsC* allele in *H. pylori* B128 did not produce the same phenotype, indicating the requirement of cardiolipin for flagellar biosynthesis is strain dependent. Thin layer chromatography analysis of ^{32}P-labelled glycerophospholipids along with matrix-assisted laser

desorption ionization time-of-flight mass spectrometry analysis of isolated glycerophospholipids was performed to evaluate the glycerophospholipid profiles in the wild-type and mutant strains. The results of the radiolabeling experiment showed a depletion in cardiolipin in both the *H. pylori* G27 *clsC* and *H. pylori* B128 *clsC* strains. Examining the mass spectrometry data showed a corresponding depletion of cardiolipin in both mutant strains. Both experiments indicated CL levels were recovered after introducing the *clsC* with its native promoter *in trans*. Interestingly, both the radiolabeled and mass spectrometry experiments revealed a small level of cardiolipin is still present in both mutant strains, meaning there exists an alternative pathway for CL synthesis in *H. pylori*.

An allelic exchange mutagenesis approach was used to identify the genetic factors that allow the *H. pylori* B128 *clsC* mutant to remain motile. Whole genome resequencing was performed on seven motile *H. pylori* G27 *clsC* recipients from two independent transformations with *H. pylori* B128 *clsC* gDNA to identify potential SNPs that rescued flagellum biosynthesis. Three alleles (*icfA*, *kdsA*, and *flgI*) from the donor were present in all seven motile *H. pylori* G27 *clsC* recipients. *kdsA* and *icfA* are adjacent genes located near the origin of replication. KdsA (3-deoxy-D-manno-octalosonicacid 8-phosphate synthetase) is involved with the CMP-KDO biosynthetic pathway required for lipopolysaccharide biosynthesis, while IcfA is a β-carbonic anhydrase that catalyzes the reversible hydration of CO_2 to carbonic acid; *flgI* encodes the flagellar P ring protein and is inserted into the peptidoglycan layer during flagellar biosynthesis. Introduction of the *kdsA* and *icfA* alleles into the *H. pylori* G27 *clsC* failed to recover motility, whereas the *flgI* allele restored flagellum biosynthesis, indicating the depletion of cardiolipin in the *H. pylori* G27 *clsC* mutant may prevent P ring assembly in this *H. pylori* strain.

Finally, very little is known about the mechanisms that mediate flagellar sheath biosynthesis in *H. pylori* or any other bacterial species. Utilizing a comparative genomics approach, I identified multiple genes that are highly conserved in sheathed *Helicobacter* species but are absent in unsheathed species. Among these genes are *clsC* and a set of genes encoding a putative efflux pump (HP1489-1486). Deletion of the gene encoding for the TolC-like protein (HP1489) in *H. pylori* B128 reduced, but did not eliminate, motility. Using the selection-counterselection cassette *kan-sacB*, the HP1488 gene (encoding a HlyD-like protein) was disrupted in the *H. pylori* B128 strain generating variants with reduced motility (designated 'RM') and highly motile (designated 'M') variants. Cryo-ET examination revealed structural components that assemble into a cage-like structure surrounding the flagellar basal body are absent in the *H. pylori* B128 HP1488:*kan-sacB* RM isolate, suggesting that the putative efflux pump participates in the formation of this structure. Whole genome re-sequencing identified a SNP in the *mreC* gene of the B128 HP1488:*kan-sacB* M isolate. Lastly, the deletion of HP1487 and HP1486, which are predicted to encode ABC-type 2 transporters, generated non-motile mutants.

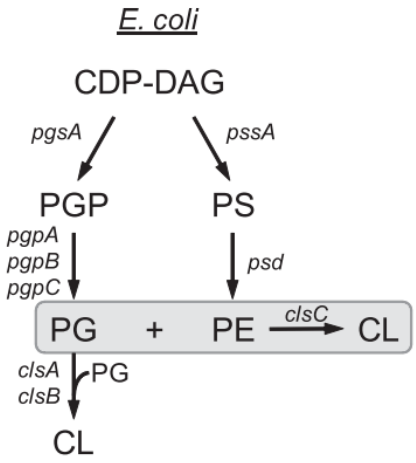

Figure 1.1. Phospholipid biosynthesis in *E. coli*. An overview of the biosynthetic pathway of the major phospholipids found in *E. coli* (129). Abbreviations are as follows: CDP-DAG, cytidine diphosphate-diacylglycerol; *pssA*, phosphatidylserine synthase; PS, phosphatidylserine; *psd*, phosphatidylserine decarboxylase; PE, phosphatidylethanolamine, *pgsA*, phosphatidylglycerolphosphate synthase; PGP, phosphatidylglycerol-phosphate; *pgp*, phosphatidylglycerol-phosphate phosphatase; *cls*, cardiolipin synthase; CL, cardiolipin.

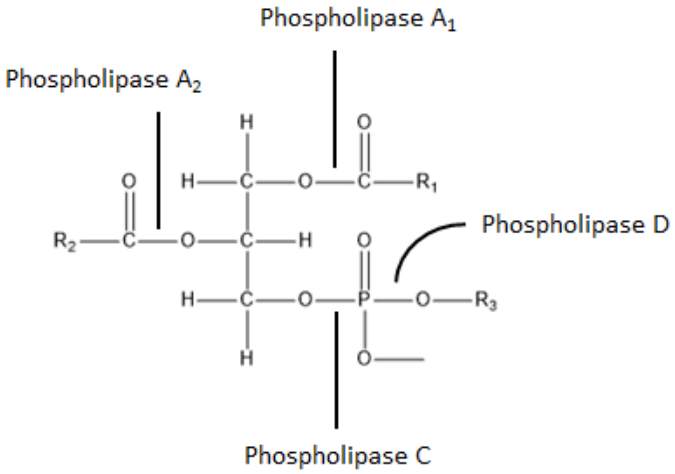

Figure 1.2: Phospholipase hydrolysis sites. Hydrolysis sites for each phospholipase enzyme are indicated in the diagram. Phospholipase B hydrolyzes the phospholipid at the same positions as phospholipase A_1 and A_2 (81).

References

1. **Atherton JC**, **Blaser MJ**. 2009. Coadaptation of *Helicobacter pylori* and humans: ancient history, modern implications. The Journal of Clinical Investigation. **119**:2475-2487. https://www.ncbi.nlm.nih.gov/pubmed/19729845.
2. **Zamani M**, **Ebrahimtabar F**, **Zamani V**, **Miller WH**, **Alizadeh-Navaei R**, **Shokri-Shirvani J**, **Derakhshan MH**. 2018. Systematic review with meta-analysis: the worldwide prevalence of *Helicobacter pylori* infection. Alimentary Pharmacology and Therapeutics. **47**:868-876. https://www.ncbi.nlm.nih.gov/pubmed/29430669.
3. **Blaser MJ**. 1993. *Helicobacter pylori*: microbiology of a 'slow' bacterial infection. Trends in Microbiology. **1**:255-260. https://www.ncbi.nlm.nih.gov/pubmed/8162405.
4. **Cover TL**, **Blaser MJ**. 1992. *Helicobacter pylori* and gastroduodenal disease. Annual Review of Medicine. **43**:135-145. https://www.ncbi.nlm.nih.gov/pubmed/1580578.
5. **Salih BA**. 2009. *Helicobacter pylori* infection in developing countries: the burden for how long? Saudi Journal of Gastroenterology. **15**:201-207. https://www.ncbi.nlm.nih.gov/pmc/articles/PMC2841423/.
6. **Moss SF**. 2016. The clinical evidence linking *Helicobacter pylori* to gastric cancer. Cellular and Molecular Gastroenterology and Hepatology. **3**:183-191. https://www.ncbi.nlm.nih.gov/pubmed/28275685.
7. **Kelley JR**, **Duggan JM**. 2003. Gastric cancer epidemiology and risk factors. Journal of Clinical Epidemiology. **56**:1-9. https://www.ncbi.nlm.nih.gov/pubmed/12589864.
8. **Ahn HJ**, **Lee DS**. 2015. *Helicobacter pylori* in gastric carcinogenesis. World Journal of Gastrointestinal Oncology. **7**:455-465. https://www.ncbi.nlm.nih.gov/pmc/articles/PMC4678392/.
9. **Brown LM**. 2000. *Helicobacter pylori* : epidemiology and routes of transmission. Epidemiologic Reviews. **22**:283-297. https://www.ncbi.nlm.nih.gov/pubmed/11218379.
10. **Yamaoka Y**. 2010. Mechanisms of disease: *Helicobacter pylori* virulence factors. Nature reviews Gastroenterology & Hepatology. **7**:629-641. https://www.ncbi.nlm.nih.gov/pubmed/20938460.
11. **Dang BN**, **Graham DY**. 2017. *Helicobacter pylori* infection and antibiotic resistance: A WHO high priority? Nature Reviews Gastroenterology and Hepatology. **14**:383-384. https://www.ncbi.nlm.nih.gov/pubmed/28465548.
12. **Alba C**, **Blanco A**, **Alarcón T**. 2017. Antibiotic resistance in *Helicobacter pylori*. Current Opinion in Infectious Diseases. **30**:489-497. https://www.ncbi.nlm.nih.gov/pubmed/28704226.
13. **Goderska K**, **Agudo Pena S**, **Alarcon T**. 2018. *Helicobacter pylori* treatment: antibiotics or probiotics. Applied Microbiology and Biotechnology. **102**:1-7. https://www.ncbi.nlm.nih.gov/pubmed/29075827.
14. **Niv Y**, **Boltin D**, **Ben-Zvi H**, **Samra Z**, **Perets TT**, **Kamenetsky Z**, **Dickman R**. 2014. Trends in secondary antibiotic resistance of *Helicobacter pylori* from 2007 to 2014: has the tide turned? Journal of Clinical Microbiology. **53**:522-527. https://www.ncbi.nlm.nih.gov/pubmed/25428158.

15. **Hooi JKY**, **Lai WY**, **Ng WK**, **Suen MMY**, **Underwood FE**, **Tanyingoh D**, **Malfertheiner P**, **Graham DY**, **Wong VWS**, **Wu JCY**, **Chan FKL**, **Sung JJY**, **Kaplan GG**, **Ng SC**. 2017. Global prevalence of *Helicobacter pylori* infection: systematic review and meta-analysis. Gastroenterology. **153**:420-429. https://www.ncbi.nlm.nih.gov/pubmed/28456631.
16. **Mégraud F**. 2004. *H. pylori* antibiotic resistance: prevalence, importance, and advances in testing. Gut. **53**:1374-1384. https://www.ncbi.nlm.nih.gov/pubmed/15306603.
17. **Mégraud F**. 2012. The challenge of *Helicobacter pylori* resistance to antibiotics: The comeback of bismuth-based quadruple therapy. Therapeutic Advances in Gastroenterology. **5**:103-109. https://www.ncbi.nlm.nih.gov/pubmed/22423259.
18. **Marshall B**, **Warren JR**. 1984. Unidentified curved bacilli in the stomach of patients with gastritis and peptic ulceration. The Lancet. **323**:1311-1315. https://www.ncbi.nlm.nih.gov/pubmed/6145023.
19. **Ernst PB**, **Gold BD**. 2000. The disease spectrum of *Helicobacter pylori*: the immunopathogenesis of gastroduodenal ulcer and gastric cancer. Annual Review of Microbiology. **54**:615-640. https://www.ncbi.nlm.nih.gov/pubmed/11018139.
20. **Gravina AG**, **Zagari RM**, **De Musis C**, **Romano L**, **Loguercio C**, **Romano M**. 2018. *Helicobacter pylori* and extragastric diseases: A review. World Journal of Gastroenterology. **24**:3204-3221. https://www.ncbi.nlm.nih.gov/pmc/articles/PMC6079286/.
21. **Argenziano G**, **Donnarumma G**, **Arnese P**, **Assunta Baldassarre M**, **Baroni A**. 2003. Incidence of anti-*Helicobacter pylori* and anti-CagA antibodies in rosacea patients. International Journal of Dermatology. **42**:601-604. https://www.ncbi.nlm.nih.gov/pubmed/12890101.
22. **Chen Y**, **Blaser MJ**. 2008. *Helicobacter pylori* colonization is inversely associated with childhood asthma. Journal of Infectious Diseases. **198**:553-560. https://www.ncbi.nlm.nih.gov/pubmed/18598192.
23. **Huang WS**, **Yang TY**, **Shen WC**, **Lin CL**, **Lin MC**, **Kao CH**. 2014. Association between *Helicobacter pylori* infection and dementia. Journal of Clinical Neuroscience. **21**:1355-1358. https://www.ncbi.nlm.nih.gov/pubmed/24629396.
24. **Hudak L**, **Jaraisy A**, **Haj S**, **Muhsen K**. 2017. An updated systematic review and meta-analysis on the association between *Helicobacter pylori* infection and iron deficiency anemia. *Helicobacter*. **22**. https://www.ncbi.nlm.nih.gov/pubmed/27411077.
25. **Lahner E**, **Persechino S**, **Annibale B**. 2012. Micronutrients (Other than iron) and *Helicobacter pylori* infection: a systematic review. *Helicobacter*. **17**:1-15. https://www.ncbi.nlm.nih.gov/pubmed/22221610.
26. **Mohebi N**, **Mamarabadi M**, **Moghaddasi M**. 2013. Relation of *Helicobacter pylori* infection and multiple sclerosis in Iranian patients. Neurology International. **5**:31-33. https://www.ncbi.nlm.nih.gov/pubmed/23888213.
27. **Oldenburg B**. 1996. High seroprevalence of *Helicobacter pylori* in diabetes mellitus patients. Digestive Diseases and Sciences. **41**:458-461. https://www.ncbi.nlm.nih.gov/pubmed/8617115.
28. **Yuan W**, **Yumin L**, **Kehu Y**, **Bin M**, **Quanlin G**, **Wang D**, **Yang L**. 2010. Iron deficiency anemia in *Helicobacter pylori* infection: meta-analysis of randomized controlled trials. Scandinavian Journal of Gastroenterology. **45**:665-676. https://www.ncbi.nlm.nih.gov/pubmed/20201716.

29. **Bégué RE**, **Gómez R**, **Compton T**, **Vargas A**. 2002. Effect of *Helicobacter pylori* eradication in the glycemia of children with type 1 diabetes: a preliminary study. Southern Medical Journal. **95**:842-845. https://www.ncbi.nlm.nih.gov/pubmed/12190218.
30. **Blaser MJ**, **Chen Y**, **Reibman J**. 2008. Does *Helicobacter pylori* protect against asthma and allergy? Gut. **57**:561-567. https://gut.bmj.com/content/57/5/561.
31. **Chen Y**, **Segers S**, **Blaser MJ**. 2013. Association between *Helicobacter pylori* and mortality in the NHANES III study. Gut. **62**:1262-1269. https://www.ncbi.nlm.nih.gov/pubmed/23303440.
32. **Hsieh MC**, **Wang SS**, **Hsieh YT**, **Kuo FC**, **Soon MS**, **Wu DC**. 2013. *Helicobacter pylori* infection associated with high HbA1c and type 2 diabetes. European Journal of Clinical Investigation. **43**:949-956. https://www.ncbi.nlm.nih.gov/pubmed/23879740.
33. **Zhou X**. 2013. Association between *Helicobacter pylori* and asthma: a meta-analysis. European Journal of Gastroenterology & Hepatology. **25**:460-468. https://www.ncbi.nlm.nih.gov/pubmed/23242126.
34. **Stone MA**. 1999. Transmission of *Helicobacter pylori.* Postgraduate Medical Journal. **75**:198-200. https://pmj.bmj.com/content/75/882/198.
35. **Eusebi LH**, **Zagari RM**, **Bazzoli F**. 2014. Epidemiology of *Helicobacter pylori* infection. Helicobacter. **19**:1-5. https://www.ncbi.nlm.nih.gov/pubmed/25167938.
36. **Li J**, **Perez-Perez GI**. 2018. *Helicobacter pylori* the latent human pathogen or an ancestral commensal organism. Frontiers in Microbiology. **9**:609. https://www.ncbi.nlm.nih.gov/pubmed/29666614.
37. **Perry S**, **Sanchez MdlL**, **Yang S**, **Haggerty TD**, **Hurst P**, **Perez-Perez G**, **Parsonnet J**. 2006. Gastroenteritis and transmission of *Helicobacter pylori* infection in households. Emerging Infectious Disease Journal. **12**:1701-1708. https://www.ncbi.nlm.nih.gov/pubmed/17283620.
38. **Mentis A**, **Lehours P**, **Mégraud F**. 2015. Epidemiology and diagnosis of *Helicobacter pylori* infection. *Helicobacter*. **20**:1-7. https://www.ncbi.nlm.nih.gov/pubmed/26372818.
39. **Linz B**, **Balloux F**, **Moodley Y**, **Manica A**, **Liu H**, **Roumagnac P**, **Falush D**, **Stamer C**, **Prugnolle F**, **van der Merwe SW**, **Yamaoka Y**, **Graham DY**, **Perez-Trallero E**, **Wadstrom T**, **Suerbaum S**, **Achtman M**. 2007. An African origin for the intimate association between humans and *Helicobacter pylori.* Nature. **445**:915-918. https://www.nature.com/articles/nature05562.
40. **Peek RM**. 2004. *Helicobacter pylori* and gastroesophageal reflux disease. Current Treatment Options in Gastroenterology. **7**:59-70. https://www.ncbi.nlm.nih.gov/pubmed/14723839.
41. **Wang Q**, **Yu C**, **Sun Y**. 2013. The association between asthma and *Helicobacter pylori*: a meta-analysis. *Helicobacter*. **18**:41-53. https://www.ncbi.nlm.nih.gov/pubmed/23067334.
42. **Saito N**, **Konishi K**, **Sato F**, **Kato M**, **Takeda H**, **Sugiyama T**, **Asaka M**. 2003. Plural transformation-processes from spiral to coccoid *Helicobacter pylori* and its viability. Journal of Infection. **46**:49-55. https://www.ncbi.nlm.nih.gov/pubmed/12504609.
43. **Chan WY**, **Hui PK**, **Leung KM**, **Chow J**, **Kwok F**, **Ng CS**. 1994. Coccoid forms of *Helicobacter pylori* in the human stomach. American Journal of Clinical Pathology. **102**:503-507. https://www.ncbi.nlm.nih.gov/pubmed/7524304.

44. **Ogata M**, **Araki K**, **Ogata T**. 1998. An electron microscopic study of *Helicobacter pylori* in the surface mucous gel layer. Histology and Histopathology. **13**:347-358. https://www.ncbi.nlm.nih.gov/pubmed/9589892.
45. **Percival SL**, **Suleman L**. 2014. Biofilms and *Helicobacter pylori:* dissemination and persistence within the environment and host. World Journal of Gastrointestinal Pathophysiology. **5**:122-132. https://www.ncbi.nlm.nih.gov/pubmed/25133015.
46. **Sarem M**, **Corti R**. 2016. Role of *Helicobacter pylori* coccoid forms in infection and recrudescence. Gastroenterología y Hepatología (English Edition). **39**:28-35. https://www.ncbi.nlm.nih.gov/pubmed/26089229.
47. **Richards CL**, **Buchholz BJ**, **Ford TE**, **Broadaway SC**, **Pyle BH**, **Camper AK**. 2011. Optimizing the growth of stressed *Helicobacter pylori.* Journal of Microbiological Methods. **84**:174-182. https://www.ncbi.nlm.nih.gov/pubmed/21129415.
48. **Albertson N**, **Wenngren I**, **Sjöström JE**. 1998. Growth and survival of *Helicobacter pylori* in defined medium and susceptibility to Brij 78. Journal of Clinical Microbiology. **36**:1232-1235. https://www.ncbi.nlm.nih.gov/pmc/articles/PMC104805/.
49. **Jiang X**, **Doyle MP**. 2000. Growth supplements for *Helicobacter pylori.* Journal of Clinical Microbiology. **38**:1984-1987. https://www.ncbi.nlm.nih.gov/pubmed/10790135.
50. **Andersen LP**, **Wadström T**. 2001. *Helicobacter pylori*: physiology and genetics. Washington (DC): ASM Press.
51. **Tomb JF**, **White O**, **Kerlavage AR**, **Clayton RA**, **Sutton GG**, **Fleischmann RD**, **Ketchum KA**, **Klenk HP**, **Gill S**, **Dougherty BA**, **Nelson K**, **Quackenbush J**, **Zhou L**, **Kirkness EF**, **Peterson S**, **Loftus B**, **Richardson D**, **Dodson R**, **Khalak HG**, **Glodek A**, **McKenney K**, **Fitzegerald LM**, **Lee N**, **Adams MD**, **Hickey EK**, **Berg DE**, **Gocayne JD**, **Utterback TR**, **Peterson JD**, **Kelley JM**, **Cotton MD**, **Weidman JM**, **Fujii C**, **Bowman C**, **Watthey L**, **Wallin E**, **Hayes WS**, **Borodovsky M**, **Karp PD**, **Smith HO**, **Fraser CM**, **Venter JC**. 1997. The complete genome sequence of the gastric pathogen *Helicobacter pylori.* Nature. **388**:539-547. https://www.ncbi.nlm.nih.gov/pubmed/9252185.
52. **Kraft C**, **Suerbaum S**. 2005. Mutation and recombination in *Helicobacter pylori*: mechanisms and role in generating strain diversity. International Journal of Medical Microbiology. **295**:299-305. https://www.ncbi.nlm.nih.gov/pubmed/16173496.
53. **Heuermann D**, **Haas R**. 1998. A stable shuttle vector system for effecient genetic complementation of *Helicobacter pylori* strains by transformation and conjugation. Mol Gen Genet. **257**:519-528. https://www.ncbi.nlm.nih.gov/pubmed/9563837.
54. **Heuermann D**, **Haas R**. 1995. Genetic organization of a small cryptic plasmid of *Helicobacter pylori.* Gene. **165**:17-24. https://www.ncbi.nlm.nih.gov/pubmed/7489910.
55. **Tsang J**, **Hoover TR**. 2014. Themes and variations: regulation of RpoN-dependent flagellar genes across diverse bacterial species. Scientifica. **2014**:14. https://www.ncbi.nlm.nih.gov/pubmed/24672734.
56. **Lowenthal AC**, **Hill M**, **Sycuro LK**, **Mehmood K**, **Salama NR**, **Ottemann KM**. 2009. Functional analysis of the *Helicobacter pylori* flagellar switch proteins. Journal of Bacteriology. **191**:7147-7156. https://www.ncbi.nlm.nih.gov/pubmed/19767432.
57. **Moore SA**, **Jia Y**. 2010. Structure of the cytoplasmic domain of the flagellar secretion apparatus component FlhA from *Helicobacter pylori.* Journal of Biological Chemistry. **285**:21060-21069. https://www.ncbi.nlm.nih.gov/pubmed/20442410.

58. **Smith TG**, **Hoover TR**. 2009. Deciphering bacterial flagellar gene regulatory networks in the genomic era. Advances in Applied Microbiology. **67**:257-295. https://www.ncbi.nlm.nih.gov/pubmed/19245942.
59. **Niehus E**, **Gressmann H**, **Ye F**, **Schlapbach R**, **Dehio M**, **Dehio C**, **Stack A**, **Meyer TF**, **Suerbaum S**, **Josenhans C**. 2004. Genome-wide analysis of transcriptional hierarchy and feedback regulation in the flagellar system of *Helicobacter pylori*. Molecular Microbiology. **52**:947-961. https://www.ncbi.nlm.nih.gov/pubmed/15130117.
60. **Beier D**, **Frank R**. 2000. Molecular characterization of two-component systems of *Helicobacter pylori*. Journal of Bacteriology. **182**:2068-2076. https://www.ncbi.nlm.nih.gov/pubmed/10735847.
61. **Spohn G**, **Scarlato V**. 1999. Motility of *Helicobacter pylori* is coordinately regulated by the transcriptional activator FlgR, an NtrC homolog. Journal of Bacteriology. **181**:593-599. https://www.ncbi.nlm.nih.gov/pubmed/9882675.
62. **Allan E**, **Dorrell N**, **Foynes S**, **Anyim M**, **Wren BW**. 2000. Mutational analysis of genes encoding the early flagellar components of *Helicobacter pylori*: evidence for transcriptional regulation of flagellin A biosynthesis. Journal of Bacteriology. **182**:5274-5277. https://www.ncbi.nlm.nih.gov/pubmed/10960117.
63. **Smith TG**, **Pereira L**, **Hoover TR**. 2009. *Helicobacter pylori* FlhB processing-deficient variants affect flagellar assembly but not flagellar gene expression. Microbiology. **155**:1170-1180. https://www.ncbi.nlm.nih.gov/pubmed/19332819.
64. **Colland F**, **Rain JC**, **Gounon P**, **Labigne A**, **Legrain P**, **De Reuse H**. 2001. Identification of the *Helicobacter pylori* anti-σ^{28} factor. Molecular Microbiology. **41**:477-487. https://www.ncbi.nlm.nih.gov/pubmed/11489132.
65. **Tsang J**, **Smith TG**, **Pereira LE**, **Hoover TR**. 2013. Insertion mutations in *Helicobacter pylori flhA* reveal strain differences in RpoN-dependent gene expression. Microbiology. **159**:58-67. https://www.ncbi.nlm.nih.gov/pubmed/23154969.
66. **Karlinsey JE**, **Tanaka S**, **Bettenworth V**, **Yamaguchi S**, **Boos W**, **Aizawa SI**, **Hughes KT**. 2000. Completion of the hook–basal body complex of the *Salmonella typhimurium* flagellum is coupled to FlgM secretion and *fliC* transcription. Molecular Microbiology. **37**:1220-1231. https://www.ncbi.nlm.nih.gov/pubmed/10972838.
67. **Rust M**, **Borchert S**, **Niehus E**, **Kuehne SA**, **Gripp E**, **Bajceta A**, **McMurry JL**, **Suerbaum S**, **Hughes KT**, **Josenhans C**. 2009. The *Helicobacter pylori* anti-sigma factor FlgM is predominantly cytoplasmic and cooperates with the flagellar basal body protein FlhA. Journal of Bacteriology. **191**:4824-4834. https://www.ncbi.nlm.nih.gov/pubmed/19465658.
68. **Parsons JB**, **Rock CO**. 2013. Bacterial lipids: metabolism and membrane homeostasis. Progress in Lipid Research. **52**:249-276. https://www.ncbi.nlm.nih.gov/pubmed/23500459.
69. **Sohlenkamp C**, **Geiger O**. 2016. Bacterial membrane lipids: diversity in structures and pathways. FEMS Microbiology Reviews. **40**:133-159. https://www.ncbi.nlm.nih.gov/pubmed/25862689.
70. **Barák I**, **Muchová K**. 2013. The role of lipid domains in bacterial cell processes. International Journal of Molecular Sciences. **14**:4050-4065. https://www.ncbi.nlm.nih.gov/pubmed/23429192.

71. **Gidden J**, **Denson J**, **Liyanage R**, **Ivey DM**, **Lay JO**. 2009. Lipid Compositions in *Escherichia coli* and *Bacillus subtilis* During Growth as Determined by MALDI-TOF and TOF/TOF Mass Spectrometry. International Journal of Mass Spectrometry. **283**:178-184. https://www.ncbi.nlm.nih.gov/pubmed/20161304.
72. **Silhavy TJ**, **Kahne D**, **Walker S**. 2010. The bacterial cell envelope. Cold Spring Harbor Perspectives in Biology. **2**:a000414. https://www.ncbi.nlm.nih.gov/pubmed/20452953.
73. **Dalebroux ZD**. 2017. Cues from the membrane: bacterial glycerophospholipids. Journal of Bacteriology. **199**:e00136-17. https://www.ncbi.nlm.nih.gov/pubmed/28439041.
74. **Raetz CR**, **Dowhan W**. 1990. Biosynthesis and function of phospholipids in *Escherichia coli*. Journal of Biological Chemistry. **265**:1235-1238. https://www.ncbi.nlm.nih.gov/pubmed/2404013.
75. **Suerbaum S**, **Josenhans C**. 2007. *Helicobacter pylori* evolution and phenotypic diversification in a changing host. Nature Reviews Microbiology. **5**:441-452. https://www.ncbi.nlm.nih.gov/pubmed/17505524.
76. **Tan BK**, **Bogdanov M**, **Zhao J**, **Dowhan W**, **Raetz CR**, **Guan Z**. 2012. Discovery of a cardiolipin synthase utilizing phosphatidylethanolamine and phosphatidylglycerol as substrates. Proceedings of the National Academy of Sciences. **109**:16504-16509. https://www.ncbi.nlm.nih.gov/pubmed/22988102.
77. **Denning EJ**, **Beckstein O**. 2013. Influence of lipids on protein-mediated transmembrane transport. Chemistry and Physics of Lipids. **169**:57-71. https://www.ncbi.nlm.nih.gov/pubmed/23473882.
78. **Jeucken A**, **Helms JB**, **Brouwers JF**. 2018. Cardiolipin synthases of *Escherichia coli* have phospholipid class specific phospholipase D activity dependent on endogenous and foreign phospholipids. BBA - Molecular and Cell Biology of Lipids. **1863**:1345-1353. https://www.ncbi.nlm.nih.gov/pubmed/29933046.
79. **Ghannoum MA**. 2000. Potential role of phospholipases in virulence and fungal pathogenesis. Clinical Microbiology Reviews. **13**:122-143. https://www.ncbi.nlm.nih.gov/pubmed/10627494.
80. **Istivan TS**, **Coloe PJ**. 2006. Phospholipase A in Gram-negative bacteria and its role in pathogenesis. Microbiology. **152**:1263-1274. https://www.ncbi.nlm.nih.gov/pubmed/16622044.
81. **Asano A**, **Nelson-Harrington JL**, **Travis AJ**. 2013. Phospholipase B Is activated in response to sterol removal and stimulates acrosome exocytosis in murine sperm. Journal of Biological Chemistry. **288**:28104-28115. https://www.ncbi.nlm.nih.gov/pubmed/23943622.
82. **Selvy PE**, **Lavieri RR**, **Lindsley CW**, **Brown HA**. 2011. Phospholipase D - enzymology, functionality, and chemical modulation. Chemical Reviews. **111**:6064-6119. https://www.ncbi.nlm.nih.gov/pubmed/21936578.
83. **Gottlin EB**, **Rudolph AE**, **Zhao Y**, **Matthews HR**, **Dixon JE**. 1998. Catalytic mechanism of the phospholipase D superfamily proceeds via a covalent phosphohistidine intermediate. Proceedings of the National Academy of Sciences. **95**:9202-9207. https://www.ncbi.nlm.nih.gov/pubmed/9689058.
84. **Frohman MA**. 2015. The phospholipase D superfamily as therapeutic targets. Trends in Pharmacological Sciences. **36**:137-144. https://www.ncbi.nlm.nih.gov/pubmed/25661257.

85. **Renesto P**, **Dehoux P**, **Gouin E**, **Touqui L**, **Cossart P**, **Raoult D**. 2003. Identification and characterization of a phospholipase D–superfamily gene in *Rickettsiae.* The Journal of Infectious Diseases. **188**:1276-1283. https://www.ncbi.nlm.nih.gov/pubmed/14593584.
86. **Waite M**. 1999. The PLD superfamily: insights into catalysis. BBA - Molecular and Cell Biology of Lipids. **1439**:187-197. https://www.ncbi.nlm.nih.gov/pubmed/10425395.
87. **Guo D**, **Tropp BE**. 2000. A second *Escherichia coli* protein with CL synthase activity. BBA - Molecular and Cell Biology of Lipids. **1483**:263-274. https://www.ncbi.nlm.nih.gov/pubmed/10634942.
88. **Koonin EV**. 1996. A duplicated catalytic motif in a new superfamily of phosphohydrolases and phospholipid synthases that includes poxvirus envelope proteins. Trends in Biochemical Sciences. **21**:242-243. https://www.ncbi.nlm.nih.gov/pubmed/8755242.
89. **Li C**, **Tan BK**, **Zhao J**, **Guan Z**. 2016. In Vivo and in Vitro Synthesis of Phosphatidylglycerol by an *Escherichia coli* Cardiolipin Synthase. Journal of Biological Chemistry. **291**:25144-25153. https://www.ncbi.nlm.nih.gov/pubmed/27760827.
90. **Koppelman CM**, **Den Blaauwen T**, **Duursma MC**, **Heeren RM**, **Nanninga N**. 2001. *Escherichia coli* minicell membranes are enriched in cardiolipin. Journal of Bacteriology. **183**:6144-6147. https://www.ncbi.nlm.nih.gov/pubmed/11567016.
91. **Paradies G**, **Paradies V**, **De Benedictis V**, **Ruggiero FM**, **Petrosillo G**. 2014. Functional role of cardiolipin in mitochondrial bioenergetics. BBA - Bioenergetics. **1837**:408-417. https://www.ncbi.nlm.nih.gov/pubmed/24183692.
92. **Tropp BE**. 1997. Cardiolipin synthase from *Escherichia coli.* BBA - Lipids and Lipid Metabolism. **1348**:192-200. https://www.ncbi.nlm.nih.gov/pubmed/9370333.
93. **Wu FG**, **Sun HY**, **Zhou Y**, **Wu RG**, **Yu ZW**. 2014. Full picture of the thermotropic phase behavior of cardiolipin bilayer in water: identification of a metastable subgel phase. RSC Advances. **4**:51171-51179. https://pubs.rsc.org/is/content/articlelanding/2014/ra/c4ra09158b#!divAbstract.
94. **Laloux G**, **Jacobs-Wagner C**. 2014. How do bacteria localize proteins to the cell pole? Journal of Cell Science. **127**:11-19. https://www.ncbi.nlm.nih.gov/pubmed/24345373.
95. **Lin TY**, **Weibel DB**. 2016. Organization and function of anionic phospholipids in bacteria. Applied Microbiology and Biotechnology. **100**:4255-4267. https://www.ncbi.nlm.nih.gov/pubmed/27026177.
96. **Romantsov T**, **Battle AR**, **Hendel JL**, **Martinac B**, **Wood JM**. 2010. Protein localization in *Escherichia coli* cells: comparison of the cytoplasmic membrane proteins ProP, LacY, ProW, AqpZ, MscS, and MscL. Journal of Bacteriology. **192**:912-924. https://www.ncbi.nlm.nih.gov/pubmed/20008071.
97. **Romantsov T**, **Helbig S**, **Culham DE**, **Gill C**, **Stalker L**, **Wood JM**. 2007. Cardiolipin promotes polar localization of osmosensory transporter ProP in *Escherichia coli.* Molecular Microbiology. **64**:1455-1465. https://www.ncbi.nlm.nih.gov/pubmed/17504273.
98. **Dudek J**. 2017. Role of cardiolipin in mitochondrial signaling pathways. Frontiers in Cell and Developmental Biology. **5**:90-90. https://www.ncbi.nlm.nih.gov/pubmed/29034233.

99. **Matsumura A**, **Higuchi J**, **Watanabe Y**, **Kato M**, **Aoki K**, **Akabane S**, **Endo T**, **Oka T**. 2018. Inactivation of cardiolipin synthase triggers changes in mitochondrial morphology. FEBS Letters. **592**:209-218. https://www.ncbi.nlm.nih.gov/pubmed/29251771.
100. **Ikon N**, **Ryan RO**. 2017. Cardiolipin and mitochondrial cristae organization. Biochimica et biophysica acta Biomembranes. **1859**:1156-1163. https://www.ncbi.nlm.nih.gov/pubmed/28336315.
101. **Mileykovskaya E**, **Dowhan W**. 2009. Cardiolipin membrane domains in prokaryotes and eukaryotes. BBA - Biomembranes. **1788**:2084-2091. https://www.ncbi.nlm.nih.gov/pubmed/19371718.
102. **Shen Z**, **Ye C**, **McCain K**, **Greenberg ML**. 2015. The role of cardiolipin in cardiovascular health. BioMed Research International. **2015**:12. https://www.ncbi.nlm.nih.gov/pubmed/26301254.
103. **El Khoury M**, **Swain J**, **Sautrey G**, **Zimmermann L**, **Van Der Smissen P**, **Décout JL**, **Mingeot-Leclercq MP**. 2017. Targeting bacterial cardiolipin enriched microdomains: an antimicrobial strategy used by amphiphilic aminoglycoside antibiotics. Scientific reports. **7**:10697-10697. https://www.ncbi.nlm.nih.gov/pubmed/28878347.
104. **Romantsov T**, **Gonzalez K**, **Sahtout N**, **Culham DE**, **Coumoundouros C**, **Garner J**, **Kerr CH**, **Chang L**, **Turner RJ**, **Wood JM**. 2018. Cardiolipin synthase A colocalizes with cardiolipin and osmosensing transporter ProP at the poles of *Escherichia coli* cells. Molecular Microbiology. **107**:623-638. https://www.ncbi.nlm.nih.gov/pubmed/29280215.
105. **Rossi RM**, **Yum L**, **Agaisse H**, **Payne SM**. 2017. Cardiolipin synthesis and outer membrane localization are required for *Shigella flexneri* virulence. mBio. **8**:e01199-01217. https://www.ncbi.nlm.nih.gov/pubmed/28851846.
106. **Mallett GE**, **Koffler H**, **Rinker JN**. 1951. The effect of shaking on bacterial flagella and motility. Journal of Bacteriology. **61**:703-708. https://www.ncbi.nlm.nih.gov/pubmed/14850428.
107. **Pijper A**. 1949. The flagella of *Spirillum volutans*. Journal of Bacteriology. **57**:111-118. https://www.ncbi.nlm.nih.gov/pubmed/16561638.
108. **Burnham JC**, **Hashimoto T**, **Conti SF**. 1970. Ultrastructure and cell division of a facultatively parasitic strain of *Bdellovibrio bacteriovorus*. Journal of Bacteriology. **101**:997-1004. https://www.ncbi.nlm.nih.gov/pubmed/4908793.
109. **Burygin GL**, **Shirokov AA**, **Shelud'ko AV**, **Katsy EI**, **Shchygolev SY**, **Matora LY**. 2007. Detection of a sheath on *Azospirillum brasilense* polar flagellum. Microbiology. **76**:728-734. https://www.ncbi.nlm.nih.gov/pubmed/18297874.
110. **Geis G**, **Leying H**, **Suerbaum S**, **Mai U**, **Opferkuch W**. 1989. Ultrastructure and chemical analysis of *Campylobacter pylori* flagella. Journal of Clinical Microbiology. **27**:436-441. https://www.ncbi.nlm.nih.gov/pubmed/2715319.
111. **Yang GC**, **Schrank GD**, **Freeman BA**. 1977. Purification of flagellar cores of *Vibrio cholerae*. Journal of Bacteriology. **129**:1121-1128. https://www.ncbi.nlm.nih.gov/pubmed/838680.
112. **Glauert AM**, **Kerridge D**, **Horne RW**. 1963. The fine structure and mode of attachment of the sheathed flagellum of *Vibrio metchnikovii*. Journal of Cell Biology. **18**:327-336. https://www.ncbi.nlm.nih.gov/pubmed/14079492.

113. **Fuerst JA**, **Hayward AC**. 1969. The sheathed flagellum of *Pseudomonas stizobbii*. Journal of General Microbiology. **58**:239-245. https://www.ncbi.nlm.nih.gov/pubmed/?term=4188225.
114. **Costerton JW**, **Thompson J**. 1972. Induced morphological changes in the stainable layers of the cell envelope of a gram-negative bacterium. Canadian Journal of Microbiology. **18**:937-940. https://www.ncbi.nlm.nih.gov/pubmed/?term=4113709.
115. **Carson KJ**, **Eagon RG**. 1966. Lysozyme sensitivity of the cell wall of *Pseudomonas aeruginosa*. Further evidence for the role of the non-peptidoglycan components in cell wall rigidity. Canadian Journal of Microbiology. **12**:105-108. https://www.ncbi.nlm.nih.gov/pubmed/?term=4958975.
116. **Hranitzky KW**, **Mulholland A**, **Larson AD**, **Eubanks ER**, **Hart LT**. 1980. Characterization of a flagellar sheath protein of *Vibrio cholerae.* Infection and Immunity. **27**:597-603. https://www.ncbi.nlm.nih.gov/pubmed/7380541.
117. **Fuerst JA**, **Perry JW**. 1988. Demonstration of lipopolysaccharide on sheathed flagella of *Vibrio cholerae* O:1 by protein A-gold immunoelectron microscopy. Journal of Bacteriology. **170**:1488-1494. https://www.ncbi.nlm.nih.gov/pubmed/?term=2450866.
118. **Geis G**, **Suerbaum S**, **Forsthoff B**, **Leying H**, **Opferkuch W**. 1993. Ultrastructure and biochemical studies of the flagellar sheath of *Helicobacter pylori*. Journal of Medical Microbiology. **38**:371-377. https://www.ncbi.nlm.nih.gov/pubmed/?term=8487294.
119. **Thomashow LS**, **Rittenberg SC**. 1985. Waveform analysis and structure of flagella and basal complexes from *Bdellovibrio bacteriovorus* 109J. Journal of Bacteriology. **163**:1038-1046. https://www.ncbi.nlm.nih.gov/pubmed/?term=4030690.
120. **Ferris FG**, **Beveridge TJ**, **Marceau-Day ML**, **Larson AD**. 1984. Structure and cell envelope associations of flagellar basal complexes of *Vibrio cholerae* and *Campylobacter fetus*. Canadian Journal of Microbiology. **30**:322-333. https://www.ncbi.nlm.nih.gov/pubmed/?term=6426766.
121. **Richardson K**, **Nixon L**, **Mostow P**, **Kaper JB**, **Michalski J**. 1990. Transposon-induced non-motile mutants of *Vibrio cholerae.* Journal of General Microbiology. **136**:717-725. https://www.ncbi.nlm.nih.gov/pubmed/1975833.
122. **Qin Z**, **Lin WT**, **Zhu S**, **Franco AT**, **Liu J**. 2017. Imaging the motility and chemotaxis machineries in *Helicobacter pylori* by cryo-electron tomography. Journal of Bacteriology. **199**:e00695-16. https://www.ncbi.nlm.nih.gov/pubmed/?term=27849173.
123. **Thomashow LS**, **Rittenberg SC**. 1985. Isolation and composition of sheathed flagella from *Bdellovibrio bacteriovorus* 109J. Journal of Bacteriology. **163**:1047-1054. https://www.ncbi.nlm.nih.gov/pubmed/?term=4030691.
124. **Geis G**, **Leying H**, **Suerbaum S**, **Opferkuch W**. 1990. Unusual fatty acid substitution in lipids and lipopolysaccharides of *Helicobacter pylori.* Journal of Clinical Microbiology. **28**:930-932. https://www.ncbi.nlm.nih.gov/pubmed/2351736.
125. **Brennan CA**, **Hunt JR**, **Kremer N**, **Krasity BC**, **Apicella MA**, **McFall-Ngai MJ**, **Ruby EG**. 2014. A model symbiosis reveals a role for sheathed-flagellum rotation in the release of immunogenic lipopolysaccharide. eLife. **3**:e01579. https://www.ncbi.nlm.nih.gov/pubmed/24596150.
126. **Yoon SS**, **Mekalanos JJ**. 2008. Decreased potency of the *Vibrio cholerae* sheathed flagellum to trigger host innate immunity. Infection and Immunity. **76**:1282-1288. https://www.ncbi.nlm.nih.gov/pubmed/18174340.

127. **Sekimizu K**, **Kornberg A**. 1988. Cardiolipin activation of dnaA protein, the initiation protein of replication in *Escherichia coli*. Journal of Biological Chemistry. **263**:7131-7135. https://www.ncbi.nlm.nih.gov/pubmed/2835364.
128. **Kusaka J**, **Shuto S**, **Imai Y**, **Ishikawa K**, **Saito T**, **Natori K**, **Matsuoka S**, **Hara H**, **Matsumoto K**. 2016. Septal localization by membrane targeting sequences and a conserved sequence essential for activity at the COOH-terminus of *Bacillus subtilis* cardiolipin synthase. Research in Microbiology. **167**:202-214. https://www.ncbi.nlm.nih.gov/pubmed/26708983.
129. **Carman GM**. 2012. An unusual phosphatidylethanolamine-utilizing cardiolipin synthase is discovered in bacteria. Proceedings of the National Academy of Sciences. **109**:16402-16403. https://www.ncbi.nlm.nih.gov/pubmed/23012456.

CHAPTER 2

LOSS OF A CARDIOLIPIN SYNTHASE IN *HELICOBACTER PYLORI* G27 BLOCKS FLAGELLUM ASSEMBLY[1]

[1]**Chu, J., S. Zhu, C. M. Herrera, J. C. Henderson, J. Liu, M. S. Trent, and T. R. Hoover**. Submitted to *Journal of Bacteriology*, 05/30/19.

Abstract

Helicobacter pylori uses a cluster of polar, sheathed flagella for motility, which it requires for colonization of the gastric epithelium in humans. As part of a study to identify factors that contribute to localization of the flagella to the cell pole, we disrupted a gene encoding a cardiolipin synthase (*clsC*) in *H. pylori* strains G27 and B128. Flagellum biosynthesis was abolished in the *H. pylori* G27 *clsC* mutant, but not in the B128 *clsC* mutant. RNA-seq analysis showed flagellar genes encoding proteins needed early in flagellum assembly were expressed at wild-type levels in the G27 *clsC* mutant. Examination of the G27 *clsC* mutant by cryo-electron tomography indicated the mutant assembled nascent flagella that contained the MS ring, C ring, flagellar protein export apparatus and proximal rod. Motile variants of the G27 *clsC* mutant were isolated following allelic exchange mutagenesis using genomic DNA from the B128 *clsC* mutant as the donor. Genome re-sequencing of seven motile G27 *clsC* recipients revealed that each isolate contained the *flgI* (encodes the P ring protein) allele from B128. Replacing the *flgI* allele in the G27 *clsC* mutant with the B128 *flgI* allele rescued flagellum biosynthesis. We postulate that *H. pylori* G27 FlgI fails to form the P ring when cardiolipin levels in the cell envelope are low, which blocks flagellum assembly at this point. In contrast, *H. pylori* B128 FlgI can form the P ring when cardiolipin levels are low and allows for the biosynthesis of mature flagella.

Introduction

Helicobacter pylori is a member of the subphylum Epsilonproteobacteria that colonizes the stomach of about half the human population worldwide (1, 2). Infection of the gastric mucosa by *H. pylori* can lead to a variety of diseases, including chronic gastritis, peptic ulcer disease, gastric cancer and mucosa-associated lymphoid tissue lymphoma (3-5). *H. pylori* cells have a cluster of

flagella at one cell pole that they use for motility, which is required for colonization of the gastric mucosa by the bacterium (6, 7).

The bacterial flagellum is composed of three basic parts, namely the basal body, hook and filament (8-10). The basal body is the most complex of these structures and includes the flagellar motor. The flagellar motor consists of the MS ring (base for the motor), C ring (switch complex regulating motor rotation), rod (connects MS ring to hook), and stator, which is a membrane protein complex of MotA and MotB. The stator is the torque generator for the flagellar motor and is powered by the proton motive force (11). In addition to regulating motor rotation, the C ring has a role in flagellum assembly (12, 13). Additional components of the basal body include a type III secretion system (fT3SS) that transports rod, hook and filament proteins across the cell membrane, and ring structures (P ring and L ring) that act as bushings embedded in the cell envelope. The hook and filament are located outside the cell envelope. The filament functions as a helical propeller, while the hook serves as a flexible joint that transmits torque from the motor to the flagellar filament over a wide range of angles between the motor axis and filament. Structural analysis of the *H. pylori* flagellar motor using cryo-electron tomography revealed that it is one of the largest flagellar motors in bacteria, accommodating up to 18 torque generators (14). The large *H. pylori* flagellar motor may provide the higher torque required for the bacterium to swim in high viscosity medium.

Flagellum biosynthesis is a complex process that involves the coordinated expression of dozens of flagellar genes with the assembly of the flagellum. Expression of flagellar genes in *H. pylori* is controlled by a transcriptional hierarchy that is organized according to the sigma factor (σ) required for transcription of specific sets of genes (15, 16). These sigma factors are RpoD (σ^{80}), RpoN (σ^{54}), and FliA (σ^{28}). Genes encoding proteins required early in flagellum assembly

(i.e., basal body formation) and some regulatory proteins rely on σ^{80} for their transcription (15). A master regulator that initiates the transcriptional hierarchy has been identified for many bacteria (17), but not for *H. pylori*. Transcription of genes whose products are required midway in flagellum assembly (e.g., hook and hook-associated proteins) requires σ^{54} and a two-component system consisting of the sensor kinase FlgS and the response regulator FlgR (16, 18, 19). FlgS may recognize an assembly checkpoint associated with the fT3SS to initiate the signaling cascade that results in transcriptional activation of the σ^{54}-dependent regulon, as disrupting genes encoding components of the fT3SS interferes with expression of σ^{54}-dependent genes (15, 20-24). Consistent with this hypothesis, FlgS binds a peptide that corresponds to the N-terminus of the fT3SS component FlhA with high affinity (25). Transcription of the late flagellar genes in *H. pylori* requires σ^{28} and is negatively regulated by the anti- σ^{28} factor FlgM (26, 27). In *Salmonella enterica* serovar Typhimurium (*S*. Typhimurium), inhibition of σ^{28} activity by FlgM is alleviated by transport of FlgM by the fT3SS (28). FlgM does not appear to be exported by the fT3SS in *H. pylori*, but rather, its inhibition on σ^{28} may be relieved by binding to FlhA (29).

As part of a study to learn how *H. pylori* localizes its flagella to the cell pole, we knocked out a putative cardiolipin synthase gene in *H. pylori* since cardiolipin (CL) is required for polar localization of certain proteins in *Escherichia coli* (30). The putative *H. pylori* G27 CL synthase shares homology with *E. coli* cardiolipin synthase C (ClsC). We found that the *H. pylori clsC* homolog is required for wild-type levels of CL, and so we designated it as *clsC*. Disrupting *clsC* abolished flagellum biosynthesis in *H. pylori* G27, but not in *H. pylori* B128, even though CL levels in the two *clsC* mutants were similarly reduced. RNA-seq analysis revealed that the *H. pylori* G27 *clsC* mutant expressed many of the genes in the σ^{54} regulon at wild-type levels or higher, suggesting the mutant expressed a functional fT3SS but was blocked in flagellum

assembly. Consistent with this hypothesis, cryo-electron tomography (cryo-ET) revealed nascent flagellar structures arrested at an early stage in the assembly process in the *H. pylori* G27 *clsC* mutant. Introduction of the *H. pylori* B128 *flgI* allele (encodes the flagellar P ring protein) into the *H. pylori* G27 *clsC* mutant restored flagellum biogenesis. We infer from these data that assembly of the P ring in *H. pylori* G27, but not *H. pylori* B128, requires normal levels or specific species of CL in the cell envelope.

Materials and Methods

Bacterial strains and growth conditions. *E. coli* DH5α was used for cloning and plasmid construction. *E. coli* strains were grown in Luria-Bertani broth or agar medium. Medium was supplemented with ampicillin (100 μg/ml), chloramphenicol (30 μg/mL) or kanamycin (30 μg/ml) when appropriate. For routine growth of *H. pylori* strains, the cultures were grown microaerobically under an atmosphere consisting of 10% CO_2, 4% O_2 and 86% N_2 at 37°C on tryptic soy agar (TSA) supplemented with 5% horse serum, or in tryptic soy broth (TSB) supplemented with 5% heat-inactivated horse serum with shaking under an atmosphere consisting of 5% CO_2, 10% H_2, 10% O_2 and 75% N_2. Growth of *H. pylori* strains for glycerophospholipid extraction was done at 37°C in Mueller-Hinton broth (MHB) with 10% horse serum and 20 mM 2-(4-morpholino)-ethane sulfonic acid (MES; pH 6.0) under an atmosphere consisting of 10% CO_2, 5% O_2 and 85% N_2. Kanamycin (30 μg/ml) or chloramphenicol (30 μg/ml) was added to the medium used to culture *H. pylori* when appropriate.

Strain construction. All primers used for PCR in the construction of *H. pylori* mutants are listed in Supplemental Table 1. Genomic DNA from *H. pylori* B128 was purified using the Wizard genomic DNA purification kit (Promega) and used as the PCR template to construct the *clsC*

knockout. DNA was amplified from *H. pylori* B128 genomic DNA (gDNA) using Phusion polymerase (New England Biolabs) and the resulting amplicons were incubated with *Taq* polymerase (Promega) at 72^{o} C for 10 min to add 3'-A overhangs for T/A cloning with pGEM-T Easy plasmid (Promega). To disrupt *clsC* in *H. pylori* G27 and B128, a 634 bp upstream DNA fragment was amplified that included 493 bp of *frdB* (gene immediately upstream of *clsC*; encodes succinate dehydrogenase subunit B), an intergenic region of 21 bp, and 99 bp of the 5'-end of *clsC* that includes a 21 bp sequence complementary to a chloramphenicol-resistance (*cat*) cassette using primers M54 and M55. A 604 bp downstream DNA fragment that included 508 bp downstream of *clsC* and 75 bp of the 3'-end of *clsC* together with 21 bp sequence complementary to the *cat* cassette was amplified using primers M56 and M57. A *cat* cassette was PCR-amplified from pUC20 *cat* using primers cat5 and cat6, generating a 742 bp fragment (31). PCR SOEing was used to join the upstream and downstream regions to the *cat* cassette, and the resulting amplicon was cloned into pGEM-T Easy to generate the suicide plasmid pJC030, which was introduced into *H. pylori* strains G27 and B128 by natural transformation. Chloramphenicol-resistant transformants were selected on TSA supplemented with horse serum and chloramphenicol. Replacement of *clsC* with the *cat* cassette in the *H. pylori* G27 and B128 chromosome was confirmed by PCR using primers that flanked the *clsC* locus. The resulting amplicons were sequenced (Eton Bioscience) to verify that *clsC* had been replaced with the *cat* cassette.

Complementation of the *clsC* mutation. Plasmid pJC032 is a derivative of the shuttle vector pHel3 (32) that carries *H. pylori* G27 *clsC* under control of its native promoter located upstream of *frdA*. To construct pJC032, the *frdA* promoter and *clsC* coding regions were amplified using the primer pairs 'P069 and P070' and 'P071 and P072', respectively, and *H. pylori* G27 gDNA as the template. The resulting amplicons were joined by overlapping PCR. Primers that contained 25

bp of homologous sequence with pHel3 were used to amplify the fusion product, and the resulting amplicon was cloned into pHel3 cut with SphI using the sequence- and ligation-independent cloning (SLIC) method (33) to generate pJC032. For complementation assays, pJC032 was introduced into the *H. pylori clsC* mutants by natural transformation, which were then examined for CL, motility and the presence of flagella as described below.

Motility assay. Motility was assessed using a soft-agar medium comprised of MHB, 10% heat-inactivated horse serum, 20 mM MES (pH 6.0), 5 μM $FeSO_4$ and 0.4% Noble agar. Plates were stab-inoculated with cells from TSA plates grown for 5 days using wooden sticks and incubated at 37^o C under an atmospheric condition consisting of 10% CO_2, 4% O_2 and 86% N_2. Diameters of swim halos were measured after 7 days of incubation. The two-sample *t* test was used to determine statistical significance.

Transmission electron microscopy. *H. pylori* strains were grown to late-log phase in TSB supplemented with 10% heat-inactivated horse serum to an OD_{600} of ~1.0. One milliliter of culture was collected by centrifugation (550 x g) then resuspended in 125 μL of 0.1 M phosphate-buffered saline. Cells were fixed by adding 50 μL of 16% EM grade formaldehyde and 25 μL of 8% EM grade glutaraldehyde to the cell resuspension. Following incubation at room temperature for 5 min, 10 μL of the cell suspension were added to 300 mesh, formvar-coated copper grids and incubated at room temperature for 5 min. The cell suspension was wicked off the grids using a filter paper, and the grids were washed 3 times with 10 μL of water. Cells were stained by applying 10 μL of 1% uranyl acetate to the grids for 30 s. After removing the stain with filter paper, the grids were washed 3 times with 10 μL of water and then air-dried. Cells were visualized using a JEOL JEM 1011 transmission electron microscope. Flagella counts were determined for at least

100 cells for each strain. The Mann-Whitney U test was used to determine whether there were statistically significant differences in number of flagella per cell for the various *H. pylori* strains.

RNA extraction and cDNA synthesis. *H. pylori* cultures were grown in TSB supplemented with 5% horse serum for 24 h, diluted in fresh medium to a cell density of 5 Klett units, then allowed to grow to a cell density of 90 Klett units. RNA was harvested from the *H. pylori* cultures using the Zymo Direct-zol RNA MiniPrep Plus kit and quantified using a NanoDrop Lite instrument (Thermo Scientific). RNA quality was assessed using a 1% bleach gel (34). RNA preparations were treated with Turbo DNA-free kit (Ambion) according to the manufacturer's protocol to eliminate contaminating gDNA, and the absence of gDNA was confirmed by PCR. RNA samples were analyzed using a Bioanalyzer 2100 instrument (Agilent), and each sample had a minimum RNA integrity number of 9.5. Single-strand cDNA was synthesized from 200 ng of RNA using the iScript cDNA synthesis kit (Bio-Rad).

RNA-seq assay. Ribosomal RNAs were depleted from RNA preparations and libraries were prepared using 5 μg of total RNA. Illumina sequencing was performed using a NextSeq500 instrument at the University of Georgia Genomics Facility. Quality of the reads were assessed using FastQC and trimmed using Trimmomatic, and the resulting reads were assembled to the *H. pylori* G27 genome (Accession no.: NC_011333.1) using Bowtie2 and visualized using Geneious (35, 36). The DESeq2 package in RStudio was used to analyze raw fragment counts and differentially regulated genes were identified with a log2-fold cutoff of 1.5 (37).

RT-qPCR. Transcript levels of *flhA, fliF, flgE, flaB* and *flaA* were monitored by RT-qPCR as previously described (25, 38). Primers used for this experiment are listed in Table 2. RT-qPCR was performed on serially diluted cDNA samples and concentrations for all samples were determined using a standard curve of serially diluted gDNA. Each RT-qPCR mixture totaled 20

μL, consisting of 10 μL of Luna Universal qPCR mix (New England BioLabs), 5 μL of 100-fold diluted cDNA, and 5 μl of the primers (final concentration 250 nM final for each primer). Evaluation of single products in all reactions was performed after each experiment by a melt curve analysis. The Applied Biosystems StepOnePlus Real-Time PCR system was used to perform all experiments in technical triplicates for three biological replicates of each condition. The $2^{-\Delta\Delta Cq}$ method (39) was used to quantify gene expression levels and statistical significance determined using the two-sample *t* test.

Allelic exchange mutagenesis. gDNA was isolated from the *H. pylori* B128 *clsC* mutant using the Wizard Genomic DNA Purification kit (Promega) and used to transform the *H. pylori* G27 *clsC* mutant as follows. The recipient strain was patched onto fresh TSA plates and incubated for 4 days. The cells were collected and transferred to a fresh plate, then transformed with 3 μg of gDNA. Following 24 h of incubation, the cells were collected and resuspended in 1 mL TSB and spot plated onto the soft agar medium used for motility assays. After 7 d of incubation, cells from the edge of the swim halo were used to inoculate fresh soft agar medium and the inoculated plates were incubated for 7 d. Cells from the edge of the swim halo were streaked onto TSA supplemented with 5% horse serum and chloramphenicol, and the resulting isolated colonies were screened for motility in the soft agar medium.

DNA sequencing and analysis. Following the instructions supplied with the Illumina iTruSeq adaptor kit, genomic libraries were prepared using 500 ng of gDNA from various *H. pylori* strains. The resulting genomic libraries were sequenced at the University of Georgia Genomics Facility by Illumina sequencing. Quality of the reads were assessed using FastQC and trimmed using Trimmomatic (35, 36). Reads for *H. pylori* G27 gDNA sequences were mapped using Bowtie2 using the published NCBI genome for *H. pylori* G27 (Accession no.: NC_011333.1) and visualized

in Geneious. The alignment generated was used to align the gDNA sequence of the *H. pylori* G27 *clsC* mutant, which served as the backbone for aligning the gDNA sequences of the suppressor mutant strains. SNPs were identified in the genome sequences of the motile recipient strains using Geneious. Candidate genes were identified by using RStudio to cross-reference SNPs that were common to all the motile G27 *clsC* recipients.

Replacement of specific alleles in the *H. pylori* G27 *clsC* mutant. For the following PCR and cloning steps, target DNA was amplified using Phusion polymerase and the resulting amplicons were incubated with *Taq* polymerase at 72^{o} C for 10 min to add 3'-A overhangs to facilitate T/A cloning into plasmid pGEM-T Easy. Primer pair P079 and P080 were used to amplify 558 bp of the *ureA* promoter from *H. pylori* G27. Using the pKSF plasmid (40) as a template, a 2,978 bp DNA fragment was amplified that included the kanamycin cassette and a promoter-less *sacB* gene. The two amplicons were joined by PCR SOEing, which generated a 3,536 bp product and was cloned into pGEM-T Easy that resulted in the plasmid pJC038. Regions upstream (568 bp) and downstream (393 bp) of *H. pylori* B128 *icfA* were amplified using the primer pairs 'P165 and P166' and 'P167 and P168', respectively. The resulting amplicons were joined by PCR SOEing and cloned into pGEM-T Easy to generate plasmid pJC068. The *kan-sacB* cassette was introduced into unique NheI and XhoI sites in plasmid pJC068 to generate a suicide vector (pJC069) that was used to replace the *icfA* and *kdsA* alleles in the *H. pylori* G27 *clsC* mutant with the corresponding alleles from *H. pylori* B128. The primers 'P165' and 'P189' were used to amplify 495 bp of DNA upstream of *H. pylori* G27 *icfA*. Primers 'P190' and 'P168' were used to amplify a region of *H. pylori* B128 gDNA corresponding to the entire coding region of *icfA* and the first 164 bp of the *kdsA* coding region. The resulting amplicons were joined using PCR SOEing and cloned into pGEM-T Easy to generate plasmid pJC075. Plasmid pJC075 was introduced by natural

transformation into the *H. pylori* G27 *clsC* strain that carried the *kan-sacB* cassette in the *icfA* locus. Transformants in which the *kan-sacB* cassette was replaced with the *icfA-kdsA* alleles carried on pJC075 were isolated following a sucrose-based counter-selection as described. The *icfA-kdsA* regions for several kanamycin-sensitive, sucrose-resistant isolates were amplified by PCR, and the resulting amplicons were sequenced to confirm that the *H. pylori* G27 *clsC* mutant contained the B128 *ifcA-kdsA* alleles.

Primer pairs 'P169' and 'P170' and 'P187' and 'P188' were used to amplify 616 bp and 503 bp of DNA sequence upstream and downstream of *H. pylori* G27 *flgI*, respectively. The two amplicons were joined using PCR SOEing, and the resulting amplicon was cloned into pGEM-T Easy to generate plasmid pJC074. A *kan-sacB* cassette was inserted in unique NheI and XhoI sites in pJC074 to generate the suicide vector pJC077 that was used to replace *flgI* coding sequence in the *H. pylori* G27 *clsC* mutant with the *kan-sacB* cassette. Primer pairs 'P169' and 'P191' were used to amplify 552 bp of DNA upstream of *H. pylori* G27 *flgI*, primer pair 'P192' and 'P172' were used to amplify 552 bp of DNA downstream of *H. pylori* G27 *flgI*, and primer pair 'P193' and 'P194' were used to amplify *H. pylori* B128 *flgI* (1029 bp of DNA sequence). The three amplicons were joined using PCR SOEing, and the resulting amplicon was cloned into pGEM-T Easy to generate plasmid pJC078. Plasmid pJC078 was transformed into the *H. pylori* G27 *clsC* strain where *flgI* had been replaced with the *kan-sacB* cassette to introduce the *H. pylori* B128 *flgI* allele into the strain using a sucrose-based counter-selection.

Glycerophospholipid extraction. Cells were harvested, and pellets were washed once with 5 ml phosphate buffered saline (PBS). Isolation of glycerophospholipids was carried out using a modified method of Bligh and Dyer as described (41). Briefly, cell pellets were resuspended in 5 ml of single-phase Bligh-Dyer mixture consisting of chloroform:methanol:water (1:2:0.8, v/v/v),

then incubated for 20 min at room temperature. Samples were centrifuged at 1,800 x g for 10 min. The resulting supernatants were transferred to clean glass tubes and converted into a two-phase Bligh-Dyer mixture consisting of chloroform:methanol:water (2:2:1.8, v/v/v). This mixture was vortexed and centrifuged to separate the organic and aqueous phases. The lower organic phase was removed into clean glass tube. A second extraction was performed by adding 2.6 ml chloroform back to the tube containing the upper phase. The mixture was vortexed and centrifuged. The resulting lower phase was pooled with the previous lower phase and converted again into a two-phase Bligh-Dyer mixture by adding 5.2 ml methanol and 4.7 ml water. The resulting mixture was vortexed and centrifuged. Finally, the lower phase containing glycerophospholipids was removed and placed into a new tube, which was subsequently dried under a stream of nitrogen.

Analysis of ^{32}P-labeled glycerophospholipids. Bacterial glycerophospholipids were uniformly radiolabeled with ^{32}P (20 µCi/ ml) following a dilution to ~0.1 OD_{600} using an overnight liquid culture and incubated for 24 h. Bacteria were transferred from growth bottles into Teflon screw-cap glass tubes (16 x 125 mm) and pelleted by centrifugation at 1800 x g for 15 min. Cells were re-suspended in PBS, then re-pelleted by centrifugation at 1800 x g for 15 min. ^{32}P-glycerophospholipds were extracted, spotted on a Silica Gel 60 thin layer chromatography (TLC) plate (20,000 cpm), and separated in a glass solvent chamber using a mobile phase consisting of chloroform, methanol and acetic acid (65:25:5, v:v:v). Upon migration of the solvent front to the top of the TLC plate (~2 h), plates were dried, covered in plastic wrap and exposed overnight to a phosphorscreen. Visualization of the ^{32}P-labelled glycerophospholipids was performed using an Amersham Typhoon imager.

Mass spectrometry. All solvents were HPLC grade. Glycerophospholipid samples from unlabeled cells were resuspended in 100 µl chloroform: methanol (4:1, v/v). Solution of 9-

aminoacridine matrix (Sigma) was prepared at a concentration of 15 mg/ml in chloroform: methanol (2:1, v/v). Sample solutions were mixed with matrix solution (1:1, v/v) and 1 μl of the mixture was loaded on the target plate. A peptide standard mixture (s6104-10ug, ProteoChem Inc.) was prepared following manufacturer's recommendations and used as external calibrant. MALDI-TOF mass spectra of glycerophospholipid extracts were acquired in reflector mode on Autoflex Speed mass spectrometer (Bruker Daltonics). A total of 500 single laser shots were averaged from each mass spectrum. Data were acquired in negative ion mode and processed using FlexControl 3.4 and FlexAnalysis 3.4 software (Bruker Daltonics).

Sample preparation for cryo-EM observation. *H. pylori* strains were cultured on plates for 4 d. The cells on the agar surface were collected then washed with PBS buffer. Colloidal gold solution (10 nm diameter) was added to the diluted *H. pylori* samples to yield a 10-fold dilution and then deposited on a freshly glow-discharged, holey carbon grid for 30 seconds. The grid was blotted with filter paper and rapidly plunge-frozen in liquid ethane in a homemade plunger apparatus as described (42).

Cryo-ET data collection and image processing. The frozen-hydrated specimens of *H.pylori* G27 *clsC* mutant were transferred to Titan Krios electron microscope equipped with a 300-kV field emission gun and a Direct Electron Detector (Gatan K2 Summit). The images were collected at a defocus near to 0 um using Volta Phase Plate and the energy filter with 20 eV slit. The data was acquired automatically with SerialEM software (43). During the data collection, the phase shift is monitored at the range of pi/3~pi2/3; when the phase shift is out of above range, next spot of phase plate will be switched to be charged for the use. A total dose of 50 e−/Å2 is distributed among 35 tilt images covering angles from −51° to +51° at tilt steps of 3°. The starting tilting angle is +36˚ instead of 0˚. For every single tilt series collection, the dose-fractionated mode was used

to generate 8–10 frames per projection image. Collected dose-fractionated data were first subjected to the motion correction program to generate drift-corrected stack files (44-46). The stack files were aligned using gold fiducial markers and volumes reconstructed by the weighted back-projection method using IMOD and Tomo3d software to generate tomograms (47, 48).

Sub-tomogram analysis with i3 packages. Bacterial flagellar motors were detected manually using the i3 program (49, 50). The orientation and geographic coordinates of selected particles were then estimated. In total, 6 sub-tomograms of *H. pylori* G27 *clsC* flagellar motors were used to sub-tomogram averaging analysis. The i3 tomographic package was used on the basis of the "alignment by classification" method with missing wedge compensation for generating the averaged structure of the motor as described .

Nucleotide sequence accession numbers. The raw data used for analysis is available in NCBI GenBank under accession numbers PRJNA545123 (DNA sequencing; https://www.ncbi.nlm.nih.gov/bioproject/PRJNA545123) and PRJNA545152 (RNA-seq; https://www.ncbi.nlm.nih.gov/bioproject/PRJNA545152).

Results

Identification of a CL synthase in *H. pylori*. The proposed *clsC* homolog in *H. pylori* G27 encodes a protein belonging to the phospholipase D (PLD) superfamily, members of which catalyze the hydrolysis of phosphodiester bonds. A large subset of enzymes belonging to the PLD superfamily possess a conserved $HxKx_4Dx_6GSxN$ motif (HKD motif) (51). The HKD motif is found in all known bacterial CL synthases including the *H. pylori* G27 homolog, which contains two HKD motifs and shares 32% amino acid identity with *E. coli* ClsC and 21-24% identity with the other two *E. coli* CL synthases, ClsA and ClsB. The predicted amino acid sequence of the

B128 homolog in both the NCBI and the JGI Integrated Microbial Genomes & Microbiomes databases indicate it consists of two open reading frames that overlap by 59 bp. Re-sequencing this region, however, revealed a single open reading frame of the same length as that of the *H. pylori* G27 *clsC* allele and having a sequence identical to a homologous open reading frame in *H. pylori* B8, a gerbil-adaptive strain derived from *H. pylori* B128 (52).

Since CL is required for polar localization of certain membrane proteins in *E. coli* (30), we hypothesized that interrupting the putative *clsC* homologs would eliminate CL levels and negatively impact the localization of flagella to the cell pole in the *H. pylori clsC* mutants. We disrupted the *clsC* homologs in the *H. pylori* G27 and B128 strains with a chloramphenicol resistance (*cat*) cassette to assess their role in CL biosynthesis and examined motility of the resulting mutants in soft agar medium. *H. pylori* G27 *clsC* failed to swim from the stab-inoculation point, indicating a severe defect in motility or chemotaxis (Fig 2.1A). Reintroducing the *clsC* homolog from *H. pylori* G27 into the mutant on plasmid pHel3 (plasmid pCls) rescued motility (Fig. 2.1A). In contrast, we observed no motility defects in the *H. pylori* B128 *clsC* mutant (Fig. 2.1A). Examination of the *H. pylori* G27 *clsC* mutant by transmission electron microscopy (TEM) revealed the cells lacked flagella, while more than 85% of the wild-type cells were flagellated, and most of the cells possessed multiple flagella (Fig. 2.1B). Plasmid pCls restored the wild-type flagellation pattern in the *clsC* mutant (Fig. 2.1B), indicating that ClsC is required for flagellum biosynthesis in *H. pylori* G27. Unlike the *H. pylori* G27 *clsC* mutant, we did not observe a reduction in flagellated cells in the *H. pylori* B128 *clsC* mutant (Fig. 2.1C).

Analysis of the ^{32}P-labeled glycerophospholipids from the wild-type and mutant strains revealed that CL levels were reduced in the putative CL synthase mutants in *H. pylori* G27 and B128 (Fig. 2.2). The glycerophospholipid composition of the wild-type G27 and B128 strains

was similar to that of *H. pylori* NCTC 11638 and ATCC 43504 , but there were some differences in the glycerophospholipid composition of the two strains we analyzed (Table 2.4). Most notably, CL levels appeared to be slightly higher in G27 compared to B128. Introducing plasmid pCls into both G27 and B128 mutants, but not the empty pHel3 shuttle vector, restored CL to wild-type levels (Fig. 2.2 and Table 2.4). These data provide compelling evidence that the *clsC* gene from *H. pylori* G27 encodes a CL synthase.

Matrix-assisted laser desorption ionization time-of-flight (MALDI/TOF) mass spectrometry of the glycerophospholipids of the *H. pylori* strains showed several molecular ions in the CL range (approximately *m/z* 1150-1400) (Fig. 2.3A). These peaks had approximate *m/z* values of 1189, 1261, 1329 and 1397 that correspond to CL species that differ with respect to acyl chain composition – i.e., length; degrees of unsaturation and cyclopropanation. The major fatty acids reported for CL from *H. pylori* NCTC 11638 include the saturated fatty acids myristic acid ($C_{14:0}$), palmitic acid ($C_{16:0}$), stearic acid ($C_{18:0}$), the unsaturated fatty acids oleic acid ($C_{18:1}$) and linoleic acid ($C_{18:2}$), and cyclopropane nonadecanoic acid ($C_{19:0}$ cyc) (53). $C_{14:0}$ and $C_{19:0}$ cyc were the most abundant fatty acids found in *H. pylori* CL, accounting for about 70% of the fatty acid content . Zhou and co-workers analyzed CL from *H. pylori* NCTC 11637 (ATCC 43504), and proposed structures for the main CL and monolysocardiolipin (MLCL; glycerophospholipid with three fatty acid chains) species (54). Proposed MLCL species included $C_{14:0}/C_{14:0}/C_{14:0}$ (*m/z* 1030), $C_{19:0}$ cyc/$C_{14:0}/C_{14:0}$ (*m/z* 1098) and $C_{19:0}$ cyc/$C_{14:0}/C_{19:0}$ cyc (*m/z* 1166); while proposed CL species included $C_{14:0}/C_{14:0}/C_{14:0}/C_{14:0}$ (*m/z* 1240), $C_{14:0}/C_{14:0}/C_{14:0}/C_{19:0}$ cyc (*m/z* 1308) and $C_{19:0}$ cyc/$C_{14:0}/C_{14:0}/C_{19:0}$ cyc (*m/z* 1376) . Peaks with approximate *m/z* values of 1261 and 1329 were absent in the *H. pylori* G27 *clsC* mutant, while 1261, 1329, and 1397 were absent in the *H. pylori* B128 *clsC* mutant, and likely correspond to CL species missing in the TLC analysis (Fig. 2.2).

The peak with the approximate *m/z* value of 1189 was observed in all strains, and likely represents the slower migrating CL species in the TLC (Fig. 2.2). Proposed structures for the CL species identified in the mass spectrometry, with the addition of a sodium adduct, are consistent with the previously proposed structures mentioned above (Fig 2.3B). Since residual amounts of CL were present in the *clsC* mutants (Fig. 2.2 and 2.3A), this suggests both *H. pylori* strains possess an alternative method to synthesize CL. At present, we do not know the identity of the enzyme(s) responsible for the synthesis of the residual amounts of CL in the *clsC* mutants.

Flagellum assembly is blocked at an early stage in the *H. pylori* G27 *clsC* mutant. We reasoned that the lesion in flagellum biosynthesis in the *H. pylori* G27 *clsC* mutant was due to the inhibition of expression of specific flagellar genes or resulted from a block in flagellum assembly. To distinguish between these two hypotheses, we compared global gene expression in the *H. pylori* G27 and *H. pylori* G27 *clsC* mutant strains by RNA-seq. Comparing the *clsC* mutant to the wild-type strain, we identified 26 genes that were differentially regulated and exhibited a $\log_2$-fold change of ≥ 1.5 in the *clsC* mutant (Fig. 2.4). Seventeen genes were downregulated in the *clsC* mutant, most of which are pseudogenes or encode hypothetical proteins of unknown function. One of the downregulated genes, *cagB*, is located within the *cag* pathogenicity island, while HPG27_RS03555 encodes a protein that belongs to the 50S ribosome-binding GTPase protein family (pfam01926). Nine genes were upregulated in the *clsC* mutant, five of which (*flgE*, *flaB*, *flgK*, *flgL*, and *flgJ*) are dependent on σ^{54} for their transcription (15).

To confirm that flagellar genes were differentially regulated in the *H. pylori* G27 *clsC* mutant, we assessed transcript levels of representative genes from the three flagellar regulons in the mutant by RT-qPCR. *flhA* (encodes a component of the fT3SS) and *fliF* (encodes MS ring protein) are dependent on the housekeeping σ factor of *H. pylori* (σ^{80}) for their transcription and

encode proteins that are required at early stages in flagellum assembly. *flgE* (encodes hook protein) and *flaB* (encodes a minor flagellin) are σ^{54}-dependent genes and their products are required at later steps in flagellum assembly. The final gene we examined, *flaA* (encodes the major flagellin), is dependent on σ^{28} for its transcription and encodes a protein that is required near the end of flagellum assembly. Transcript levels of *flhA* and *fliF* in the *clsC* mutant were indistinguishable from those in wild type (both were ~90% of wild type; *p*-values = 0.57 and 0.38, respectively; Fig. 2.5). Consistent with the RNA-seq data, transcript levels of *flaB* and *flgE* in the G27 *clsC* mutant were higher (~1.9-fold, *p*-value = 0.0021; and ~2.3-fold, *p*-value = 0.0017, respectively) than those in wild type (Fig. 2.5). In contrast to the σ^{80}-dependent and σ^{54}-dependent flagellar genes, transcript levels of *flaA* in the G27 *clsC* mutant were slightly lower (~60%; *p*-value = 0.0017) than those in wild type (Fig. 2.5).

Since the fT3SS is intimately linked with expression of the σ^{54}-dependent flagellar genes in *H. pylori* (15, 20-25, 55), the upregulation of σ^{54}-dependent flagellar genes in the G27 *clsC* mutant suggested the mutant assembles a nascent flagellum structure that includes the fT3SS. Examining the ultrastructure of the *H. pylori* G27 *clsC* mutant by cryo-ET revealed nascent flagellum structures in the cell envelope (Fig. 2.6). The MS ring, C ring, fT3SS and proximal rod were clearly visible within the nascent flagellum structures, while other basal body and flagellar motor components are not apparent, including the P ring, L ring, distal rod and stator (Fig. 2.6). The *H. pylori* flagellum has a unique cage-like structure that surrounds the motor (14), and this structure was also absent in the nascent flagellum structures of the *H. pylori* G27 *clsC* mutant (Fig. 2.6). Taken together with the RNA-seq and RT-qPCR data, the results of the cryo-ET study indicate that reduced CL levels in the cell envelope of the *H. pylori* G27 *clsC* mutant interfere with an early step in flagellum assembly.

The P ring protein from *H. pylori* B128 rescues flagellum biosynthesis in the *H. pylori* G27 *clsC* mutant. To determine the genetic basis for the disruption in flagellum assembly in the *H. pylori* G27 *clsC* mutant, we isolated seven motile variants (designated mv49, mv50, mv51, mv65, mv70, mv76 and mv77) of the *H. pylori* G27 *clsC* mutant following two independent transformations of the strain with gDNA from the *H. pylori* B128 *clsC* mutant (Fig. 2.7A). TEM analysis revealed that the motile variants were flagellated, but varied significantly in their flagellation patterns (Fig. 2.7B). The motile variant mv49 was highly flagellated, with about 98% of the cells possessing multiple flagella, which was higher than that observed for the other motile variants and wild type (Fig. 2.7B). The highly flagellated nature of mv49 corresponded with the enhanced motility of the strain in soft agar medium relative to that of wild type and the other motile variants (Fig. 2.7A). In contrast, the motility of mv50, mv51, mv65, mv70, mv76 and mv77 were similar to that of wild type (Fig. 2.7A), and the flagellation patterns of the motile variants were similar to wild type, although the motile variants had a higher proportion of cells that lacked flagella or had a single flagellum compared to wild type (Fig. 2.7B).

Genomes of the motile variants were re-sequenced to identify B128 alleles that may have rescued flagellum biosynthesis in the G27 *clsC* mutant. DNA sequences derived from the B128 donor were identified as regions with clusters of single nucleotide polymorphisms (SNPs), which ranged from 438 to 2664 in the motile G27 *clsC* recipients. The number of B128 alleles identified in the G27 *clsC* recipients ranged from 23 to 104. Motile variant mv49 was very different from the other motile variants in its genetic makeup as it contained 98 B128 alleles (2492 SNPs) that were not present in the other motile variants. In contrast, the other motile variants only possessed between 4 and 6 unique B128 alleles.

Only three B128 alleles (*kdsA*, *icfA* and *flgI*) were present in all seven motile variants. *kdsA* and *icfA* are adjacent genes located near the origin of replication. KdsA (3-deoxy-D-manno-octalosonicacid 8-phosphate synthetase) is part of the CMP-KDO biosynthetic pathway required for lipopolysaccharide biosynthesis, while IcfA is a β-carbonic anhydrase that catalyzes the reversible hydration of CO_2 to carbonic acid. *flgI* encodes the flagellar P ring protein and is located ~250 kb from *icfA*.

The coding regions of *kdsA*, *icfA* and *flgI* in the G27 *clsC* mutant were replaced with the corresponding regions from B128 to determine if any of the alleles restored flagellum biosynthesis in the G27 *clsC* mutant. Substitution of *kdsA* and *icfA* in the G27 *clsC* mutant with the B128 alleles failed to rescue motility (Fig. 2.8A) or flagellar biosynthesis (data not shown) in the G27 *clsC* mutant. The *icfA kdsA* locus is near the origin of replication and may be a recombination hotspot, which might have accounted for the presence of the B128 *kdsA* and *icfA* alleles in all seven of the motile variants. In contrast to *kdsA* and *icfA*, introducing the B128 *flgI* allele into the G27 *clsC* mutant restored motility (Fig. 2.8A) and flagellum biosynthesis (Fig. 2.8B), suggesting that the lesion in flagellum biosynthesis in the *H. pylori* G27 *clsC* mutant results, at least in part, from the failure to assemble the flagellar P ring.

Discussion

We show here that disrupting *clsC* in *H. pylori* G27 interferes with flagellum assembly, which is relieved by introducing the *flgI* allele from *H. pylori* B128. Disrupting *clsC* in *H. pylori* strains G27 and B128 resulted in reduced amount of total CL, as well as the apparent loss of specific CL species (Figs. 2.2 and 2.3A). The *clsC* mutants contains a single, predominant CL species, which we predict to be the monolysocardiolipin $C_{18:0}/C_{16:0}/C_{18:1}$ (Fig. 2.3B). Our data

suggest that assembly of the flagellar P ring in *H. pylori* G27 requires either specific CL species or high levels of CL, but the *H. pylori* B128 P ring protein is not constrained by these limitations. An intriguing question is what accounts for the differences between the G27 and B128 FlgI proteins that allows one to form the P ring in the *H. pylori* G27 *clsC* mutant but not the other? The G27 and B128 FlgI proteins differ at five amino acid positions, but only three of these differences (T140V, N151H and F216L) were identified in the *H. pylori* G27 *clsC* motile variants from the genome re-sequencing. One or more of these amino acid differences may affect the stability or transport of FlgI, or may influence interactions of the protein with itself or other proteins, which could account for the failure of the G27 FlgI protein to assemble the P ring in the absence of ClsC.

CL plays roles in the localization, oligomeric state and function of various membrane proteins (56-59), and it is possible that the lesion in flagellum assembly in the *H. pylori* G27 *clsC* mutant is due to interference in one or more of these roles. CL has a small glycerol head group and a large hydrophobic tail consisting of four acyl chains, which gives the molecule a conical shape that results in an intrinsic curvature (60). The shape of the CL molecule favors its localization in negatively curved regions of bacterial membranes, such as the cell poles and septa in rod-shaped bacteria (61-63). The preferential localization of CL to the cell pole presumably accounts for the polar localization of some proteins in *E. coli*, such as the osmotic stress protein ProP (59) and the CL synthase ClsA (58). While ProP and ClsA are inner membrane proteins, CL also has an apparent role in the polar localization of the outer membrane protein IcsA in *Shigella flexneri* (64), and is hypothesized to play a role in the localization or display of adhesion proteins in the outer membrane of *Moraxella catarrhalis* (65). It is possible that FlgI fails to localize to the cell pole in the absence of normal levels of CL or specific CL species in *H. pylori* G27. It is unlikely though that FlgI interacts directly with CL since FlgI is not associated with the inner or

outer membranes. Thus, if CL does affect localization of FlgI to the cell pole, then it is likely mediated through another protein that interacts directly with CL.

In *S.* Typhimurium, the Sec machinery transports FlgI into the periplasmic space where it assembles into the P ring surrounding flagellar rod (66, 67). The bacterial Sec system consists of the SecYEG protein channel complex and SecA ATPase, which work together to secrete preproteins across the cell membrane in a process that is powered by ATP hydrolysis and the proton motive force. The Sec machinery in *E. coli* requires CL for the efficient translocation of preproteins across the cell membrane (68). CL binds the SecYEG complex to stabilize formation of dimers, which creates a binding platform for SecA and stimulates ATP hydrolysis (69). Corey and co-workers identified two specific CL binding sites in SecYEG that potentiate the role of CL in ATPase and protein transport activity (56). It is possible that the G27 FlgI is not transported by the Sec machinery as efficiently as the B128 protein due to the reduced levels of CL or absence of specific CL species. The amino acid differences in B128 FlgI may overcome the CL deficiency in the *clsC* mutant by stabilizing the protein-translocation complex to facilitate assembly of the P ring and restore motility.

The first 19 amino acids of *E. coli* FlgI constitute a signal peptide that is cleaved by the Sec machinery as the protein is translocated across the cell membrane. Signal peptide prediction programs (e.g., SignalP-5.0 or Phobius) identify the first 19 amino acids of *H. pylori* FlgI as a signal peptide. The 120 amino acid residues at the N-terminus of the processed *E. coli* FlgI protein form a conserved region that is rich in glycine and proline residues, and has been suggested to have roles in stabilizing the protein or interacting with other FlgI monomers or other flagellar proteins (70). The corresponding region of *H. pylori* FlgI shares 55% identity and 75% similarity with that of *E. coli* FlgI and is similarly rich in glycine and proline residues. Two of the amino

acid positions where the G27 and B128 FlgI proteins differ (positions 140 and 151) are adjacent to the glycine-/proline-rich region, which could impact the function of this region. For example, the affinity of the G27 and B128 FlgI proteins for themselves or other interaction partners may differ as a result of the amino acid differences at position 140 or 151. In *Salmonella*, 26 copies of FlgI are predicted to assemble to form the P ring (71). In addition to interacting with itself, FlgI interacts strongly with FlgH, which forms the L ring. As is the case with FlgI, FlgH is transported into the periplasmic space by the Sec machinery (66, 67). FlgI may also interact with peptidoglycan, the flagellar rod proteins, the MotA/B stator complex, or other flagellar components found in the periplasmic space (70). If transport of FlgI and/or any of its interaction partners in the periplasmic space is impaired in the *clsC* mutant, the reduced levels of these proteins combined with the lower affinity of the G27 FlgI for itself or its interaction partners may account for its failure to assemble the P ring in the *clsC* mutant.

Another FlgI interaction partner is FlgA, which is predicted to be a chaperone that aids in P ring assembly by facilitating polymerization of FlgI (72). Although *flgA* is required for motility in *S.* Typhimurium under normal conditions, overproducing FlgI in a *flgA* mutant restores flagellum synthesis, indicating that FlgA plays an auxiliary role in assembly of the P ring (72). *H. pylori* strains possess an *flgA* homolog, although we are unaware of any report demonstrating the requirement of this gene for flagellum biosynthesis in *H. pylori*. *S.* Typhimurium FlgA is transported by the Sec machinery (72). Sec-dependent transport of FlgA may be inhibited in the *H. pylori* G27 *clsC* mutant, which could account for the failure of the P ring to assemble in this mutant. If the B128 FlgI protein has a higher affinity for itself and is less dependent on FlgA for assembling the P ring or has a higher affinity for FlgA, this might account for the ability of this protein to form the P ring in the presence of reduced amounts of FlgA. Future work in our lab will

attempt to understand the molecular basis for how the B128 FlgI protein is able to assemble the P ring in the *clsC* mutant.

Acknowledgements

We thank Abigail Courtney and Zachary Lewis for advice on analyzing the genome re-sequencing data. This work was supported by NIH grant AI140444 to T.R.H., NIH grants AI138576 and AI064184 to M.S.T., and NIH grants GM107629 and AI087946 to J.L.

Author Contributions

JC and TRH designed the research project and wrote the manuscript. Most of the experiments and data analysis were performed by JC. SZ and JL carried out the cryo-electron tomography studies. CMH and JCH assisted with the ^{32}P-labelling studies and mass spectrometry analysis of the *H. pylori* glycerophospholipids, and MST helped with the design of these experiments. MST, SZ and JL assisted in the writing of the manuscript.

Table 2.1: Primers and RT-qPCR primers used in this study.

Primer No.	Primer name	Sequence
M54	HP0190 up f	5’ - CCT AAC TTC TAG CTT TGA AAG C - 3’
M55	HP0190 up r	5’ - ATC CAC TTT TCA ATC TAT ATC ATC ATA AGA GAT AGG AGA GCT TG - 3’
M56	HP0190 down f	5’ - CCC AGT TTG TCG CAC TGA TAA ACT TCG CCT GAC ACT TCC TTC - 3’
M57	HP0190 down r	5’ - TTG CCA CTC GTT GGT TGC TAG - 3’
Cat5	cat5	5’ – GAT ATA GAT TGA AAA GTG GAT – 3’
Cat6	cat6	5’ – TTA TCA GTG CGA CAA ACT GGG – 3’
P069	Promoter F Comp pHel3	5’ – CCT CTA GAG TCG ACC TGC AGG CAT GGC TTT CTT TTA AAA GCG TTC G - 3’
P070	Promoter R Comp HP0190	5’ – GCT TAA AAG GAC TAA AAA GAT TTT CAA AAA AAC TGC TCC TAA AAA CTC AAA - 3’
P071	HP0190 F Comp Promoter	5’ – TTT GAG TTT TTA GGA GCA GTT TTT TTG AAA ATC TTT TTA GTC CTT TTA AGC – 3’
P072	HP0190 R Comp pHel3	5’ – GAG CTC GCG AAA GCT AGC TTG CAT GTT AAA GCT CTC TTT CAG GAA GG – 3’
P079	NheI *ureA* Promoter F	5’ – GCT AGC CAT GCG ATA GAG TTT GGC ATG – 3’
P080	*ureA* Promoter R	5’ – TTG TTT TGC AAA CTT TTT GAT GTT CAT CTT ATT CTC CTA TTC TTA AAG TGT TTT – 3’
P081	XhoI *kan* gene F	5’ – CTC GAG CCC GGC GAA CCA TTT GAT – 3’
P082	*sacB* gene R	5’ – AAA ACA CTT TAA GAA TAG GAG AAT AAG ATG AAC ATC AAA AAG TTT GCA AAA CAA – 3’
P165	*icfA* upstream F	5’ – AAT TCC TCT TCG CTA AAG – 3’
P166	*icfA* upstream R	5’ – CTC GAG GAT CGA ATC GCT AGC CTC TCA TAA AGC TCT TTA AGC – 3’
P167	*icfA* downstream F	5’ – GCT AGC GAT TCG ATC CTC GAG CAA TTC AGC AAC CAT TT – 3’
P168	*icfA* downstream R	5’ – CGG TTA GCC TTA TCA AA – 3’
P189	*icfA* upstream G27	5’ – TCC TAA AAA CGC TTC CAC TCT TTA ACC CTT AAA TCT CAT – 3’
P190	*icfA* allele from B128	5’ – ATG AGA TTT AAG GGT TAA AGA GTG GAA GCG TTT TTA GGA – 3’
P169	*flgI* US F	5’ – GGT TTT AGT CCT GGT GTG – 3’
P170	*flgI* US R	5’ – CTC GAG GAT CGA ATC GCT AGC CGC TAT ATC GCC TAT TTT TTC – 3’
P172	*flgI* DS R	5’ – AAT TCC TTT TCT ACC TTG TAG – 3’
P187	*flgI* DS F.1	5’ – GCT AGC GAT TCG ATC CTC GAG TTT GGC AAT AAA GTA GCC – 3’
P188	*flgI* DS R.1	5’ – TTC GCT CGC TAA TTT AGA – 3’
P191	G27 *flgI* US R	5’ – TCA AAC CCT TTC TTT ATT CC – 3’
P192	G27 *flgI* DS F	5’ – TAA ACA ACA ATA AAG CCA TG – 3’

P193	B128 *flgI* F	5’ – GGA ATA AAG AAA GGG TTT GAT TGA AAC GGG TGT TTT TAT – 3’
P194	B128 *flgI* R	5’ – CAT GGC TTT ATT GTT GTT TAT CAT AGT ATC TCC ATT TCA GC – 3’
qP007	*rpoD* F	5’ – CCC CAC TTC TTC AGC CAC CAC TTC – 3’
qP008	*rpoD* R	5’ – CCC GCA CTA TCC GCA TCC CTA TTC – 3’
qP009	*rpoA* F	5’ – ACA GGA GCA TAC CCC ACA GAG C – 3’
qP010	*rpoA* R	5’ – TGC TAG AGA AAG AGG GCA ATC GGG – 3’
qP013	*flhA* F	5’ – GGG GTG TGG GGT TTG ATT TTG GAG C – 3’
qP014	*flhA* R	5’ – GCA GGG AGG GAA AGG ACG GGT TGC – 3’
qP015	*fliF* F	5’ – CGT GCC TGG GGT TGT GAG CA – 3’
qP016	*fliF* R	5’ – TGC CAA ACT CGC CCT TAA TCT CGC T – 3’
qP017	*flaB* F	5’ – CCT TGA GCG GAA TGA AAG CCC ACA T – 3’
qP018	*flaB* R	5’ – GGA TTT CTG GGA CAC AAC ATG CGG T – 3’
qP019	*flgE* F	5’ – CGC TGT CTG AAG AAT ACC CGC TCA C – 3’
qP020	*flgE* R	5’ – CGG ACA ATT ACC AGG ACT CAG CCG – 3’
qP021	*flaA* F	5’ – AGT TCA GCA GGC ACA GGG ATC G – 3’
qP022	*flaA* R	5’ – TCG CTT GTG GTG ATA ACG CTC GC – 3’

Primer3 was used to design RT-qPCR primers. The production of a single PCR product from each primer set was confirmed using gDNA as a template. In addition, a melting curve analysis was done of the products synthesized by reverse transcription quantitative (RT-qPCR) to confirm that each product produced a single melting curve.

geNorm was used to calculate the M-values for each gene analyzed in the RT-qPCR assay and produce a pairwise plot to identify the minimum number of genes required for normalization. NormFinder was used to estimate the variation of gene expression within and between groups. The geomean for each gene was calculated utilizing the rankings from geNorm and NormFinder, which subsequently led to *rpoA* and *rpoD* being selected as the reference gene pair (citation for R and packages).

Table 2.2: Genes that are differentially regulated in the *H. pylori* G27 *clsC* mutant.

Locus tag	Gene	Upregulated genes Function	Log2	p-value
HPG27_RS04255	*flgE*	Flagellar hook protein	2.33	0.10
HPG27_RS00600	*flaB*	flagellin	2.23	0.13
HPG27_RS06175	*flgJ*	putative flagellar muraminidase	1.66	0.15
HPG27_RS05560	*flgK*	flagellar hook-associated protein	1.60	0.31
HPG27_RS01480	*flgL*	flagellar hook-associated protein	1.58	0.31
HPG27_RS06670		potential copper resistance determinant	1.93	$2.32e^{-06}$
HPG27_RS03510	*sabA*	outer membrane protein	1.51	0.02
HPG27_RS07220		LPP20 lipoprotein	1.59	$1.36e^{-15}$
HPG27_RS08135		hypothetical protein	1.72	0.36
Locus tag	**Gene**	**Downregulated genes Function**	**Log2**	**p-value**
HPG27_RS08290		pseudogene downstream of 16S rRNA gene	-3.75	$1.9e^{-04}$
HPG27_RS08195		hypothetical protein; potential pseudogenes	-3.37	$3.98e^{-109}$
HPG27_RS03555		50S ribosome-binding GTPase	-2.64	$1.63e^{-44}$
HPG27_RS05040		hypothetical protein	-2.29	0.01
HPG27_RS02975		hypothetical protein	-2.21	0.04
HPG27_RS02590		pseudogene in cag pathogenicity island	-2.14	$2.59e^{-05}$
HPG27_RS08070		pseudogene	-2.06	0.10
HPG27_RS02650	*cagB*	cag pathogenicity island protein B	-1.93	$7.74e^{-10}$

HPG27_RS08115	pseudogene	-1.93	0.001
HPG27_RS08230	pseudogene	-1.93	0.047
HPG27_RS04995	hypothetical protein	-1.85	0.18
HPG27_RS04305	hypothetical protein	-1.78	0.001
HPG27_RS02970	hypothetical protein	-1.75	0.008
HPG27_RS08300	pseudogene	-1.70	$4.98e^{-08}$
HPG27_RS05035	hypothetical protein	-1.58	0.062
HPG27_RS02345	hypothetical protein	-1.56	0.001
HPG27_RS08140	hypothetical protein	-1.51	0.26

Table 2.3: Strains and plasmids used in this study.

Strain	Relevant Genotype	Resistance	Source
H. pylori			
HP003	B128 wild-type		
HP004	G27 wild-type		
HP013	G27 *clsC*	Cat	This study
HP020	G27 pHel3	Kan	This study
HP025	G27 pHel3 p*clsC*	Kan	This study
HP027	G27 *clsC* pHel3 p*clsC*	Cat, Kan	This study
HP030	G27 *clsC* pHel3	Cat, Kan	This study
HP035	B128 *clsC*	Cat	This study
HP036	B128 pHel3 *clsC*	Cat, Kan	This study
HP037	B128 pHel3	Kan	This study
HP039	B128 *clsC* pHel3	Cat, Kan	This study
HP040	B128 *clsC* pHel3 *clsC*	Cat, Kan	This study
HP049	G27 *clsC* B128 gDNA	Cat	This study
HP050	G27 *clsC* B128 gDNA	Cat	This study
HP051	G27 *clsC* B128 gDNA	Cat	This study
HP065	G27 *clsC* B128 *clsC* gDNA	Cat	This study
HP070	G27 *clsC* B128 *clsC* gDNA	Cat	This study
HP076	G27 *clsC* B128 *clsC* gDNA	Cat	This study
HP077	G27 *clsC* B128 *clsC* gDNA	Cat	This study
HP138	G27 *clsC icfA*:*kan-sacB*	Cat, Kan	This study
HP146	G27 *clsC* B128 *icfA kdsA*	Cat	This study
HP147	G27 *clsC* B128 *icfA kdsA*	Cat	This study
HP148	G27 *clsC* B128 *icfA kdsA*	Cat	This study
HP152	G27 *clsC flgI*:*kan-sacB*	Cat, Kan	This study
HP164	G27 *clsC* B128 *flgI*	Cat	This study
HP168	G27 *clsC* B128 *flgI*	Cat	This study
HP169	G27 *clsC* B128 *flgI*	Cat	This study
Escherichia coli			
JC011	DH5α pHel3 p*clsC*	Kan	This study
JC042	DH5α pGEM-T Easy *clsC*:*cat*	Amp, Cat	This study
JC044	DH5α pHel3 p*clsC*	Kan	This study
JC053	DH5α pGEM-T Easy *kan-sacB*	Amp, Kan	This study
JC083	DH5α pGEM-T Easy *icfA*	Amp	This study
JC084	DH5α pGEM-T Easy *icfA*:*kan-sacB*	Amp, Kan	This study
JC089	DH5α pGEM-T Easy *flgI*	Amp	This study
JC090	DH5α pGEM-T Easy *icfA*	Amp	This study
JC092	DH5α pGEM-T Easy *flgI*:*kan-sacB*	Amp, Kan	This study
JC093	DH5α pGEM-T Easy *flgI*	Amp	This study

Plasmids	Relevant Genotype	Resistance	Source
pJC001	pHel3	Kan	
pJC030	pGEM-T Easy *clsC*:*cat*	Amp, Cat	This study
pJC032	pHel3 p*clsC*	Kan	This study
pJC038	pGEM-T Easy *kan-sacB*	Amp, Kan	This study
pJC068	pGEM-T Easy *icfA*	Amp	This study
pJC069	pGEM-T Easy *icfA*:*kan-sacB*	Amp, Kan	This study
pJC074	pGEM-T Easy *flgI*	Amp	This study
pJC075	pGEM-T Easy *icfA*	Amp	This study
pJC077	pGEM-T Easy *flgI*:*kan-sacB*	Amp, Kan	This study
pJC078	pGEM-T Easy *flgI*	Amp	This study

Table 2.4: Glycerophospholipid distribution of *H. pylori* strains.

	Wild-type		*clsC*		*clsC* pHel3		*clsC* pHel3 *clsC*	
	G27	B128	G27	B128	G27	B128	G27	B128
PE	68%	80%	87%	92%	87%	92%	69%	77%
CL	29%	17%	10%	4%	10%	4%	27%	20%
PG	2%	3%	3%	3%	3%	3%	3%	2%

The glycerophospholipid composition was determined using the Amershan Typhoon Scanner Control Software 2.0. Percentages represent the distribution for each glycerophospholipid isolated from whole cells.

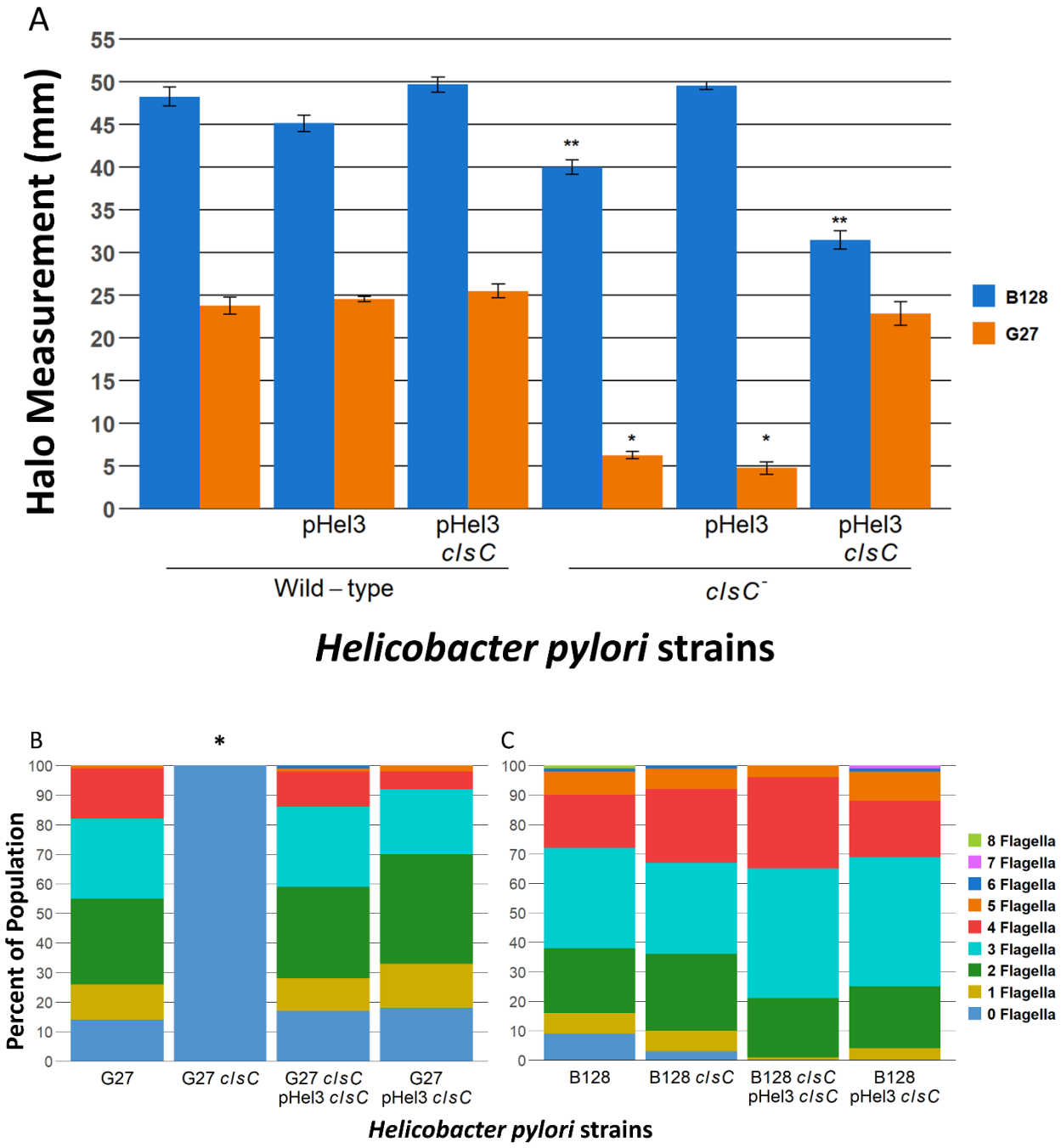

Figure 2.1: Effects of *clsC* knockouts on motility and number of flagella per cell in *H. pylori* G27 and B128. (A) Motility was assessed on soft agar medium. Measurements indicate the halo diameters surrounding the point of inoculation 7 d post-inoculation. Asterisks indicate values that were significantly different (p-value < 0.01) from that of the parental strain. Statistical significance

was determined using the two-sample *t* test. (B and C) The number of flagella per cell was determined by TEM following negative staining (n = 100 per strain). Asterisks indicate values that were significantly different from that of the parental strain (*p*-value < 0.05). Statistical significance was determined using the Mann-Whitney U test.

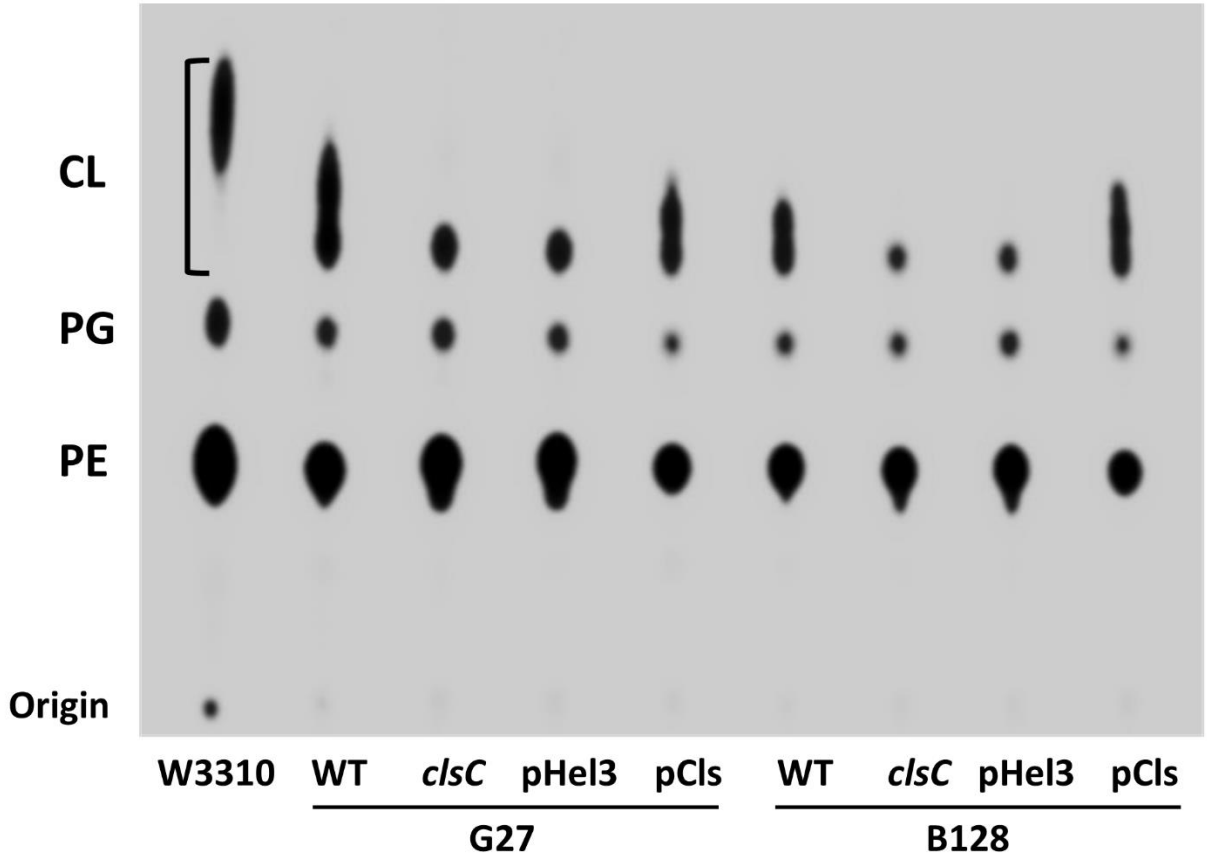

Figure 2.2: ClsC from *H. pylori* strains G27 and B128 is involved in CL synthesis. Radiolabeled glycerophospholipids from *E. coli* W3310 (lane 1; standard) and various *H. pylori* strains (lanes 2 through 9) were isolated and separated by TLC. Glycerophospholipids were separated in the following order (bottom to top): phosphatidylethanolamine (PE), phosphatidylglycerol (PG) and cardiolipin (CL). Wild-type strains of *H. pylori* G27 and B128 (lanes 2 and 6) displayed similar patterns for glycerophospholipid species with two unique spots for CL. The CL deficient strains (lanes 3 and 7) show a loss of the top CL spot in both strains. Introducing the complementing plasmid, but not the empty shuttle vector (lanes 4 and 8), in both mutants (lanes 5 and 9) recovers CL levels, indicated by the presence of the top CL spot for these strains.

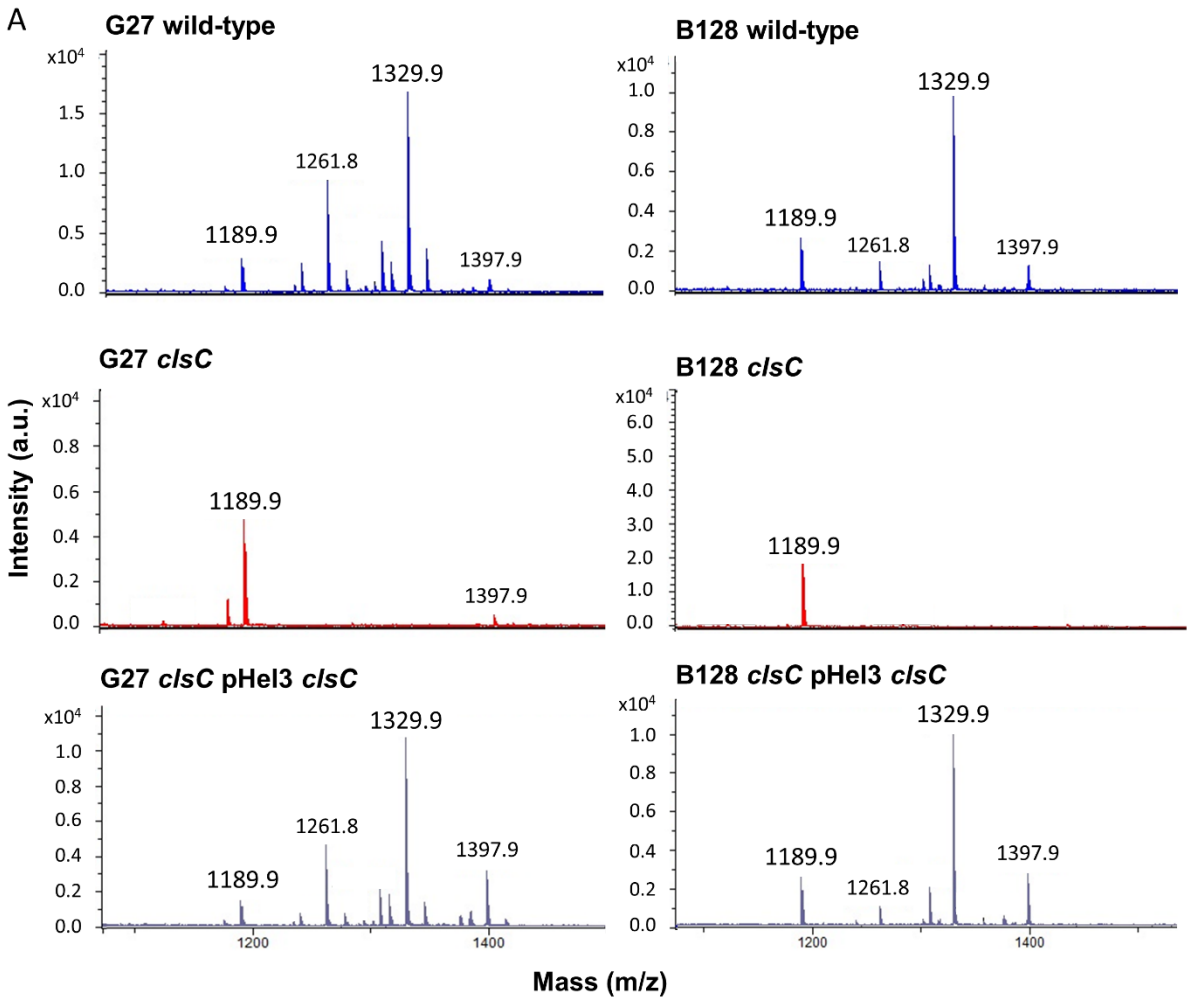

B

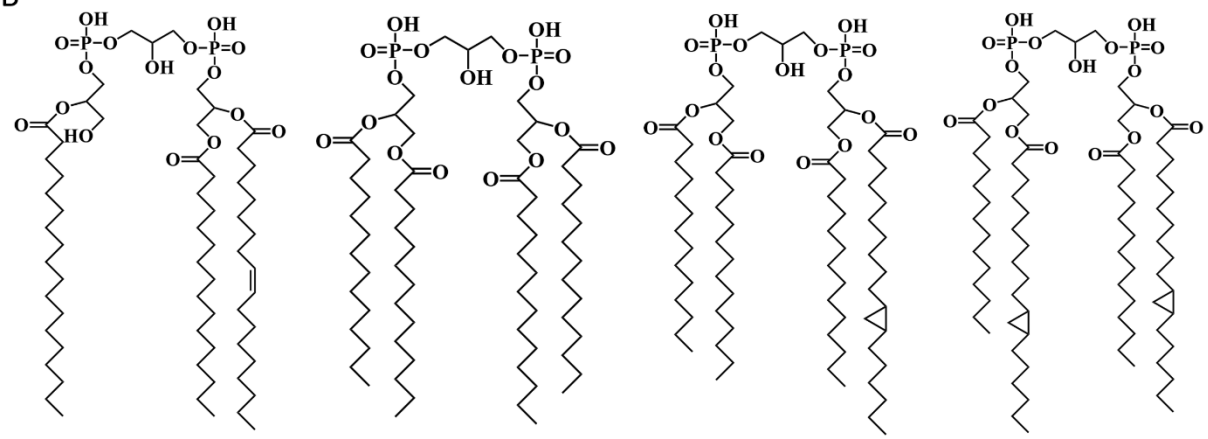

Exact mass: 1168.8
Na adduct: 1191.8

Exact mass: 1240.8
Na adduct: 1263.8

Exact mass: 1308.9
Na adduct: 1331.9

Exact mass: 1377.0
Na adduct: 1400.0

Figure 2.3: MALDI-TOF mass spectrometry of *clsC* mutants in *H. pylori* G27 and B128. (A) The wild-type and complemented strains produced peaks in the CL range of 1150 and 1400 *m/z* as reported for *H. pylori* (54). Samples from the wild-type and complemented strains displayed peaks with *m/z* values of 1189.9, 1261.8, 1329.9 and 1397.9. In contrast, the sample from the B128 *clsC* mutant only displayed a peak with a *m/z* value of 1189.9, while the G27 *clsC* mutant showed peaks with *m/z* values of 1189.9 and 1397.9. (B) Predicted structures for the cardiolipin species corresponding to the peaks from the mass spectrometry analysis.

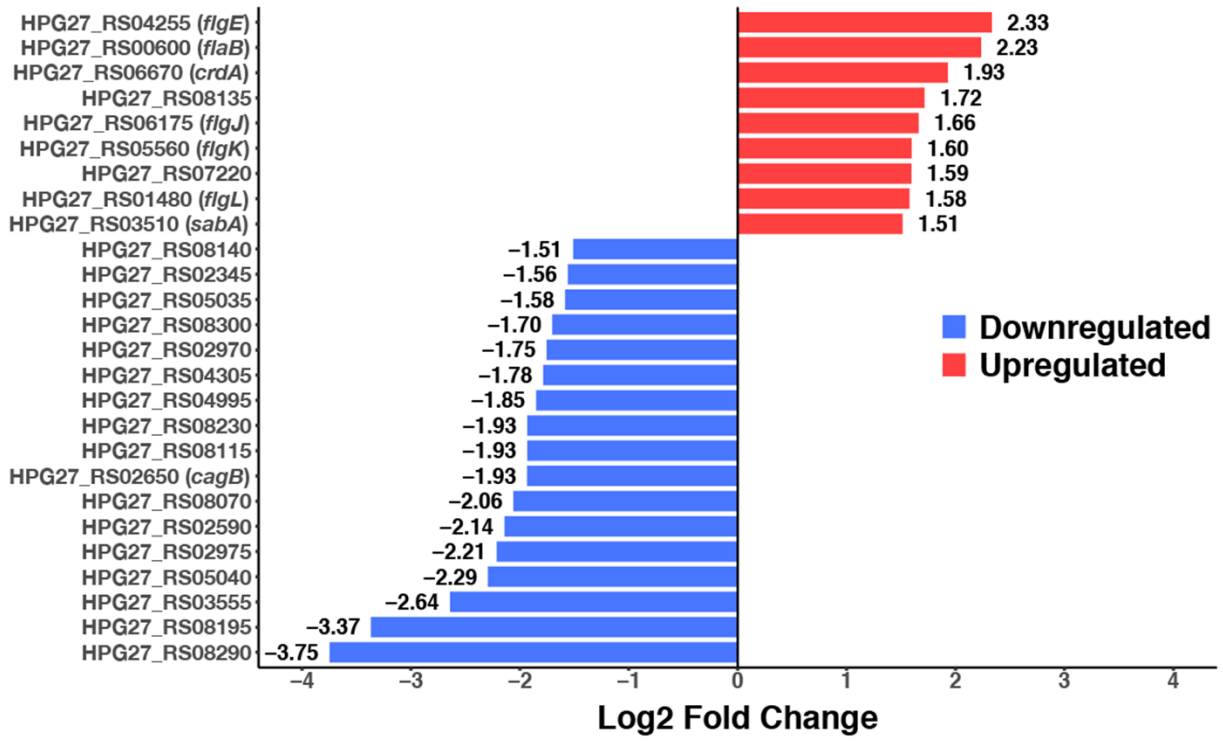

Figure 2.4: Genes identified in RNA-seq to be differentially regulated. Each bar represents a gene with a log2-fold change of ±1.5 in the G27 *clsC* mutant. Functions for the genes indicated are as follows: *flgE*, flagellar hook protein; *flaB*, minor flagellin B; *crdA*, copper resistance determinant; *flgJ*, predicted muramidase; *flgK*, flagellar hook-associated protein; *flgL*, flagellar hook-associated protein; *sabA*, outer membrane protein; and *cagB*, cag pathogenicity island protein B. The remaining genes either encode proteins of unknown function or are pseudogenes.

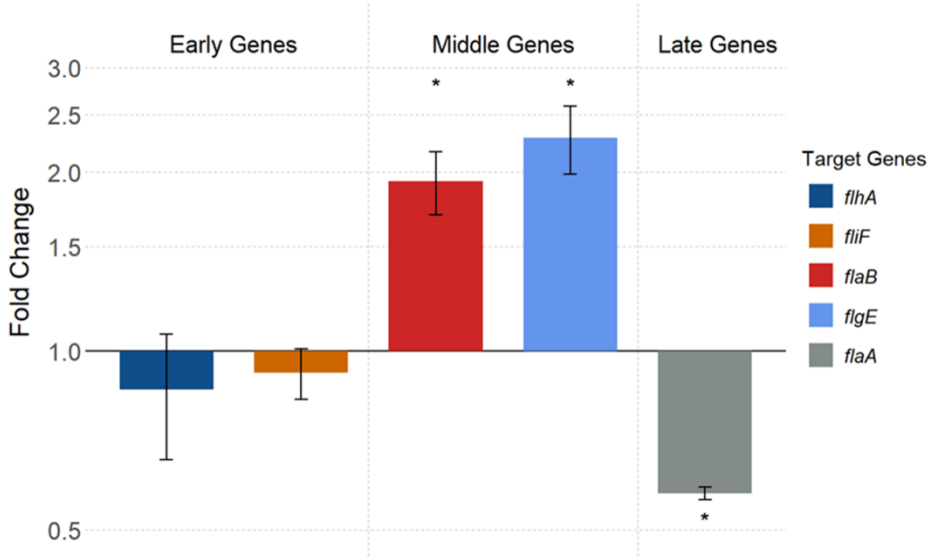

Figure 2.5: Expression levels of select flagellar genes as determined by RT-qPCR. Each bar indicates the mean fold-change for three biological replicates in a comparison of transcript levels of the target genes from the G27 *clsC* and the G27 wild-type strain. Fold-change values for all target genes were calculated using the ΔΔCt method (39) using *rpoA* and *rpoD* as reference genes. The asterisks indicate a statistically significant difference between the mutant and wild-type strains using the two-sample *t* test (p-value < 0.01).

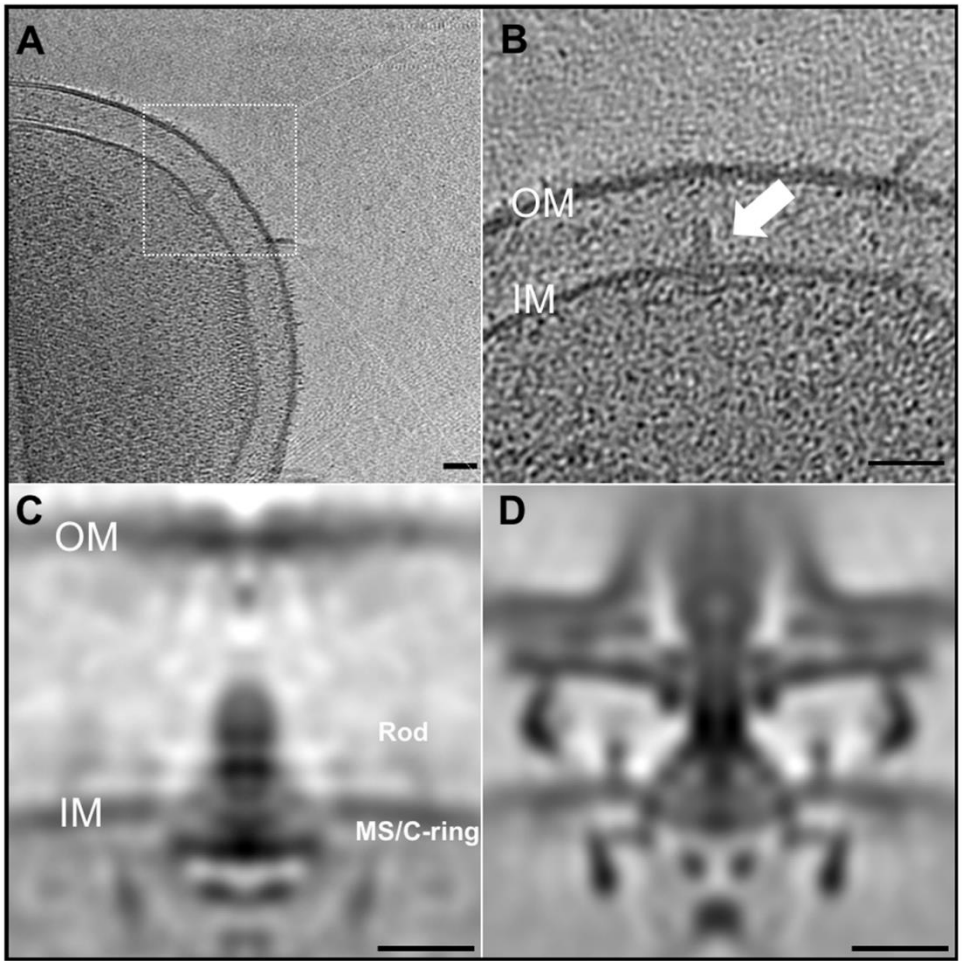

Figure 2.6: In-situ structure of the nascent flagellum from the *H. pylori* G27 *clsC* mutant. (A) A representative slice of a 3D reconstruction of *H. pylori* G27 *clsC*. (B) A zoom-in view showing MS/C-ring together with the partial rod density. (C) A central section slice of sub-tomogram averaged structure from *H. pylori* G27 *clsC*. (D) A central section slice from wild-type motor averaged structure. Bar in A and B is 50 nm; in C and D is 20 nm. OM, outer membrane, IM, inner membrane.

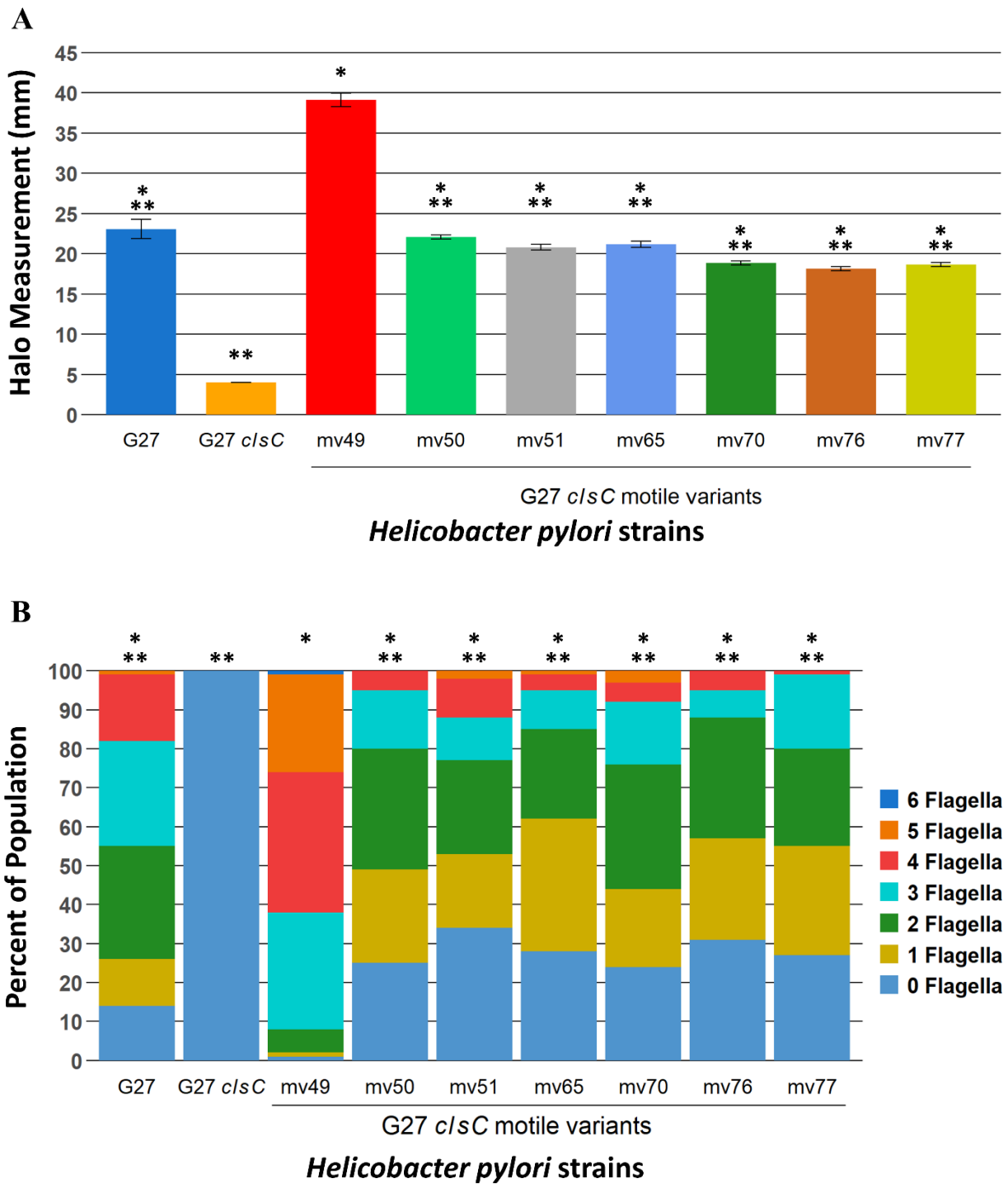

Figure 2.7: Motility and number of flagella per cell for the G27 *clsC* motile variants isolated following allelic exchange mutagenesis. (A) Motility was assessed on soft agar medium. Measurements indicate the halo diameters surrounding the point of inoculation 7 d post-

inoculation. Statistical significance was determined using the two-sample *t* test. (B) The number of flagella per cell was assessed by TEM after negative staining (n = 100 per strain). Statistical significance was determined using the Mann-Whitney U test. For both panels, the ***** indicates a strain is statistically different compared to the *H. pylori* G27 *clsC* parental strain (*p*-value < 0.01) and the ****** indicates a strain is statistically different compared to the motile variant mv49 (*p*-value < 0.01).

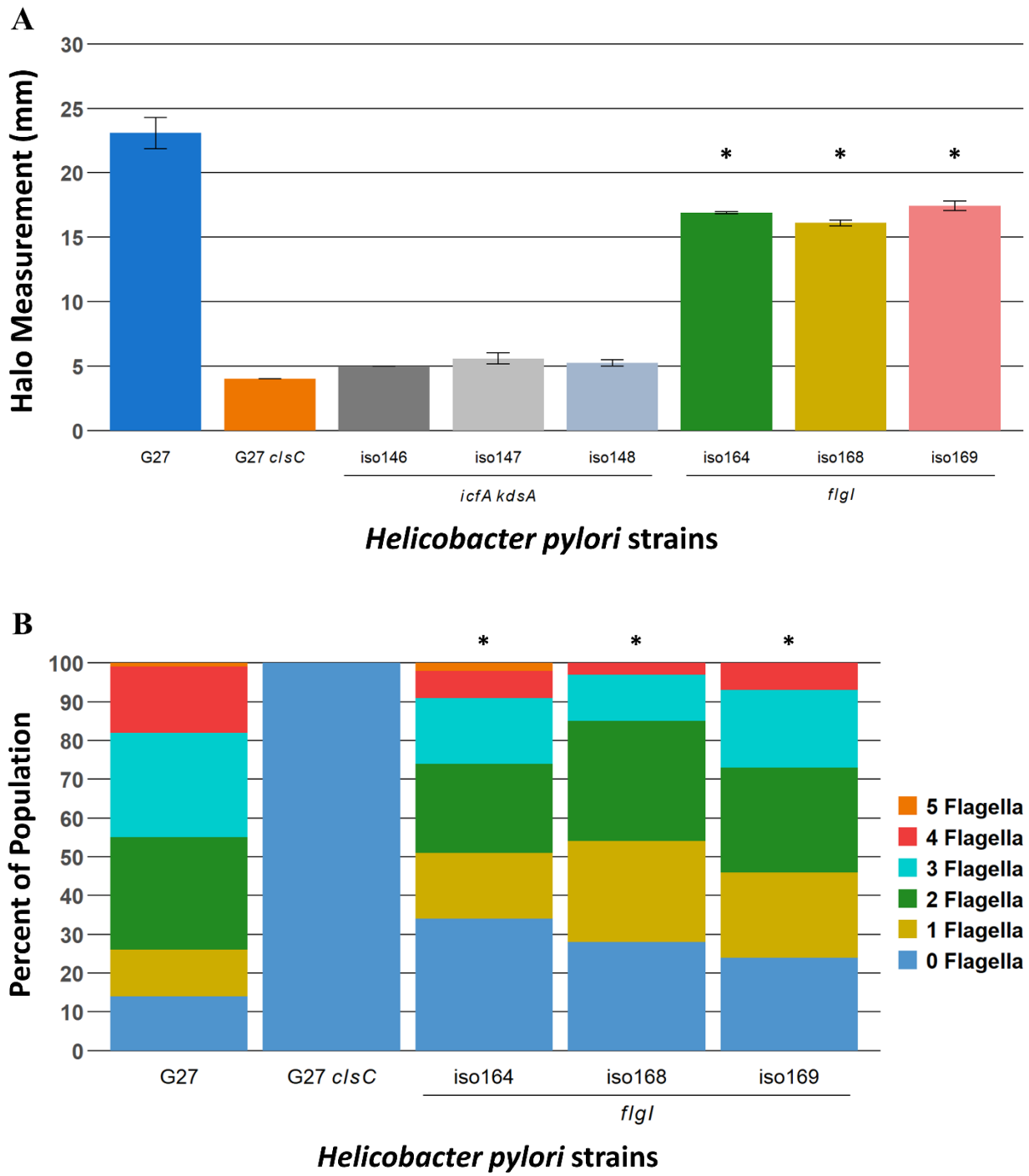

Figure 2.8: Motility and flagella count results for the G27 *clsC* mutant strains in which specific B128 alleles were introduced. (A) Motility was assessed on soft agar medium. Measurements indicate the halo size surrounding the point of inoculation after 7 d. The G27 wild-type and G27 *clsC* strains are used as references. Three isolates of the G27 *clsC* mutant in which

the B128 *icfA* and *kdsA* alleles (iso146, iso147 and iso148) or the B128 *flgI* allele (iso164, iso168 and iso169) had been introduced were examined in the motility assay. Statistical significance was determined using the two-sample *t* test. (B) The number of flagella per cell was assessed by TEM after negative staining (n = 100 per strain). Statistical significance was determined using the Mann-Whitney U test. The ***** indicates a statistically significant difference in the number of flagella per cell for the G27 *clsC* mutants bearing the B128 *flgI* allele (iso164, iso168 and iso169) compared to the G27 *clsC* parental strain (p-value < 0.01).

References

1. **Amieva MR**, **El-Omar EM**. 2008. Host-bacterial interactions in *Helicobacter pylori* infection. Gastroenterology. **134**:306-23. https://www.ncbi.nlm.nih.gov/pubmed/18166359.
2. **Atherton JC**, **Blaser MJ**. 2009. Coadaptation of *Helicobacter pylori* and humans: ancient history, modern implications. The Journal of Clinical Investigation. **119**:2475-2487. https://www.ncbi.nlm.nih.gov/pubmed/19729845.
3. **Blaser MJ**. 1993. *Helicobacter pylori*: microbiology of a 'slow' bacterial infection. Trends in Microbiology. **1**:255-260. https://www.ncbi.nlm.nih.gov/pubmed/8162405.
4. **Cover TL**, **Blaser MJ**. 1992. *Helicobacter pylori* and gastroduodenal disease. Annual Review of Medicine. **43**:135-145. https://www.ncbi.nlm.nih.gov/pubmed/1580578.
5. **Kuipers EJ**. 1997. *Helicobacter pylori* and the risk and management of associated diseases: gastritis, ulcer disease, atrophic gastritis and gastric cancer. Alimentary Pharmacology & Therapeutics. **1**:71-88. https://www.ncbi.nlm.nih.gov/pubmed/9146793.
6. **Eaton KA**, **Morgan DR**, **Krakowka S**. 1992. Motility as a factor in the colonisation of gnotobiotic piglets by *Helicobacter pylori.* Journal of Medical Microbiology. **37**:123-127. https://www.ncbi.nlm.nih.gov/pubmed/1629897.
7. **Ottemann KM**, **Lowenthal AC**. 2002. *Helicobacter pylori* uses motility for initial colonization and to attain robust infection. Infection and Immunity. **70**:1984-90. https://www.ncbi.nlm.nih.gov/pubmed/11895962.
8. **Berg HC**. 2003. The rotary motor of bacterial flagella. Annual Review of Biochemistry. **72**:19-54. https://www.ncbi.nlm.nih.gov/pubmed/12500982.
9. **Chevance FFV**, **Hughes KT**. 2008. Coordinating assembly of a bacterial macromolecular machine. Nature Reviews Microbiology. **6**:455-465. https://www.ncbi.nlm.nih.gov/pubmed/18483484.
10. **Macnab RM**. 2003. How bacteria assemble flagella. Annual Review of Microbiology. **57**:77-100. https://www.ncbi.nlm.nih.gov/pubmed/12730325.
11. **Manson MD**, **Tedesco P**, **Berg HC**, **Harold FM**, **Van der Drift C**. 1977. A protonmotive force drives bacterial flagella. Proceedings of the National Academy of Sciences. **74**:3060-3064. https://www.ncbi.nlm.nih.gov/pubmed/19741.
12. **Irikura VM**, **Kihara M**, **Yamaguchi S**, **Sockett H**, **Macnab RM**. 1993. *Salmonella typhimurium fliG* and *fliN* mutations causing defects in assembly, rotation, and switching of the flagellar motor. Journal of Bacteriology. **175**:802-10. https://www.ncbi.nlm.nih.gov/pubmed/8423152.
13. **Yamaguchi S**, **Aizawa S**, **Kihara M**, **Isomura M**, **Jones CJ**, **Macnab RM**. 1986. Genetic evidence for a switching and energy-transducing complex in the flagellar motor of *Salmonella typhimurium*. Journal of Bacteriology. **168**:1172-1179. https://www.ncbi.nlm.nih.gov/pubmed/3536867.
14. **Qin Z**, **Lin WT**, **Zhu S**, **Franco AT**, **Liu J**. 2017. Imaging the motility and chemotaxis machineries in *Helicobacter pylori* by cryo-electron tomography. Journal of Bacteriology. **199**:e00695-16. https://www.ncbi.nlm.nih.gov/pubmed/?term=27849173.
15. **Niehus E**, **Gressmann H**, **Ye F**, **Schlapbach R**, **Dehio M**, **Dehio C**, **Stack A**, **Meyer TF**, **Suerbaum S**, **Josenhans C**. 2004. Genome-wide analysis of transcriptional hierarchy and feedback regulation in the flagellar system of *Helicobacter pylori*. Molecular Microbiology. **52**:947-961. https://www.ncbi.nlm.nih.gov/pubmed/15130117.

16. **Spohn G**, **Scarlato V**. 1999. Motility of *Helicobacter pylori* is coordinately regulated by the transcriptional activator FlgR, an NtrC homolog. Journal of Bacteriology. **181**:593-599. https://www.ncbi.nlm.nih.gov/pubmed/9882675.
17. **Smith TG**, **Hoover TR**. 2009. Deciphering bacterial flagellar gene regulatory networks in the genomic era. Advances in Applied Microbiology. **67**:257-295. https://www.ncbi.nlm.nih.gov/pubmed/19245942.
18. **Beier D**, **Frank R**. 2000. Molecular characterization of two-component systems of *Helicobacter pylori*. Journal of Bacteriology. **182**:2068-2076. https://www.ncbi.nlm.nih.gov/pubmed/10735847.
19. **Brahmachary P**, **Dashti MG**, **Olson JW**, **Hoover TR**. 2004. *Helicobacter pylori* FlgR is an enhancer-independent activator of σ^{54}-RNA polymerase holoenzyme. Journal of Bacteriology. **186**:4535-4542. https://www.ncbi.nlm.nih.gov/pubmed/15231786.
20. **Allan E**, **Dorrell N**, **Foynes S**, **Anyim M**, **Wren BW**. 2000. Mutational analysis of genes encoding the early flagellar components of *Helicobacter pylori*: evidence for transcriptional regulation of flagellin A biosynthesis. Journal of Bacteriology. **182**:5274-5277. https://www.ncbi.nlm.nih.gov/pubmed/10960117.
21. **Schmitz A**, **Josenhans C**, **Suerbaum S**. 1997. Cloning and characterization of the *Helicobacter pylori flbA* gene, which codes for a membrane protein involved in coordinated expression of flagellar genes. Journal of Bacteriology. **179**:987-997. https://www.ncbi.nlm.nih.gov/pubmed/9023175.
22. **Smith TG**, **Pereira L**, **Hoover TR**. 2009. *Helicobacter pylori* FlhB processing-deficient variants affect flagellar assembly but not flagellar gene expression. Microbiology. **155**:1170-1180. https://www.ncbi.nlm.nih.gov/pubmed/19332819.
23. **Tsang J**, **Hoover TR**. 2014. Requirement of the flagellar protein export apparatus component FliO for optimal expression of flagellar genes in *Helicobacter pylori*. Journal of Bacteriology. **196**:2709-17. https://www.ncbi.nlm.nih.gov/pubmed/24837287.
24. **Tsang J**, **Smith TG**, **Pereira LE**, **Hoover TR**. 2013. Insertion mutations in *Helicobacter pylori flhA* reveal strain differences in RpoN-dependent gene expression. Microbiology. **159**:58-67. https://www.ncbi.nlm.nih.gov/pubmed/23154969.
25. **Tsang J**, **Hirano T**, **Hoover TR**, **McMurry JL**. 2015. *Helicobacter pylori* FlhA binds the sensor kinase and flagellar gene regulatory protein FlgS with high affinity. Journal of Bacteriology. **197**:1886-1892. https://www.ncbi.nlm.nih.gov/pubmed/25802298.
26. **Colland F**, **Rain JC**, **Gounon P**, **Labigne A**, **Legrain P**, **De Reuse H**. 2001. Identification of the *Helicobacter pylori* anti-σ^{28} factor. Molecular Microbiology. **41**:477-487. https://www.ncbi.nlm.nih.gov/pubmed/11489132.
27. **Josenhans C**, **Niehus E**, **Amersbach S**, **Hörster A**, **Betz C**, **Drescher B**, **Hughes KT**, **Suerbaum S**. 2002. Functional characterization of the antagonistic flagellar late regulators FliA and FlgM of *Helicobacter pylori* and their effects on the *H. pylori* transcriptome. Molecular Microbiology. **43**:307-322. https://www.ncbi.nlm.nih.gov/pubmed/11985711.
28. **Hughes KT**, **Gillen KL**, **Semon MJ**, **Karlinsey JE**. 1993. Sensing structural intermediates in bacterial flagellar assembly by export of a negative regulator. Science. **262**:1277-1280. https://www.ncbi.nlm.nih.gov/pubmed/8235660.

29. **Rust M**, **Borchert S**, **Niehus E**, **Kuehne SA**, **Gripp E**, **Bajceta A**, **McMurry JL**, **Suerbaum S**, **Hughes KT**, **Josenhans C**. 2009. The *Helicobacter pylori* anti-sigma factor FlgM is predominantly cytoplasmic and cooperates with the flagellar basal body protein FlhA. Journal of Bacteriology. **191**:4824-4834. https://www.ncbi.nlm.nih.gov/pubmed/19465658.
30. **Romantsov T**, **Battle AR**, **Hendel JL**, **Martinac B**, **Wood JM**. 2010. Protein localization in *Escherichia coli* cells: comparison of the cytoplasmic membrane proteins ProP, LacY, ProW, AqpZ, MscS, and MscL. Journal of Bacteriology. **192**:912-924. https://www.ncbi.nlm.nih.gov/pubmed/20008071.
31. **Wang Y**, **Taylor DE**. 1990. Chloramphenicol resistance in *Campylobacter coli*: nucleotide sequence, expression, and cloning vector construction. Gene. **94**:23-28. https://www.ncbi.nlm.nih.gov/pubmed/2227449.
32. **Heuermann D**, **Haas R**. 1998. A stable shuttle vector system for effecient genetic complementation of *Helicobacter pylori* strains by transformation and conjugation. Mol Gen Genet. **257**:519-528. https://www.ncbi.nlm.nih.gov/pubmed/9563837.
33. **Li MZ**, **Elledge SJ**. 2012. SLIC: a method for sequence- and ligation-independent cloning. Methods Mol Biol. **852**:51-59. https://www.ncbi.nlm.nih.gov/pubmed/22328425.
34. **Aranda PS**, **LaJoie DM**, **Jorcyk CL**. 2012. Bleach gel: a simple agarose gel for analyzing RNA quality. Electrophoresis. **33**:366-369. https://www.ncbi.nlm.nih.gov/pubmed/22222980.
35. **Andrews S**. 2010. FastQC: a quality control tool for high throughput sequence data.
36. **Bolger AM**, **Lohse M**, **Usadel B**. 2014. Trimmomatic: a flexible trimmer for Illumina sequence data. *Bioinformatics*. **30**:2114-2120. https://www.ncbi.nlm.nih.gov/pubmed/24695404.
37. **Love MI**, **Huber W**, **Anders S**. 2014. Moderated estimation of fold change and dispersion for RNA-seq data with DESeq2. Genome Biology. **15**:550. https://www.ncbi.nlm.nih.gov/pubmed/25516281.
38. **Tsang J**, **Hoover TR**. 2015. Basal body structures differentially affect transcription of RpoN- and FliA-dependent flagellar genes in *Helicobacter pylori*. Journal of Bacteriology. **197**:1921-1930. https://www.ncbi.nlm.nih.gov/pubmed/25825427.
39. **Schmittgen TD**, **Livak KJ**. 2008. Analyzing real-time PCR data by the comparative CT method. Nature Protocols. **3**:1101-1108. https://www.ncbi.nlm.nih.gov/pubmed/18546601.
40. **Copass M**, **Grandi G**, **Rappuoli R**. 1997. Introduction of unmarked mutations in the *Helicobacter pylori vacA* gene with a sucrose sensitivity marker. Infection and Immunity. **65**:1949-1952. https://www.ncbi.nlm.nih.gov/pubmed/9125586.
41. **Henderson JC**, **Herrera CM**, **Trent MS**. **2017**. AlmG, responsible for polymyxin resistance in pandemic *Vibrio cholerae*, is a glycyltransferase distantly related to lipid A late acyltransferases. Journal of Biological Chemistry. **292**:21205-21215. https://www.ncbi.nlm.nih.gov/pubmed/29101229.
42. **Zhu S**, **Qin Z**, **Wang J**, **Morado DR**, **Liu J**. 2017. In situ structural analysis of the spirochetal flagellar motor by cryo-electron tomography. Methods Mol Biol. **1593**:229-242. https://www.ncbi.nlm.nih.gov/pubmed/28389958.

43. **Mastronarde DN**. 2005. Automated electron microscope tomography using robust prediction of specimen movements. Journal of Structural Biology. **152**:36-51. https://www.ncbi.nlm.nih.gov/pubmed/16182563.
44. **Li X**, **Mooney P**, **Zheng S**, **Booth CR**, **Braunfeld MB**, **Gubbens S**, **Agard DA**, **Cheng Y**. 2013. Electron counting and beam-induced motion correction enable near-atomic-resolution single-particle cryo-EM. Nature Methods. **10**:584-590. https://www.ncbi.nlm.nih.gov/pubmed/23644547.
45. **Morado DR**, **Hu B**, **Liu J**. 2016. Using Tomoauto: a protocol for high-throughput automated cryo-electron tomography. Journal of Visualized Experiments.e53608-e53608. https://www.ncbi.nlm.nih.gov/pubmed/26863591.
46. **Zheng SQ**, **Palovcak E**, **Armache J-P**, **Verba KA**, **Cheng Y**, **Agard DA**. 2017. MotionCor2: anisotropic correction of beam-induced motion for improved cryo-electron microscopy. Nature Methods. **14**:331-332. https://www.ncbi.nlm.nih.gov/pubmed/28250466.
47. **Agulleiro JI**, **Fernandez JJ**. 2015. Tomo3D 2.0 – exploitation of advanced vector eXtensions (AVX) for 3D reconstruction. Journal of Structural Biology. **189**:147-152. https://www.ncbi.nlm.nih.gov/pubmed/25528570.
48. **Kremer JR**, **Mastronarde DN**, **McIntosh JR**. 1996. Computer visualization of three-dimensional image data using IMOD. Journal of Structural Biology. **116**:71-76. https://www.ncbi.nlm.nih.gov/pubmed/8742726.
49. **Winkler H**. 2007. 3D reconstruction and processing of volumetric data in cryo-electron tomography. Journal of Structural Biology. **157**:126-137. https://www.ncbi.nlm.nih.gov/pubmed/16973379.
50. **Winkler H**, **Zhu P**, **Liu J**, **Ye F**, **Roux KH**, **Taylor KA**. 2009. Tomographic subvolume alignment and subvolume classification applied to myosin V and SIV envelope spikes. Journal of Structural Biology. **165**:64-77. https://www.ncbi.nlm.nih.gov/pubmed/19032983.
51. **Selvy PE**, **Lavieri RR**, **Lindsley CW**, **Brown HA**. 2011. Phospholipase D - enzymology, functionality, and chemical modulation. Chemical Reviews. **111**:6064-6119. https://www.ncbi.nlm.nih.gov/pubmed/21936578.
52. **Farnbacher M**, **Jahns T**, **Willrodt D**, **Daniel R**, **Haas R**, **Goesmann A**, **Kurtz S**, **Rieder G**. 2010. Sequencing, annotation, and comparative genome analysis of the gerbil-adapted *Helicobacter pylori* strain B8. BMC Genomics. **11**:335. https://www.ncbi.nlm.nih.gov/pubmed/20507619.
53. **Hirai Y**, **Haque M**, **Yoshida T**, **Yokota K**, **Yasuda T**, **Oguma K**. 1995. Unique cholesteryl glucosides in *Helicobacter pylori*: composition and structural analysis. Journal of Bacteriology. **177**:5327-5333. https://www.ncbi.nlm.nih.gov/pubmed/7665522.
54. **Zhou P**, **Hu R**, **Chandan V**, **KuoLee R**, **Liu X**, **Chen W**, **Liu B**, **Altman E**, **Li J**. 2012. Simultaneous analysis of cardiolipin and lipid A from *Helicobacter pylori* by matrix-assisted laser desorption/ionization time-of-flight mass spectrometry. Molecular BioSystems. **8**:720-725. https://www.ncbi.nlm.nih.gov/pubmed/22266632.
55. **Porwollik S**, **Noonan B**, **O'Toole PW**. 1999. Molecular characterization of a flagellar export locus of *Helicobacter pylori*. Infection and Immunity. **67**:2060-2070. https://www.ncbi.nlm.nih.gov/pubmed/10225855.

56. **Corey RA**, **Pyle E**, **Allen WJ**, **Watkins DW**, **Casiraghi M**, **Miroux B**, **Arechaga I**, **Politis A**, **Collinson I**. 2018. Specific cardiolipin-SecY interactions are required for proton-motive force stimulation of protein secretion. Proceedings of the National Academy of Sciences. **115**:7967-7972. https://www.ncbi.nlm.nih.gov/pubmed/30012626.
57. **Gupta K**, **Donlan JAC**, **Hopper JTS**, **Uzdavinys P**, **Landreh M**, **Struwe WB**, **Drew D**, **Baldwin AJ**, **Stansfeld PJ**, **Robinson CV**. 2017. The role of interfacial lipids in stabilizing membrane protein oligomers. Nature. **541**:421-424. https://www.ncbi.nlm.nih.gov/pubmed/28077870.
58. **Romantsov T**, **Gonzalez K**, **Sahtout N**, **Culham DE**, **Coumoundouros C**, **Garner J**, **Kerr CH**, **Chang L**, **Turner RJ**, **Wood JM**. 2018. Cardiolipin synthase A colocalizes with cardiolipin and osmosensing transporter ProP at the poles of *Escherichia coli* cells. Molecular Microbiology. **107**:623-638. https://www.ncbi.nlm.nih.gov/pubmed/29280215.
59. **Romantsov T**, **Helbig S**, **Culham DE**, **Gill C**, **Stalker L**, **Wood JM**. 2007. Cardiolipin promotes polar localization of osmosensory transporter ProP in *Escherichia coli*. Molecular Microbiology. **64**:1455-1465. https://www.ncbi.nlm.nih.gov/pubmed/17504273.
60. **Huang KC**, **Ramamurthi KS**. 2010. Macromolecules that prefer their membranes curvy. Molecular Microbiology. **76**:822-832. https://www.ncbi.nlm.nih.gov/pubmed/20444099.
61. **Bernal P**, **Muñoz-Rojas J**, **Hurtado A**, **Ramos JL**, **Segura A**. 2007. A *Pseudomonas putida* cardiolipin synthesis mutant exhibits increased sensitivity to drugs related to transport functionality. Environmental Microbiology. **9**:1135-1145. https://www.ncbi.nlm.nih.gov/pubmed/17472630.
62. **Kawai F**, **Shoda M**, **Harashima R**, **Sadaie Y**, **Hara H**, **Matsumoto K**. 2004. Cardiolipin domains in *Bacillus subtilis* marburg membranes. Journal of Bacteriology. **186**:1475-1483. https://www.ncbi.nlm.nih.gov/pubmed/14973018.
63. **Mileykovskaya E**, **Dowhan W**. 2000. Visualization of phospholipid domains in *Escherichia coli* by using the cardiolipin-specific fluorescent dye 10-N-nonyl acridine orange. Journal of Bacteriology. **182**:1172-1175. https://www.ncbi.nlm.nih.gov/pubmed/10648548.
64. **Rossi RM**, **Yum L**, **Agaisse H**, **Payne SM**. 2017. Cardiolipin synthesis and outer membrane localization are required for *Shigella flexneri* virulence. mBio. **8**:e01199-01217. https://www.ncbi.nlm.nih.gov/pubmed/28851846.
65. **Buskirk SW**, **Lafontaine ER**. 2014. *Moraxella catarrhalis* expresses a cardiolipin synthase that impacts adherence to human epithelial cells. Journal of Bacteriology. **196**:107-120. https://www.ncbi.nlm.nih.gov/pubmed/24142255.
66. **Homma M**, **Komeda Y**, **Iino T**, **Macnab RM**. 1987. The *flaFIX* gene product of *Salmonella typhimurium* is a flagellar basal body component with a signal peptide for export. Journal of Bacteriology. **169**:1493-1498. https://www.ncbi.nlm.nih.gov/pubmed/3549691.
67. **Jones CJ**, **Homma M**, **Macnab RM**. 1989. L-, P-, and M-ring proteins of the flagellar basal body of *Salmonella typhimurium*: gene sequences and deduced protein sequences. Journal of Bacteriology. **171**:3890-3900. https://www.ncbi.nlm.nih.gov/pubmed/2544561.

68. **de Vrije T**, **de Swart RL**, **Dowhan W**, **Tommassen J**, **de Kruijff B**. 1988. Phosphatidylglycerol is involved in protein translocation across *Escherichia coli* inner membranes. Nature. **334**:173-175. https://www.ncbi.nlm.nih.gov/pubmed/3290692.
69. **Gold VAM**, **Robson A**, **Bao H**, **Romantsov T**, **Duong F**, **Collinson I**. 2010. The action of cardiolipin on the bacterial translocon. Proceedings of the National Academy of Sciences. **107**:10044-10049. https://www.ncbi.nlm.nih.gov/pubmed/20479269.
70. **Hizukuri Y**, **Kojima S**, **Yakushi T**, **Kawagishi I**, **Homma M**. 2008. Systematic Cys mutagenesis of FlgI, the flagellar P-ring component of *Escherichia coli.* Microbiology. **154**:810-817. https://www.ncbi.nlm.nih.gov/pubmed/18310027.
71. **Jones CJ**, **Macnab RM**, **Okino H**, **Aizawa S**. 1990. Stoichiometric analysis of the flagellar hook-(basal-body) complex of *Salmonella typhimurium.* Journal of Molecular Biology. **212**:377-387. https://www.ncbi.nlm.nih.gov/pubmed/2181149.
72. **Nambu T**, **Kutsukake K**. 2000. The *Salmonella* FlgA protein, a putative periplasmic chaperone essential for flagellar P ring formation. Microbiology. **146**:1171-1178. https://www.ncbi.nlm.nih.gov/pubmed/10832645.

CHAPTER 3

CHARACTERIZING A PUTATIVE CARDIOLIPIN TRANSPORT SYSTEM REQUIRED FOR FLAGELLUM BIOSYNTHESIS[1]

[1]**Chu, J., S. Zhu, J. Liu, J. Mrázek and T. R. Hoover**.
To be submitted to *Journal of Bacteriology*.

Abstract

Helicobacter pylori uses a cluster of polar, sheathed flagella for motility, which it requires for colonization of the human stomach epithelial cells. The function of sheathed flagella is unknown for any bacterial species. As part of a study to identify proteins required for the function and/or biogenesis of the flagellar sheath, we identified an operon that encodes a putative efflux pump that we hypothesized to be required for flagellar sheath biosynthesis. Deleting the genes that encode the efflux pump proteins in *H. pylori* B128 resulted in decreased motility and number of flagella per cell. During the construction of the *H. pylori* B128 HP1488:*kan-sacB* strain, the motilities of the individual isolates ranged from motility impaired ('RM') to highly motile ('M'). Cryo-electron tomography revealed part of a cage-like structure uniquely associated with the flagellar basal body of *H. pylori* is absent in the 'RM' isolate. Genome re-sequencing of the 'RM' and 'M' isolates identified a single-nucleotide polymorphism in the *mreC* gene from the 'M' isolate that substitutes a tyrosine for a histidine at position 220 ($MreC^{Y220H}$). The *mreC* gene encodes a protein that forms a complex with MreB and MreD in *Escherichia coli* and is responsible for the maintenance of rod-shaped cells. In *Caulobacter crescentus*, the MreC protein interacts with outer membrane proteins and may support membrane stability. *H. pylori* lacks an MreD homolog, which suggests the *H. pylori* MreC protein participates in a more central role in maintaining the rod shape membrane stability of cells. Disrupting HP1488 may have resulted in a membrane stress that does not support the assembly of the flagellum in the absence of the cage-like structure. The $MreC^{Y220H}$ variant may allow the assembly of the flagellum by reducing or eliminating the membrane stress by interacting with other structural components.

Introduction

Helicobacter pylori is a member of the Epsilonproteobacteria that colonizes the human gastric mucosa and is responsible for causing a variety of diseases, including chronic gastritis, peptic and duodenal ulcers, B cell MALT lymphoma and gastric adenocarcinoma (1, 2). Approximately 50% of the world's population is infected with *H. pylori*, however, only a subset of individuals develops clinical symptoms. *H. pylori* possesses 2 to 6 polar sheathed flagella that it uses to migrate through the viscous mucosa layer covering the stomach epithelium. In the absence of flagella, cells are rendered non-motile and unable to colonize the epithelial layer of the stomach (3).

Flagellar biogenesis is a complex process that involves the coordination of gene expression and assembly of the gene products into a nascent flagellum. The temporal regulation of gene expression in *H. pylori* is controlled by three different sigma factors: RpoD (σ^{80}), RpoN (σ^{54}), and FliA (σ^{28}). Flagellar genes are arranged into one of three regulons according to the specific sigma factor required for their transcription. Early genes are under the control of RpoD and encode major structural proteins required for the assembly of the basal body. Transcription of genes whose products are needed midway through flagellum assembly (e.g., hook protein and hook-filament junction proteins) are dependent on RpoN and a two-component system consisting of FlgS (a sensor kinase) and FlgR (a response regulator) for their transcription (4). FlgS is a cytoplasmic protein that responds to a flagellum assembly checkpoint to initiate a signaling cascade that culminates in transcription of the RpoN-dependent flagellar genes. The identity of the assembly checkpoint is not known, but it appears to include components of the flagellar protein export apparatus and/or flagellar C ring (5-7). The transcription of the late flagellar genes is regulated by FliA, the activity of which is negatively regulated by the anti-sigma factor FlgM (8).

The bacterial flagellum is comprised of three main parts: the basal body, hook and filament (9). The basal body consists of several distinct structures, which includes the cytoplasmic ring (C ring), flagellar protein export apparatus, a rotary motor powered by the proton motive force, rod and rings (P ring and L ring) embedded in the cell envelope that act as a bushing to hold the rotating rod. The flagellar protein export apparatus is a Type III secretion system (fT3SS) that consists of six membrane proteins (FlhA, FlhB, FliO, FliP, FliQ and FliR) and three cytoplasmic proteins (FliH, FliI and FliJ) and is responsible for transporting axial components of the flagellum across the inner membrane. The *H. pylori* C ring is made of four different proteins, FliG, FliM, FliN and FliY. In *Salmonella enterica* serovar Typhimurium (*S.* Typhimurium), the C ring plays a role in determining the direction of rotation of the flagellum, but also facilitates the loading of protein substrates in the fT33SS. The MS ring-rod junction protein (FliE) is the first protein secreted by the fT3SS, followed by the rod proteins (FlgB and FlgC), hook protein (FlgE), hook-filament junction proteins (FlgK and FlgL) and flagellins (10). Torque is transmitted to the filament through the flexible hook, which acts as a universal joint in allowing torque transfer over a range of angles between the rod and filament axes. The filament is a long, rigid, helical structure that propels the cell as it rotates. The *H. pylori* flagellar filament contains a minor flagellin (FlaB) that localizes near the hook and is dependent on RpoN for its expression, and a major flagellin (FlaA) that forms the distal portion of the filament and is dependent on FliA for its expression (6).

The flagellar sheath is a unique structure restricted to a limited number of bacteria that includes *Vibrio* species, *Pseudomonas* species, *H. pylori*, *Bdellovibrio bacteriovorus* and *Azospirillum brasilense* (11-14). The membranous sheath appears to be a contiguous extension of the outer membrane, but the biological function of the sheath is unclear. Additionally, a mechanism responsible for the coordination of flagellum biosynthesis and outer membrane

remodeling must exist as the hook and filament structures progress past the cell body. Yoon and Mekalonas proposed that the sheath aids *Vibrio cholerae* in avoiding surveillance by the host immune system (15), although rotation of the flagellum in *V. cholerae* promotes the release of the potent immune response stimulant lipopolysaccharide (LPS), which may be derived from the sheath (16). A recent cryo-electron tomography (cryo-ET) study of the *H. pylori* flagellum identified a series of nascent structures that suggested flagellum assembly and outer membrane remodeling related to formation of the sheath are tightly coupled (17). In opposition to the hypothesis that flagellum assembly and sheath biosynthesis are tightly linked, Richardson and co-workers identified several non-motile, transposon-induced mutants in *V. cholerae* that produced structures resembling a flagellar sheath but lacking an internal flagellar core (18). Interestingly, the sheaths that lacked the flagellar filament often extended from the sides of the bacteria instead of the poles where the flagellum is normally located, suggesting proper localization of the sheath requires the flagellar filament (18).

An unexplored aspect of flagellar sheath biosynthesis is whether the glycerophospholipid composition differs from that of the outer membrane and, if so, how is such a disparateness in glycerophospholipid distribution maintained. Geis and co-workers identified the major fatty acids of glycerophospholipids associated with isolated *H. pylori* flagellar sheaths as myristic acid ($C_{14:0}$), stearic acid ($C_{18:0}$) and cyclopropane nonadecanoic acid ($C_{19:0}$ cyc) (ref). Hirai and colleagues reported $C_{14:0}$ and $C_{19:0}$ cyc as the most abundant fatty acids in *H. pylori* cardiolipin (CL) (19), indicating that CL may be a significant component of the *H. pylori* flagellar sheath. CL is an anionic glycerophospholipid that has a small glycerol head group and a large hydrophobic tail consisting of four acyl chains, which gives the molecule a conical shape that results in an intrinsic curvature (20). The shape of the CL molecule favors its localization in negatively curved regions

of bacterial membranes (20, 21). The flagellar sheath is a long, narrow tube with extensive negative curvature, and so it seems reasonable to expect CL in the outer membrane to localize to the sheath.

The mechanisms that mediate glycerophospholipid trafficking between the inner and outer membranes in Gram-negative bacteria are not fully understood. MsbA and PbgA are two proteins that facilitate the movement of glycerophospholipids between the membranes. Glycerophospholipids and lipid A are synthesized on the cytoplasmic side of the inner membrane and then flipped to the outer leaflet where they can be translocated across the periplasm to the outer membrane (22). MsbA, a member of the ATP-binding cassette (ABC) transport protein superfamily, participates in moving lipid A across the cell membrane bilayer (23, 24). Dalebroux *et al*. found that *S*. Typhimurium PbgA regulates the movement of CL from the inner to outer membrane (25). PbgA contains a large periplasmic domain that is believed to span the periplasm during CL translocation in a process that is dependent on the PhoPQ two-component system (25). *H. pylori* strains possess a MsbA homolog, but lack a PbgA homolog, suggesting another component or system exists to support the translocation of CL across the membranes.

While most *Helicobacter* species possess a flagellar sheath, several species lack a flagellar sheath. To identify genes that may have a role in flagellar sheath biosynthesis, we used a comparative genomics approach to search for genes that were prevalent in *Helicobacter* species that possessed a sheath, but were absent in *Helicobacter* species that lacked a sheath. Notably, one of the genes we identified encodes a cardiolipin synthase (*clsC*), which suggests further a role for CL in flagellar sheath biosynthesis in *H. pylori*. Four other genes that are conserved in *Helicobacter* species that have flagellar sheaths, but not in species lacking a sheath, are part of a larger operon and encode a predicted RND (resistance, nodulation and cell division) efflux system

that we hypothesized to play a role in flagellar sheath biosynthesis. The genes of the efflux system encode a TolC-like protein (HP1489), HlyD-like protein (HP1488), and two ABC type-2 transporters (HP1487 and HP1486) in *H. pylori* 26695. Following the targeted deletion of the corresponding genes in *H. pylori* B128, we observed a range of motility defects in the resulting mutants, with deletion of the gene encoding the HlyD-like protein (HPB128_199g41) resulting in the greatest reduction in motility. Examination of the HPB128_199g41 mutant by cryo-ET revealed that part of a unique cage-like structure that surrounds the flagellar motor within the periplasm was missing (17). We hypothesize that the cage-like structure surrounding the flagellar motor is an RND efflux pump that transports CL or other components to the outer membrane for insertion into the flagellar sheath.

Materials and Methods

Bacterial strains and growth conditions. *Escherichia coli* DH5α was used for cloning and plasmid construction. *E. coli* strains were grown in Luria-Bertani broth or agar medium. Medium was supplemented with ampicillin (100 μg/ml), chloramphenicol (30 ug/mL) or kanamycin (30 μg/ml) when appropriate. *H. pylori* strains used in the study were G27 and B128. *H. pylori* G27 displayed reduced motility and less flagellated with repeated passage in the laboratory. Highly motile variants of *H. pylori* G27 were obtained as follows. *H. pylori* G27 was stab-inoculated into a soft agar medium containing Mueller-Hinton broth, 10% heat-inactivated horse serum, 20 mM 2-(4-morpholino)-ethane sulfonic acid (pH 6.0), 5 μM $FeSO_4$ and 0.4 % Noble agar. The culture was incubated for 7 days at 37° C under an atmospheric condition consisting of 10% CO_2, 4% O_2 and 86% N_2 to allow the cells to migrate from the point of inoculation. The enrichment for motile cells was repeated by picking cells from the edge to the resulting swim halo and inoculating a fresh

soft agar medium plate. After the second enrichment on soft agar medium, cells from the edge of the swim halo were streaked on tryptic soy agar (TSA) supplemented with 5% heat-inactivated horse serum and grown at 37°C under an atmosphere consisting of 10% CO_2, 4% O_2, and 86% N_2 to obtain single colonies. One of the isolates that was highly motile was saved and designated as strain G27M. For routine culturing of *H. pylori*, cells were grown at 37°C on TSA supplemented with 5% heat-inactivated horse serum under an atmosphere consisting of 10% CO_2, 4% O_2, and 86% N_2, or grown at 37°C in liquid cultures with shaking under an atmosphere consisting of 5% CO_2, 10% H_2, 10% O_2 and 75% N_2 in Mueller-Hinton broth (MHB) supplemented with 5% heat-inactivated horse serum. Kanamycin (30 μg/ml) or chloramphenicol (30 μg/ml) was added to the medium used to culture *H. pylori* when appropriate.

Strain construction. Primers used for all PCR steps are listed in Table 3.1. Genomic DNA from *H. pylori* G27 was purified using the Wizard genomic DNA purification kit (Promega) and used as the template to construct all transporter deletions. DNA was amplified using Phusion polymerase (New England Biolabs) and the resulting amplicons were incubated with *Taq* polymerase (Promega) at 72° C for 10 min to add a 3'-A overhangs to facilitate T/A cloning with pGEM-T Easy plasmid (Promega).

The HP1489 homologs in *H. pylori* B128 and *H. pylori* G27M, HPB128_199g42 and HPG27_1412, respectively, were deleted as follows. A 792 bp upstream DNA fragment was amplified that included 696 bp of the upstream gene, 72 bp of the target gene and 24 bp of DNA complementary to the region downstream of the target gene using primers P117 and P118. An 805 bp DNA sequence corresponding to the region downstream of the target gene was amplified using primers P119 and P120. The resulting amplicon contained 700 bp of the downstream gene, 81 bp of the target gene and 24 bp of DNA complementary to the upstream region. The

complementary DNA for the two amplicons included unique restriction sites NheI and XhoI. PCR SOEing was used to join the two amplicons, and the resulting fragment was cloned into pGEM-T Easy to generate the suicide plasmid pJC049. The *kan-sacB* cassette described in Chapter 2 was introduced into unique NheI and XhoI sites in plasmid pJC049 to generate the suicide plasmid pJC051 that was used to replace the target gene in the *H. pylori* chromosome with the *kan-sacB* cassette. Plasmid pJC051 was introduced by natural transformation into the strains *H. pylori* B128 and G27M, and transformants were screened for kanamycin resistance. The target gene was removed by transforming the kanamycin-resistant isolates with plasmid pJC049, and transformants in which the *kan-sacB* cassette was replaced with the unmarked deletion were isolated following a sucrose-based counter-selection as described (26). Regions flanking the targeted genes were amplified by PCR using primers P117 and P120, and the resulting amplicons were sequenced to confirm the target gene was removed (Eton Bioscience).

Primer pair P139 and P140 together with primer pair P141 and P142 were used to amplify 566 bp and 459 bp of DNA sequence upstream and downstream, respectively, of the HP1488 homolog (HPB128_199g41) in *H. pylori* B128. The upstream region included 423 bp of the upstream gene, a 11 bp intergenic region, 111 bp of the target gene and 21 bp of DNA that was complementary to the downstream amplicon. The downstream amplicon included 223 bp of downstream gene, a 11 bp intergenic region, 225 bp of the target gene and 21 bp of DNA that was complementary to the upstream region. The complementary sequences included unique restriction sites NheI and XhoI. The amplicons were joined using PCR SOEing and subsequently cloned into pGEM-T Easy to generate the plasmid pJC062. A *kan-sacB* cassette was introduced into unique NheI and XhoI sites in plasmid pJC062 to generate the suicide plasmid pJC063, which was used to replace the target gene in the *H. pylori* B128 chromosome with the *kan-sacB* cassette. Plasmid

pJC062 was transformed into the kanamycin-resistant isolates to replace the *kan-sacB* cassette with the unmarked deletion, which was selected for using a sucrose-based counter-selection (26). Introduction of the unmarked deletion in the target gene was confirmed by PCR and DNA sequencing of the resulting amplicon (Eton Bioscience).

The genes that encoded both ABC type-2 transporters in the *H. pylori* B128 strain were deleted concurrently (HPB128_199g40 and HPB128_199g39). Primer pair P177 and P178 was used to amplify the 617 bp upstream region that included 546 bp of the gene that encoded the HlyD-like protein, 11 bp intergenic region, 39 bp of the target gene and 21 bp of DNA that was complementary to the downstream amplicon. Primer pair P179 and P180 was used to amplify the 690 bp downstream amplicon that included 537 bp of a hypothetical protein (HPB128_199g38), 132 bp of the target gene and 21 bp of DNA that was complementary to the upstream amplicon. Each amplicon included restriction sites NheI and XhoI. Both amplicons were joined using PCR SOEing and the resulting DNA fragment was cloned into pGEM-T Easy to generate plasmid pJC076. A *kan-sacB* cassette was introduced into unique NheI and XhoI sites in plasmid pJC076 to generate the suicide plasmid pJC080. The resulting plasmid was introduced by natural transformation into the *H. pylori* B128 strain and transformants were screened for kanamycin resistance. The target gene was removed by naturally transforming kanamycin resistant isolates with plasmid pJC076 and transformants with the allele removed were isolated following a sucrose-based counter-selection as previously described (26). DNA isolated from sucrose-resistant isolates were amplified by PCR, and the resulting amplicons were sequenced to confirm the target gene was removed.

Flagellar sheath preparation. All strains were resuspended in 50 mL of phosphate buffered saline (PBS, pH 7.4) from approximately 30 plates. *H. pylori* cells were harvested by

centrifugation and resuspended in 25 mL of PBS. Flagella were sheared using a Waring commercial blender for 3 min. Cells were removed by centrifugation (7000 x g for 15 min at 4° C). Flagella together with the associated flagellar sheaths were pelleted from the resulting supernatant by ultracentrifugation (270,000 x g for 60 min at 4° C). The resulting pellet was resuspended with 4 mL of 20 mM HEPES, pH 7.2, and applied to a discontinuous sucrose gradient (30-60% sucrose in 20 mM HEPES, pH 7.2, plus 1 mM EDTA). The gradients were centrifuged for ~20 h at 100,000 x g at 4° C, after which 1 mL fractions were collected (37 fractions). A_{280} was monitored for each fraction following a 1:50 dilution, and the sucrose concentration was determined using a Baucsh and Lomb refractometer (Fig 3.1B). Fractions with the highest A_{280} readings were pooled and diluted with 20 mM HEPES, pH 7.2. The flagella and flagellar sheaths were then pelleted by ultracentrifugation (100,000 x g for 60 min at 4° C), and the resulting pellets were resuspended in PBS.

Cells were harvested and cell pellets were washed once with 5 mL of PBS. Isolation of glycerophospholipids was carried out as previously described (27). Briefly, cell pellets were resuspended in 5 mL of single-phase Bligh-Dyer mixture consisting of chloroform:methanol:water (1:2:0.8, v/v/v) then incubated for 20 min at room temperature. Samples were centrifuged at 1,800 x g for 10 min and the resulting supernatant solutions were transferred to clean glass tubes. The mixture was converted into two-phase Bligh-Dyer consisting of chloroform:methanol:water (2:2:1.8, v/v/v). This mixture was vortexed and centrifuged to separate the organic and aqueous phases. The lower organic phase was transferred to a clean glass tube. A second extraction was performed adding 2.6 mL chloroform to the tube containing the upper aqueous phase. The mixture was vortexed and centrifuged. The resulting lower phase was pooled with the previous lower phase and converted again into two-phase Bligh-Dyer by adding 5.2 mL methanol and 4.7 mL water.

The resulting mixture was vortexed and centrifuged. The lower phase was transferred to a clean glass tube and the organic solvent was evaporated under a stream of nitrogen yielding the purified glycerophospholipids.

Motility assay. Motility was evaluated using a semisolid medium containing Mueller-Hinton broth, 10% heat-inactivated horse serum, 20 mM 2-(4-morpholino)-ethane sulfonic acid (pH 6.0), 5 μM $FeSO_4$ and 0.4 % Noble agar. A minimum of 3 biological samples and 3 technical replicates were used for all experiments. Using sterile wooden sticks, with *H. pylori* cells grown on TSA supplemented with 10% heat-inactivated horse serum for 4 days were stab-inoculated into the motility agar and incubated at 37° C under an atmospheric condition consisting of 10% CO_2, 4% O_2 and 86% N_2. Swim halo diameters were measured 7 d post-inoculation. The two-sample *t* test was used to determine statistical significance.

Transmission electron microscopy (TEM). *H. pylori* strains were grown to late-log phase in MHB supplemented with 10% heat-inactivated horse serum to an OD_{600} of ~1.0. Cells from 1 mL of culture were pelleted by centrifugation (550 x g) and then resuspended in 125 μL of 0.1 M phosphate-buffered saline. Cells were fixed by adding 50 μL of 16% EM grade formaldehyde and 25 μL of 8% EM grade glutaraldehyde to the cell resuspension. Following incubation at room temperature for 5 min, 10 μL of the cell suspension were added to 400 mesh, formvar-coated copper grids and incubated at room temperature for 5 min. The cell suspension was wicked off the grids using a filter paper, and the grids were washed 3 times with 10 μL of water. Cells were stained by applying 10 μL of 1% uranyl acetate to the grids for 30 s. After removing the stain with filter paper, the grids were washed 3 times with 10 μL of water and then air-dried. Cells were visualized using a JEOL JEM 1011 transmission electron microscope. Flagella counts were determined (n=100) for each strain. The Mann-Whitney U test was used to determine whether

there were statistically significant differences in number of flagella per cell for the various *H. pylori* strains.

DNA sequencing and analysis. The Illumina iTruSeq adaptor kit was used to prepare genomic libraries from 500 ng of gDNA from various *H. pylori* strains. The resulting libraries were sequenced at the University of Georgia Genomics Facility by Illumina sequencing. Read quality was assessed using FastQC and trimmed using Trimmomatic resulting in minimum read lengths of 50 and maximum read lengths of 140 (28, 29). Geneious 11.0 was used to align reads for the *H. pylori* gDNA sequences using the Bowtie2 algorithm, and mapping to the published NCBI genome sequence for *H. pylori* B128 to identify single-nucleotide polymorphisms (SNPs) in the re-sequenced genomes. The published NCBI genome sequence for *H. pylori* G27 was used to map the re-sequencing data for the *H. pylori* G27M strain.

Results

Cardiolipin is present in *H. pylori* flagellar sheath preparations. Since the flagellar sheath is a long tube-like structure that results in the inner leaflet of the sheath with a considerable amount of negative curvature, we hypothesized CL to be a major component of the sheath. To examine this hypothesis, we isolated sheathed flagella from *H. pylori* G27 by shearing them from the cells, removing the cells by low-speed centrifugation, and then pelleting the sheathed flagella by high-speed centrifugation. The glycerophospholipid profile of the flagellar sheaths that co-purified with the flagella were analyzed by TLC and visualized with the molybdenum blue reagent. Consistent with our hypothesis, CL appeared to be a major component of the flagellar sheath in *H. pylori* G27 (Fig. 3.1A). Phosphatidylethanolamine (PE) appeared to be the most abundant glycerophospholipid associated with the flagellar sheath, and low amounts of phosphatidylglycerol

(PG) were also present in the sheath (Fig. 3.1A). To obtain data on the glycerophospholipid profile of more highly purified preparations of the *H. pylori* flagellar sheath, we applied sheared flagella isolated from *H. pylori* B128 or *H. pylori* G27 to a discontinuous sucrose gradient. The *H. pylori* G27 flagella preparation displayed a major A_{280} peak on the sucrose gradient that corresponded to a sucrose concentration of ~42%, and a minor A_{280} peak that corresponded to a sucrose concentration of ~35% (Fig. 3.1B). The *H. pylori* B128 flagella preparation displayed similar A_{280} peaks on the sucrose gradient, although the major peak was smaller than that of the *H. pylori* G27 flagella preparation (Fig 3.1B). The major A_{280} peaks occurred at a similar sucrose concentration as that reported by Geis *et al*. (30) in their isolation of *H. pylori* sheathed flagella. The major A_{280} peaks for the flagella preparations for each of the *H. pylori* strains were pooled, and the glycerophospholipids were extracted for TLC analysis. PE was clearly present in the purified flagellar sheath preparations for both strains, although the intensity of the PE spot was much less than that of the *H. pylori* G27 flagella isolated from the high-speed centrifugation step (Figs. 3.1A and 3.1C). Faint spots for CL and PG were observed in the *H. pylori* G27 and *H. pylori* B128 samples, respectively (Fig. 3.1C). Given the low amount of glycerophospholipids recovered from the flagella purified on the sucrose gradients, the flagella preparations will need to be scaled up to obtain useful data on the glycerophospholipid profiles of the flagellar sheaths from the two *H. pylori* strains examined here.

Identification of *Helicobacter* genes correlated with the presence of a flagellar sheath. We aimed to identified candidate genes that are conserved in *Helicobacter* species possessing a flagellar sheath (FS^+), but are absent in *Helicobacter* species that lack a sheath (FS^-). Genomes of 33 FS^+ *Helicobacter* species and 7 FS^- *Helicobacter* species were searched for 1458 open reading frames present in the *H. pylori* G27 genome using blastp. An E-value of $1e^{-10}$ was used as a cutoff

when searching the 7 FS^- *Helicobacter* species genomes, while the cutoff for the 33 FS^+ *Helicobacter* species genomes was a more stringent cutoff of $1e^{-20}$. Utilizing this approach, we identified 23 proteins (Table 3.3) that are prevalent in FS^+ *Helicobacter* species, but are absent or rare in FS^- *Helicobacter* species (p-value = 0.0001 or less using the Fisher's exact test). We hypothesize that some of these proteins have roles in the biosynthesis or function of the flagellar sheath. Notable genes that are found preferentially in FS^+ *Helicobacter* species included *clsC*, which encodes cardiolipin synthase, and HP1486-HP1489, which encode a putative efflux system.

HP1486-HP1489 are required for wild-type motility. The genes corresponding to locus tag numbers HP1486-HP1489 (Table 3.3) share the organization of a tripartite efflux system found in Gram-negative bacteria. These efflux systems transport a variety of substrates, which includes proteins, oligosaccharides, small molecules and large cations (31). HP1486 and HP1487 encode an ATP-binding cassette (ABC) transporter that traverses the substrate across the inner membrane. HP1488 encodes a member of the membrane fusion protein (MFP) component of the RND (resistance, nodulation and cell division) efflux pump, which is thought to bring the inner and outer membranes together and enable substrate transport to the outer membrane (32). HP1489 encodes a member of the outer membrane efflux protein (OEP) family, which includes *E. coli* TolC. MFPs and OEPs often have roles in the export of antibiotics or other toxic compounds (31). van Amsterdam and co-workers tested the susceptibility of a HP1489-knockout mutant and found that the mutant displayed increased sensitivity to ethidium bromide (33).

To determine if HP1486-HP1489 are involved in biosynthesis of the flagellum or flagellar sheath, we deleted the genes in the *H. pylori* B128 using a sucrose-based counter-selection method (26). Since HP1486 and HP1487 are predicted to encode subunits of the same ABC transporter, we deleted both genes together. The motility of the *H. pylori* B128 ΔHP1487/ΔHP1486 mutant

was ~60% of that of the wild-type parental strain (Fig 3.2A). Examination of the ΔHP1487/ΔHP1486 double mutant by TEM revealed that its flagellation pattern differed from that of wild type (Fig 3.2B). Specifically, a higher proportion of the ΔHP1487/ΔHP1486 double mutant cells either lacked flagella or possessed a single flagellum (~25% for the mutant versus ~15% for wild type), and ~70% of the mutant cells had 2 or 3 flagella, while ~60% of the wild-type cells possessed 3 or 4 flagella (Fig. 3.2B). Motility was similarly impaired in the *H. pylori* B128 ΔHP1488 mutant compared to wild-type (Fig 3.2A). TEM analysis indicated that the flagellation pattern of the ΔHP1488 mutant differed from that of wild type, with ~40% of the mutant cells either lacking flagella or possessing a single flagellum (compared to ~15% for the wild-type cells; Fig. 3.2B). Deleting HP1489 in *H. pylori* B128 reduced motility by ~36% (Fig. 3.2A); and similar to the *H. pylori* B128 ΔHP1488 mutant, ~36% of the ΔHP1489 mutant cells either lacked flagella or had a single flagellum (Fig3.2B). *H. pylori* G27M is a derivative of strain G27 that displays enhanced motility and was selected by repeated passage on soft agar medium as described in Materials and Methods. Disrupting HP1489 in *H. pylori* G27M with the *kan-sacB* cassette reduced motility of the strain by more than 60% (Fig 3.3), suggesting that the HP1486-HP1489 efflux system is required for wild-type motility in *H. pylori* G27M, as it is in *H. pylori* B128.

Disrupting HP1488 in *H. pylori* B128 results in partial loss of the cage-like structure surrounding the *H. pylori* flagellar motor. When we disrupted HP1488 with the *kan-sacB* cassette in *H. pylori* B128, one of the isolates was highly motile (this strain was designated as HP1488:*kan-sacB* M or 'M'), while another isolate (designated as HP1488:*kan-sacB* RM or 'RM') was significantly impaired in their motility (Fig. 3.4A). Examination of the 'M' and 'RM' isolates flagellation pattern revealed the 'M' isolate was similar to that of wild-type *H. pylori* B128, while the 'RM' isolate had an increase in the number of cells that could not synthesize a flagellum (Fig.

3.4B). To determine if disrupting HP1488 affected the ultrastructure of the flagellar basal body, the 'RM' isolate was examined by cryo-ET. Interestingly, cryo-ET revealed that the flagellar basal body of the 'RM' isolate lacked part of a cage-like structure (Fig. 3.5), which the Liu lab had identified as a unique structure that surrounds the flagellar motor in *H. pylori* (17). These data suggest HP1488 protein is either a part of the cage-like structure or plays a role in the assembly of the cage-like structure. Removing the *kan-sacB* cassette following a sucrose-based counter-selection step did not restore motility to wild-type levels, indicating the motility defect is stable and is associated with loss of HP1488 (Fig 3.4A). To confirm the reduction in motility is independent of polar effects, the HP1488 gene must be reintroduced into the mutant and examined for the recovery of motility and the complete assembly of the cage-like structure.

A mutation in *mreC* appears to suppress the flagellar biosynthesis and motility defects of the *H. pylori* B128 HP1488:*kan-sacB* RM isolate. We hypothesized that the *H. pylori* B128:*kan-sacB* 'M' isolate had acquired a secondary mutation that restored flagellum biosynthesis and motility. To identify potential suppressor mutations, we re-sequenced the genomes of the 'M' and 'RM' isolates and analyzed the sequences for single nucleotide polymorphisms (SNPs). Comparing the genome sequences of the 'RM' isolate and the 'M' isolate to the parental strain revealed a SNP that resulted in a tyrosine to histidine amino acid substitution at position 220 in the MreC protein. These data suggest that the $MreC^{Y220H}$ variant suppresses the flagellum biosynthesis and motility defects in the *H. pylori* B128 HP1488:*kan-sacB* mutant.

MreC is part of a protein complex that includes MreB and MreD in *E. coli* and is required for the maintenance of rod-shaped cells (34, 35). Like *C. crescentus*, the MreB protein from *H. pylori* polymerizes into long filaments on the cytoplasmic side of the inner membrane, while MreC is a soluble periplasmic protein (36-38). The MreC from *H. pylori* has a hydrophobic zipper

domain that serves as a binding platform for interaction with the penicillin-binding protein PBP2 (36). The PBP2:MreC interface is essential for protein recognition and rod-shaped maintenance; residues that are critical in forming the binding platform are Phe-169, Phe-182 and Tyr-222 (36). Phyre^2 was used as a prediction tool to examine the spatial organization of these 3 residues that included the amino acid substitution (Fig 3.6) (39). Examining the model revealed the Y220H substitution was not predicted to change the spatial arrangement of the residues responsible for the binding platform (Fig 3.6). The histidine residue was predicted to be in a similar spatial arrangement as the native tyrosine, and all the adjacent residues, except for Thr-221, appeared to be unaffected (Figs 3.6C, 3.6D and 3.6E). Thr-221 is orthogonal to its original position, which in combination with the amino acid substitution, could alter the interaction with PBP2 or any other interacting proteins (Figs 3.6D and 3.6E).

Discussion

The biological role and mechanisms that mediate sheath biosynthesis in any bacterial species are currently unknown. In a cryo-ET study of *H. pylori*, the Lui lab visualized intermediates of sheath biogenesis where remodeling of the outer membrane was synchronized with the biogenesis of the flagellum (17). Using a comparative genomics approach, we identified 23 genes that are highly conserved in *Helicobacter* species that possess a flagellar sheath, but are absent or rare in *Helicobacter* species that lack a sheath (Table 3.1). Four of these genes (HP1486-HP1489) encode a predicted efflux system that we found to be required for wild-type motility and flagellation (Figs. 3.2A and 3.2B). This efflux system may correspond to a cage-like structure that surrounds the *H. pylori* flagellar motor (Fig. 3.5B). We hypothesize the efflux system transports CL or other macromolecules across to the outer membrane where they are incorporated into the

flagellar sheath (Fig. 3.7). Our rationale for proposing CL as the substrate for the efflux system is based on our observations that CL appears to be a major component of the flagellar sheath (Fig. 3.1) and that cardiolipin synthase (ClsC) is required for flagellum biosynthesis in *H. pylori* G27 (Fig. 2.1). Further biochemical characterization of efflux system encoded by HP1486-HP1489 is obviously needed to test our proposed model; and it may be that the efflux system transports alternative glycerophospholipids, proteins or other compounds needed for biosynthesis of the flagellar sheath or flagellum, rather than CL.

HP1486 and HP1487 are predicted to encode an ABC transporter that we hypothesize functions as a floppase to transport CL or other glycerophospholipids from the cytoplasmic face of the inner membrane to the periplasmic face (40). By disrupting these genes, we expected a major reduction in motility as a consequence of CL not being incorporated into the flagellar sheath. In addition to floppases, there are two other major transport mechanisms that can support the movement of glycerophospholipids between the two leaflets in the inner membrane. One group of enzymes are called scramblases, which are membrane-bound enzymes that non-specifically move glycerophospholipids between the two leaflets in the inner membrane (40-42). The second group of membrane-bound enzymes are called flippases, which move glycerophospholipids from the periplasmic face to the cytoplasmic face of the inner membrane (40, 42). Membrane-fusion proteins, like the HP1488 protein, in other tripartite efflux pumps are known to be involved in substrate recognition (43). Since the HP1488 gene remains undisrupted in the *H. pylori* B128 ΔHP1486/ΔHP1487 mutant, CL movement across the membrane bilayer that is facilitated by scramblases may be recognized by the HP1488 protein and transferred to the outer membrane in the absence of the ABC transporter. As a result, this reduced level of CL transport may support sheath biogenesis, but this would likely impact motility and the cells ability to synthesize multiple

flagella, which was observed in the motility and TEM experiments (Fig 3.2). Alternatively, if substrate recognition is impaired due to the absence of the ABC-transporter protein, membrane stress could incur, resulting in increased activity by flippases to reduce or eliminate this stress, which would impair the cells ability to utilize CL for sheath biogenesis.

The gene HP1488 encodes a HlyD-like or membrane-fusion protein (MFP), that spans the periplasm joining the ABC transporter and TolC-like protein (HP1489) (43). Deleting HP1488 from *H. pylori* B128 reduced motility and the degree to which the cells were flagellated. Disrupting the HP1488 gene with the *kan-sacB* cassette generated motile variants that produced severely impaired to highly motile strains (Fig 3.4). We hypothesized that during the construction of the *H. pylori* B128 ΔHP1488 strain, we gained a suppressor mutation that overcomes the absence of the cage-like structure. Following whole-genome re-sequencing, a SNP was identified in the highly motile *H. pylori* B128 HP1488:*kan-sacB* strain that was mapped to the *mreC* gene and resulted in a Y to H amino acid substitution at position 220. In *E. coli* and *Bacillus subtillis*, MreC interacts with MreB and MreD to form a membrane-bound complex that is critical for maintaining rod-shaped morphology (34, 35). The MreB protein polymerizes into a helical structure that is longitudinal to the cell underneath the cytoplasmic membrane, whereas MreC is organized on the periplasmic side of the inner membrane and MreD is inserted into the membrane (37, 44). All three Mre proteins are essential as deletion of any of the genes results in failure to maintain a rod-shaped morphology and subsequent cell lysis (34). MreC interacts with penicillin binding proteins (PBPs) in *H. pylori* and *C. crescentus* (36-38). In addition, the MreC protein in *C. crescentus* interacts with outer membrane proteins and MreC, which is thought to be involved in their spatial organization (37). *H. pylori* lacks a MreD homolog suggesting MreB and MreC are adequate for maintaining cell shape or there are other unidentified protein partners that

substitute for MreD (38). PBP2 co-crystalized with MreC from *H. pylori* indicated residues Phe-169, Phe-182, and Tyr-222 create a hydrophobic zipper on the surface of MreC that forms a binding platform that interacts with PBP2 (36). Examining a predictive model of the MreC^{Y220H} variant revealed the residue Thr-221 is rotated 90^{o} from its native position. Collectively, the amino acid substitution and the resulting positioning of the Thr-221 may alter the interaction with the PBP2 protein by enhancing binding, resulting in stabilizing the membrane at the cell pole and allowing flagellum biogenesis in the absence of the proposed CL efflux pump. Alternatively, the MreC variant may be interacting with unknown protein(s) in the periplasm or outer membrane that supports flagellum biogenesis.

The motility results following the disruption of the HP1489 allele in the *H. pylori* B128 and *H. pylori* G27M are unclear (Figs 3.2A and 3.3). The *H. pylori* G27M HP1489:*kan-sacB* swim halo was reduced nearly twice that of the *H. pylori* B128 ΔHP1489 strain, but we do not know if this is a result of polar effects on the downstream genes. Additionally, flagellar counts were not obtained for the *H. pylori* G27M HP1489:*kan-sacB* strain. Removing the *kan-sacB* cassette and enumerating the number of flagella per cell for the *H. pylori* G27M HP1489:*kan-sacB* strain will clarify the motility discrepancies.

Acknowledgements

This work was supported by NIH grant AI140444 to T.R.H.

Author Contributions

JC and TRH designed the research project and prepared the manuscript. JC performed most of the experiments and analyzed the data. SZ and JL carried out the cryo-electron tomography studies. JM did the comparative genomics analysis.

Table 3.1. Primers used in this study.

Primer No.	Primer name	Sequence
P117	HP1489 US_F	5’ – CAT CAA AAA CGC GGT GGA – 3’
P118	HP1489 US_R	5’ – GCT AGC ATA ATC GAA TTC CTC GAG AGG AAC TCC ATC AAC AGC GCT – 3’
P119	HP1489 DS_F	5’ – CTC GAG GAA TTC GAT TAT GCT AGC GCT TAT AAA TAC ATT GTT TCA TTA GCG – 3’
P120	HP1489 DS_R	5’ – CTT AGG GCT AAG CTC ACC ACC – 3’
P139	HP1488 US F	5’ – GAA GAC ATG ATC CCT AGT TGG TTT – 3’
P140	HP1488 US R	5’ – GCT AGC GAT TCG ATC CTC GAG CAC TTC AGC CTT AGG GCG – 3’
P141	HP1488 DS F	5’ – CTC GAG GAT CGA ATC GCT AGC GAG TTT AGG GTG GGT AAG GAA TTT – 3’
P142	HP1488 DS R	5’ – CCA CTT GGT ATT TGA TTT GAA GTG – 3’
P177	1487 US F	5’ – AAG CGC GAT GAA GCC TAT – 3’
P178	1487 US R	5’ – GCT AGC GAT TCG ATC CTC GAG CTT GTC TTG TAA AAC CCA TGC – 3’
P179	1486 DS F	5’ – CTC GAG GAT CGA ATC GCT AGC TTG AAT CAA ATG CAT GCG – 3’
P180	1486 DS R	5’ – AAA AAC GCT TGC AAA TTT TC – 3’

Table 3.2. Strains and plasmids used in this study.

Strain	Relevant Genotype	Resistance	Source
H. pylori			
HP003	B128 wild-type		
HP116	B128 HPG27_1411:*kan-sacB* (RM)	Kan	This study
HP117	B128 HPG27_1411:*kan-sacB* (M)	Kan	This study
HP119	B128 ΔHPG27_1411		This study
HP125	G27M wild-type		This study
HP158	G27M HPG27_1412:*kan-sacB*	Kan	This study
HP174	B128 HPB128_199g40/39:*kan-sacB*	Kan	This study
HP177	B128 HPG27_1412:*kan-sacB*	Kan	This study
HP179	B128 ΔHPG27_1412		This study
HP185	B128 ΔHPB128_199g40/39		This study
Escherichia coli			
JC064	DH5α pGEM-T Easy US_DS HPG27_1412	Amp	This study
JC066	DH5α pGEM-T Easy US_DS HPG27_1412:*kan-sacB*	Amp, Kan	This study
JC077	DH5α pGEM-T Easy US_DS HPG27_1411	Amp	This study
JC078	DH5α pGEM-T Easy US_DS HPG27_1411:*kan-sacB*	Amp, Kan	This study
JC091	DH5α pGEM-T Easy US_DS_HPB128_199g40/39	Amp	This study
JC095	DH5α pGEM-T Easy US_DS_HPB128_199g40/39:*kan-sacB*	Amp, Kan	This study

Plasmids	Relevant Genotype	Resistance	Source
pJC049	pGEM-T Easy US_DS HPG27_1412	Amp	This study
pJC051	pGEM-T Easy US_DS HPG27_1412:*kan-sacB*	Amp, Kan	This study
pJC062	pGEM-T Easy US_DS HPG27_1411	Amp	This study
pJC063	pGEM-T Easy US_DS HPG27_1411:*kan-sacB*	Amp, Kan	This study
pJC076	pGEM-T Easy US_DS_HPB128_199g40/39	Amp	This study
pJC080	pGEM-T Easy US_DS_HPB128_199g40/39:*kan-sacB*	Amp, Kan	This study

Table 3.3: Genes preferentially found in *Helicobacter* species with flagellar sheaths.

Proposed Function	Locus tag (gene name)	Refs.
phospholipid metabolism	HP0190 (*clsC*)	
efflux system protein	HP1486; HP1487; HP1488; HP1489	
[1]outer membrane protein (pfam02521)	HP0209; HP0486; HP0487; HP0782; HP0788; HP0914; HP1083	
FadL outer membrane protein family member (pfam03349)	HP0839	
lipid A modification	HP1580 (*lpxF*); HP0580	(45, 46)
metal ion homeostasis	HP0653 (*ftnA*); HP0971 (*cznC*); HP0970 (*cznB*)	(47-49)
hypothetical protein	HP0018; HP0097; HP0838; HP1028; HP1440	

[1]FS$^+$ *Helicobacter* species possess 1 to 14 members of this outer membrane protein family.

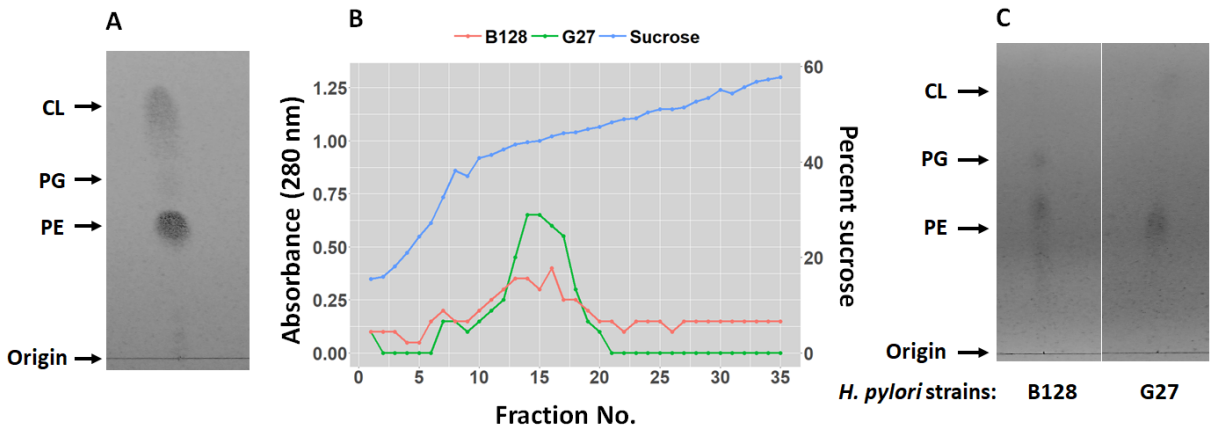

Figure 3.1: Purification of *H. pylori* G27 and *H. pylori* B128 flagella and analysis of flagellar sheath glycerophospholipids. **(A)** Flagellar sheath glycerophospholipids extracted from *H. pylori* G27 were separated by TLC and visualized with molybdenum blue reagent. Glycerophospholipids were separated in the following order, from bottom to top: phosphatidylethanolamine (PE), phosphatidylglycerol (PG), and cardiolipin (CL). **(B)** A280 values for fractions from the *H. pylori* B128 flagellar preparation (red) and *H. pylori* G27 flagellar preparation (green) are shown. Sucrose concentrations for each fraction (blue) were determined using a refractometer. **(C)** Flagellar sheath preparations from panel B were pooled for the *H. pylori* B128 and *H. pylori* G27 wild-type strains. Glycerophospholipids were extracted from the pooled fractions, separated by TLC and visualized with molybdenum blue reagent.

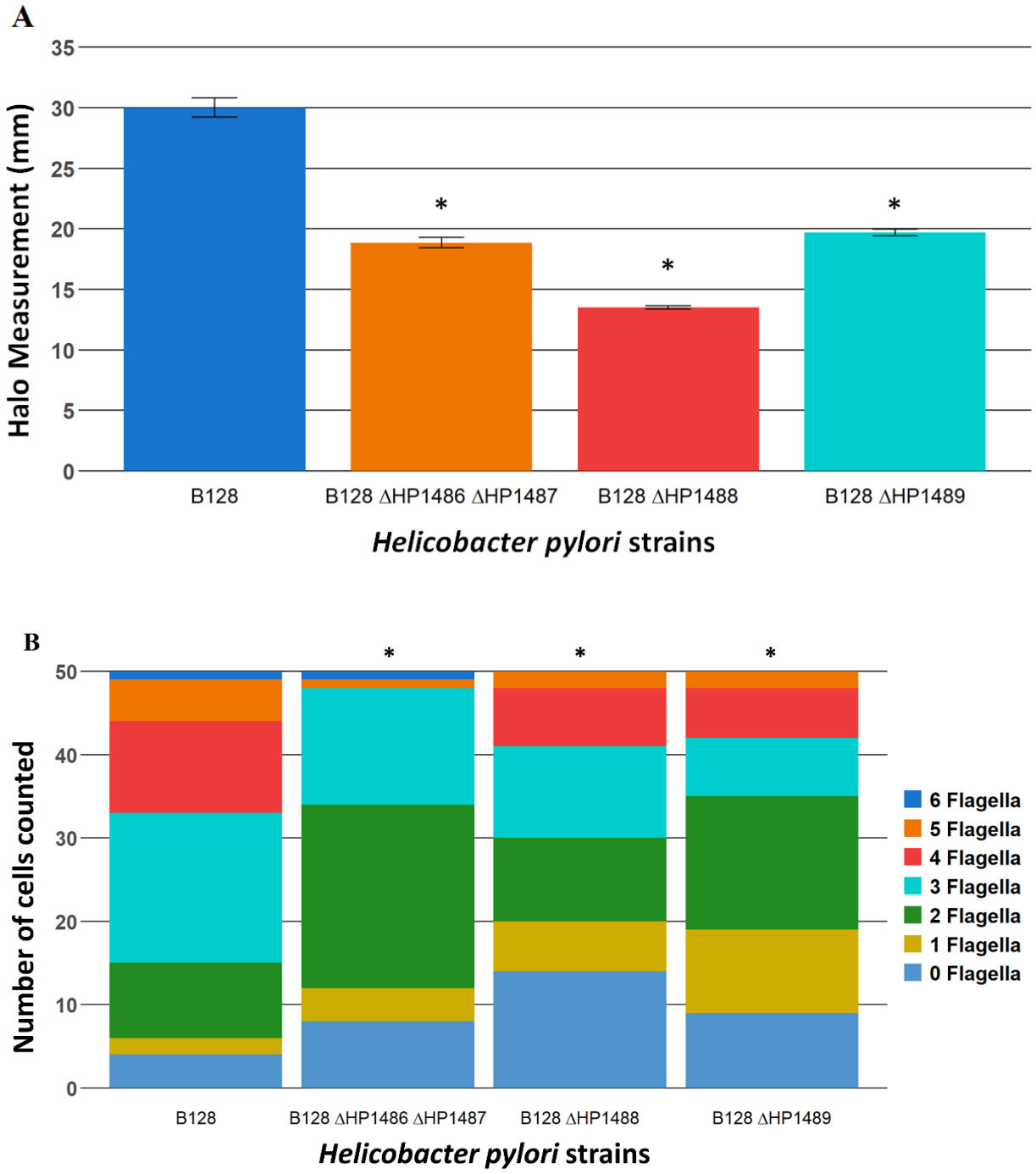

Figure 3.2: Motility and the number of flagella per cell for the efflux system mutants. (A) Motility was assessed on 0.4% soft-agar plates following 7 days of incubation under a microaerophilic environment. Measurements indicate the diameter of the swim halo that surrounded the point of inoculation. Asterisks indicate a statistically significant difference

compared to the wild-type strain (p value < 0.01). Statistical significance of was determined using the two-sample t test. (B) Flagella were analyzed and counted by electron microscopy after negative staining (n = 50). Asterisks indicate a statistically significant difference compared to the wild-type strain (p value < 0.01). Statistical significance was determined using the Mann-Whitney U test.

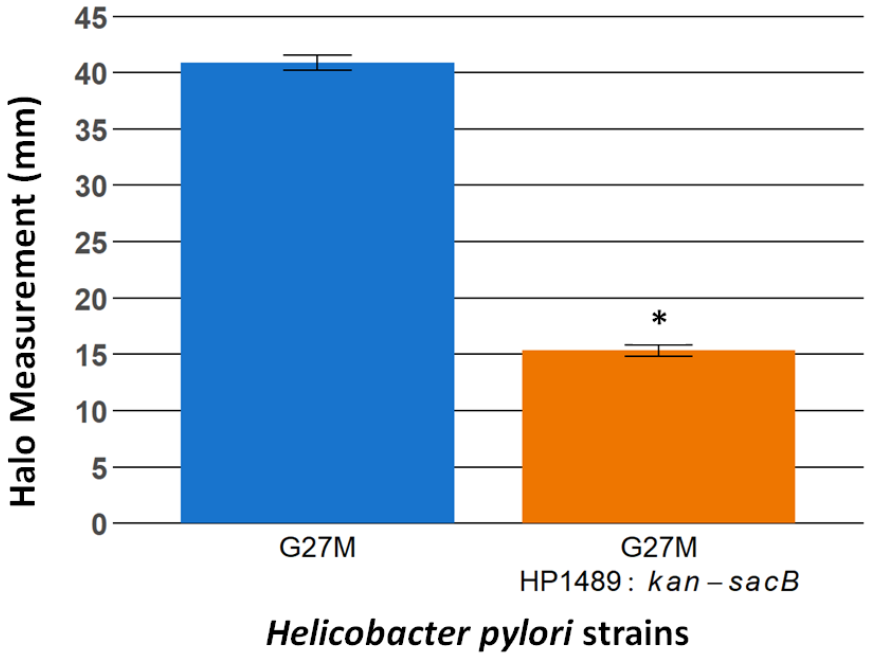

Figure 3.3: Motility results for the *H. pylori* G27M HP1489:*kan-sacB* mutant. Motility was assessed on 0.4% soft-agar plates following 7 days of incubation under a microaerophilic environment. Measurements indicate the diameter of the swim halo that surrounded the inoculation point. Asterisks indicate a statistically significant difference compared to the wild-type strain (p value < 0.01). Statistical significance of was determined using the two-sample t test.

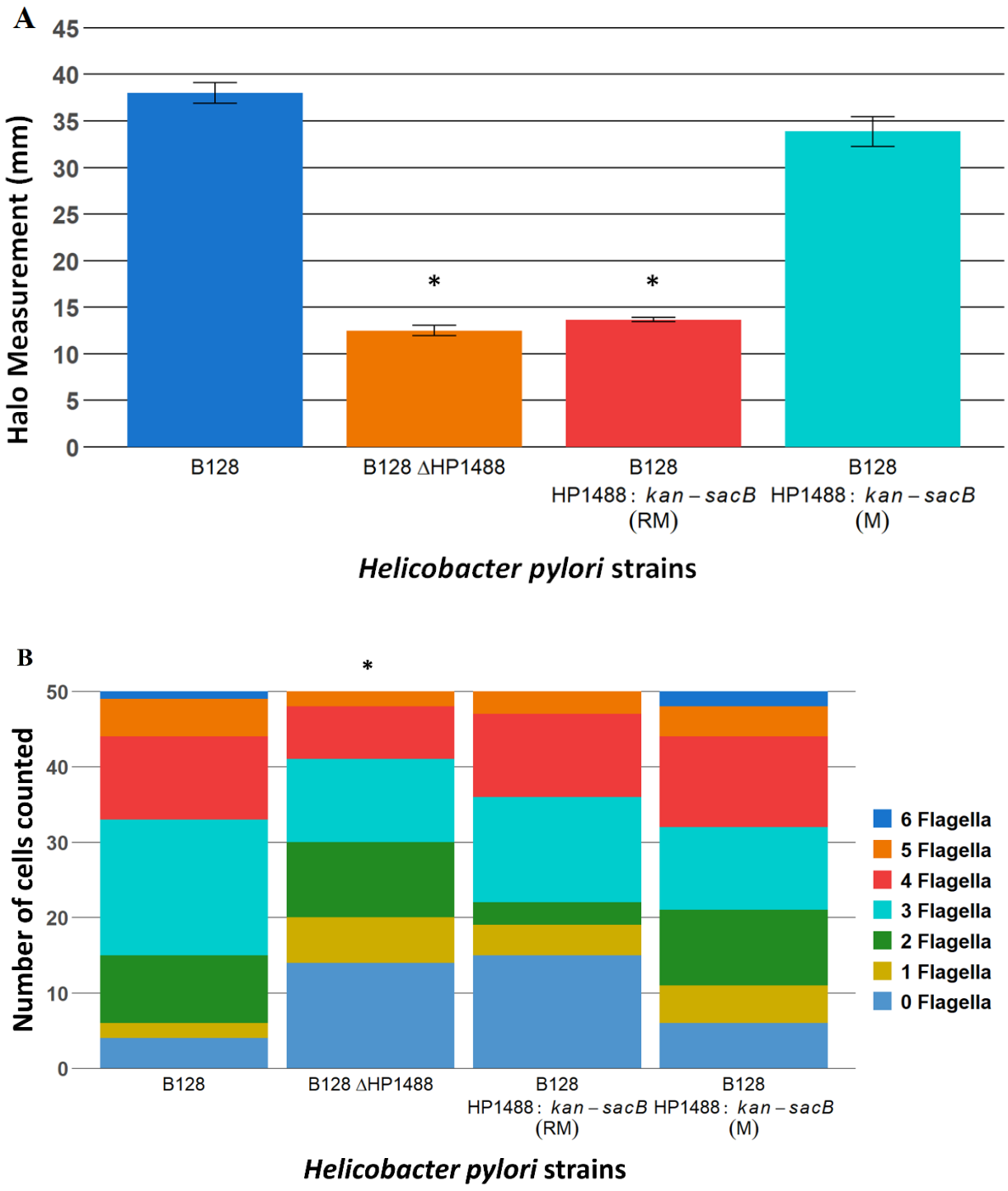

Figure 3.4: Motility and number of flagella per cell for the *H. pylori* HP1488 mutants. (A) Motility was assessed as previously described. Measurements indicate the diameter of the swim halo that surround the inoculation point. Asterisks indicate a statistically significant difference

compared to the wild-type strain (p value < 0.01). Statistical significance was determined using the two-sample t test. HP1488:*kan-sacB* 'RM' isolated displayed reduced motility compared to wild type, and was the strain from which the ΔHP1488 strain was derived. HP1488:*kan-sacB* 'M' displayed wild-type motility. (B) Flagella were counted by electron microscopy after negative staining (n = 50). Asterisks indicate a statistically significant difference compared to the wild-type strain (p value < 0.01). Statistical significance was determined using the Mann-Whitney U test.

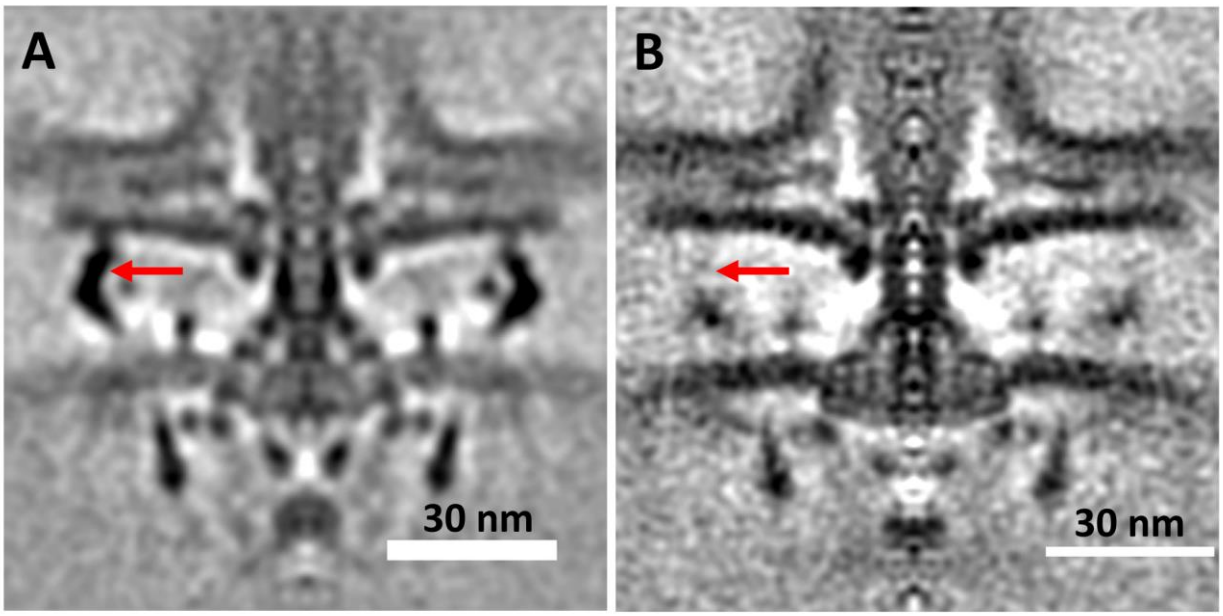

Figure 3.5: In-situ structure of the flagellar basal body of the motility-impaired *H. pylori* B128 HP1488:*kan-sacB* isolate. Flagellar basal bodies of *H. pylori* B128 wild-type strain (A) (150 motors) and *H. pylori* B128 HP1488:*kan-sacB* 'RM' isolate (B) (34 motors). The red arrow in panel A indicates the cage-like structure surrounding the flagellar motor, while the red arrow in panel B indicates the expected position of the cage-like structure for the flagellar basal body of the HP1488:*kan-sacB* 'RM' isolate.

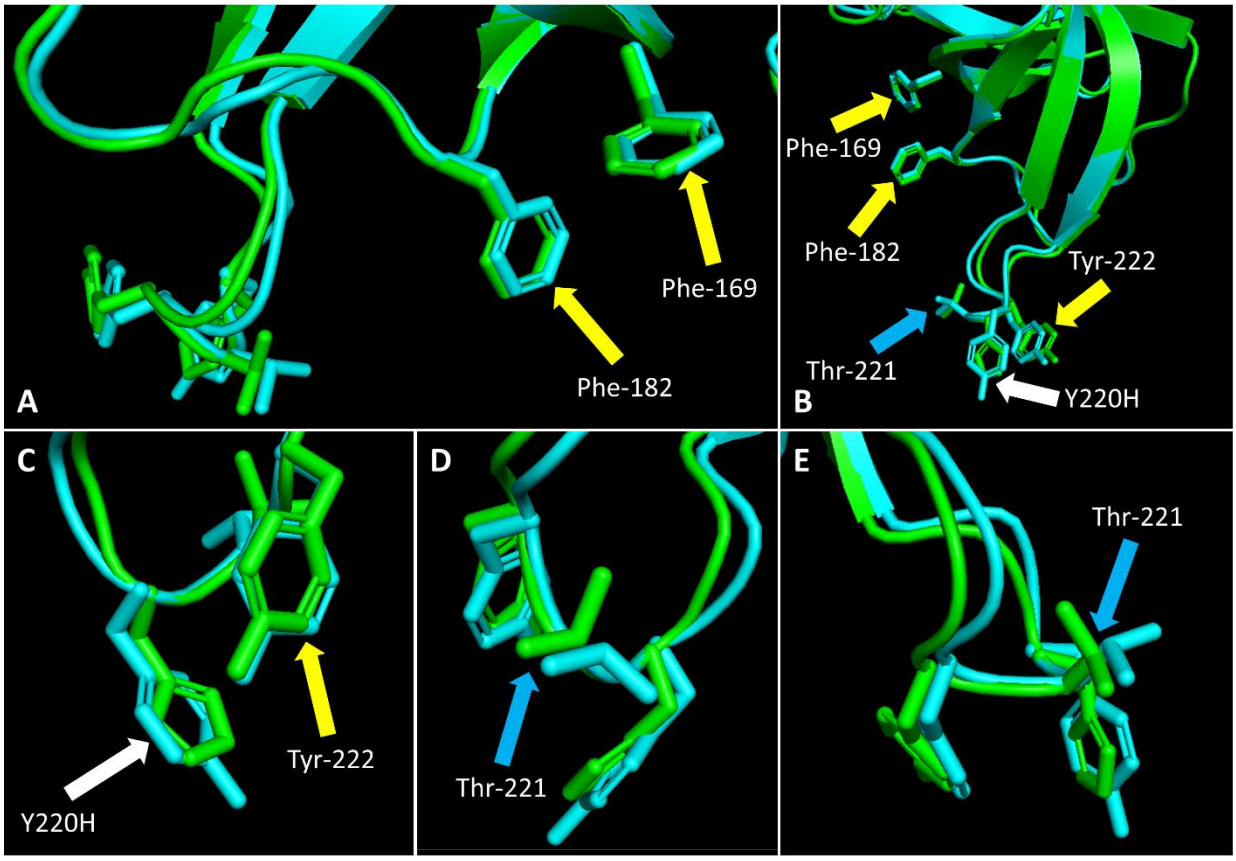

Figure 3.6: Predictive model comparing the MreC proteins from the *H. pylori* B128 1488:*kan-sacB* 'M' and *H. pylori* B128 1488:*kan-sacB* 'RM' strains. The yellow arrows indicate the residues responsible for forming the binding platform for the PBP2 protein (panels A, B and C) (36). White arrows in panels B and C indicate the Y220H amino acid substitution, which is adjacent to the binding platform. Thr-221 is specified by the blue arrows in panels B, D and E.

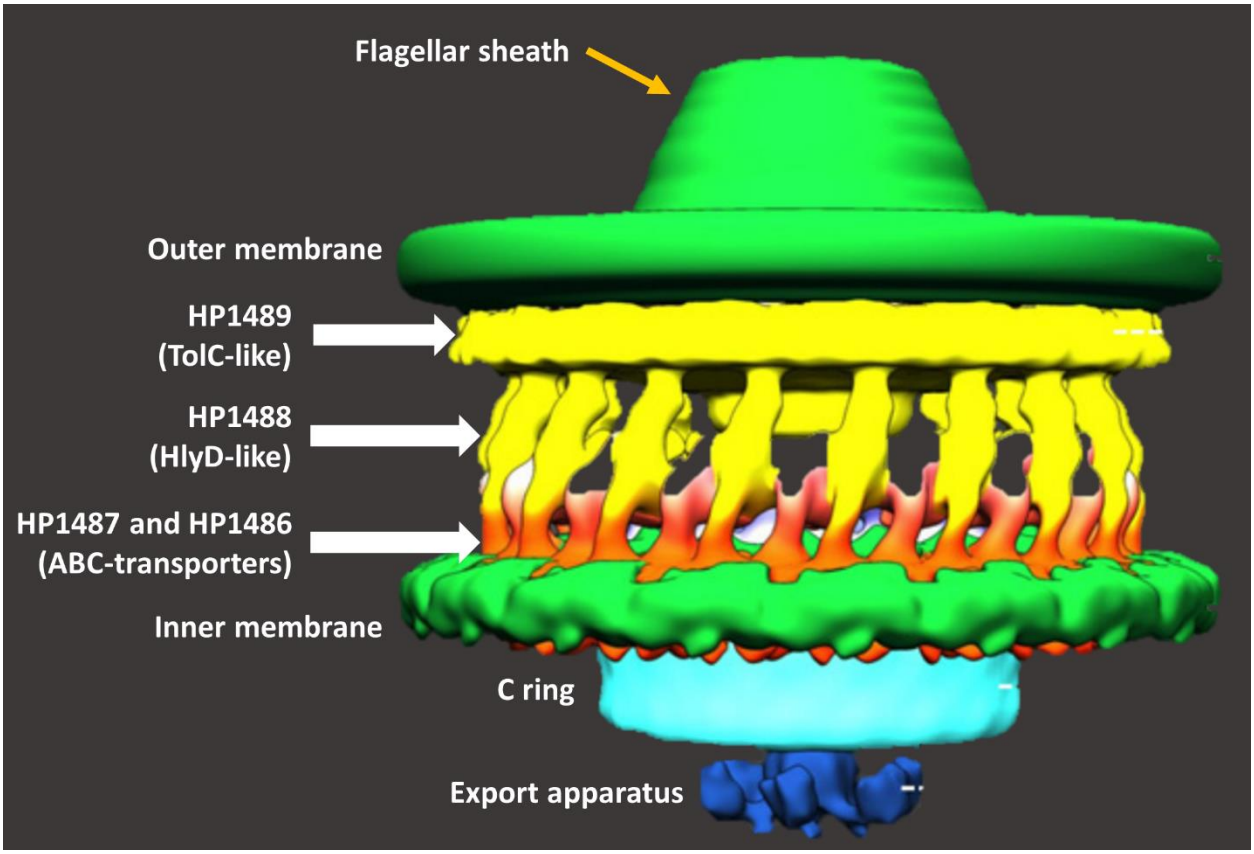

Figure 3.7: Proposed model for the HP1486-HP1489 efflux system in biosynthesis of the *H. pylori* flagellar sheath. ABC-transporter proteins encoded by the genes in locus tags HP1486 and HP1487 are responsible for traversing CL from the inner leaflet to the outer leaflet of the inner membrane. The HlyD-like protein encoded by the gene in locus tag HP1488 interacts with the ABC-transporters and facilitates the translocation of CL across the periplasm. The TolC-like protein encoded by the gene in locus tag HP1489 receives CL from the HP1488 protein and inserts the glycerophospholipid into the inner leaflet of the outer membrane where it is incorporated into the flagellar sheath. This figure was adapted from a previous study (17).

References

1. **Atherton JC**, **Blaser MJ**. 2009. Coadaptation of *Helicobacter pylori* and humans: ancient history, modern implications. The Journal of Clinical Investigation. **119**:2475-2487. https://www.ncbi.nlm.nih.gov/pubmed/19729845.
2. **Zamani M**, **Ebrahimtabar F**, **Zamani V**, **Miller WH**, **Alizadeh-Navaei R**, **Shokri-Shirvani J**, **Derakhshan MH**. 2018. Systematic review with meta-analysis: the worldwide prevalence of *Helicobacter pylori* infection. Alimentary Pharmacology and Therapeutics. **47**:868-876. https://www.ncbi.nlm.nih.gov/pubmed/29430669.
3. **Eaton KA**, **Morgan DR**, **Krakowka S**. 1992. Motility as a factor in the colonisation of gnotobiotic piglets by *Helicobacter pylori.* Journal of Medical Microbiology. **37**:123-127. https://www.ncbi.nlm.nih.gov/pubmed/1629897.
4. **Beier D**, **Frank R**. 2000. Molecular characterization of two-component systems of *Helicobacter pylori.* Journal of Bacteriology. **182**:2068-2076. https://www.ncbi.nlm.nih.gov/pubmed/10735847.
5. **Tsang J**, **Hirano T**, **Hoover TR**, **McMurry JL**. 2015. *Helicobacter pylori* FlhA binds the sensor kinase and flagellar gene regulatory protein FlgS with high affinity. Journal of Bacteriology. **197**:1886-1892. https://www.ncbi.nlm.nih.gov/pubmed/25802298.
6. **Tsang J**, **Hoover TR**. 2015. Basal body structures differentially affect transcription of RpoN- and FliA-dependent flagellar genes in *Helicobacter pylori.* Journal of Bacteriology. **197**:1921-1930. https://www.ncbi.nlm.nih.gov/pubmed/25825427.
7. **Niehus E**, **Gressmann H**, **Ye F**, **Schlapbach R**, **Dehio M**, **Dehio C**, **Stack A**, **Meyer TF**, **Suerbaum S**, **Josenhans C**. 2004. Genome-wide analysis of transcriptional hierarchy and feedback regulation in the flagellar system of *Helicobacter pylori*. Molecular Microbiology. **52**:947-961. https://www.ncbi.nlm.nih.gov/pubmed/15130117.
8. **Josenhans C**, **Niehus E**, **Amersbach S**, **Hörster A**, **Betz C**, **Drescher B**, **Hughes KT**, **Suerbaum S**. 2002. Functional characterization of the antagonistic flagellar late regulators FliA and FlgM of *Helicobacter pylori* and their effects on the *H. pylori* transcriptome. Molecular Microbiology. **43**:307-322. https://www.ncbi.nlm.nih.gov/pubmed/11985711.
9. **Macnab RM**. 2003. How bacteria assemble flagella. Annual Review of Microbiology. **57**:77-100. https://www.ncbi.nlm.nih.gov/pubmed/12730325.
10. **Minamino T**, **Yamaguchi S**, **Macnab RM**. 2000. Interaction between FliE and FlgB, a proximal rod component of the flagellar basal body of *Salmonella.* Journal of Bacteriology. **182**:3029-3036. https://www.ncbi.nlm.nih.gov/pubmed/10809679.
11. **Burnham JC**, **Hashimoto T**, **Conti SF**. 1970. Ultrastructure and cell division of a facultatively parasitic strain of *Bdellovibrio bacteriovorus*. Journal of Bacteriology. **101**:997-1004. https://www.ncbi.nlm.nih.gov/pubmed/4908793.
12. **Burygin GL**, **Shirokov AA**, **Shelud'ko AV**, **Katsy EI**, **Shchygolev SY**, **Matora LY**. 2007. Detection of a sheath on *Azospirillum brasilense* polar flagellum. Microbiology. **76**:728-734. https://www.ncbi.nlm.nih.gov/pubmed/18297874.
13. **Geis G**, **Leying H**, **Suerbaum S**, **Mai U**, **Opferkuch W**. 1989. Ultrastructure and chemical analysis of *Campylobacter pylori* flagella. Journal of Clinical Microbiology. **27**:436-441. https://www.ncbi.nlm.nih.gov/pubmed/2715319.

14. **Yang GC**, **Schrank GD**, **Freeman BA**. 1977. Purification of flagellar cores of *Vibrio cholerae*. Journal of Bacteriology. **129**:1121-1128. https://www.ncbi.nlm.nih.gov/pubmed/838680.
15. **Yoon SS**, **Mekalanos JJ**. 2008. Decreased potency of the *Vibrio cholerae* sheathed flagellum to trigger host innate immunity. Infection and Immunity. **76**:1282-1288. https://www.ncbi.nlm.nih.gov/pubmed/18174340.
16. **Brennan CA**, **Hunt JR**, **Kremer N**, **Krasity BC**, **Apicella MA**, **McFall-Ngai MJ**, **Ruby EG**. 2014. A model symbiosis reveals a role for sheathed-flagellum rotation in the release of immunogenic lipopolysaccharide. eLife. **3**:e01579. https://www.ncbi.nlm.nih.gov/pubmed/24596150.
17. **Qin Z**, **Lin WT**, **Zhu S**, **Franco AT**, **Liu J**. 2017. Imaging the motility and chemotaxis machineries in *Helicobacter pylori* by cryo-electron tomography. Journal of Bacteriology. **199**:e00695-16. https://www.ncbi.nlm.nih.gov/pubmed/?term=27849173.
18. **Richardson K**, **Nixon L**, **Mostow P**, **Kaper JB**, **Michalski J**. 1990. Transposon-induced non-motile mutants of *Vibrio cholerae.* Journal of General Microbiology. **136**:717-725. https://www.ncbi.nlm.nih.gov/pubmed/1975833.
19. **Hirai Y**, **Haque M**, **Yoshida T**, **Yokota K**, **Yasuda T**, **Oguma K**. 1995. Unique cholesteryl glucosides in *Helicobacter pylori*: composition and structural analysis. Journal of Bacteriology. **177**:5327-5333. https://www.ncbi.nlm.nih.gov/pubmed/7665522.
20. **Huang KC**, **Mukhopadhyay R**, **Wingreen NS**. 2006. A curvature-mediated mechanism for localization of lipids to bacterial poles. PLOS Computational Biology. **2**:e151. https://www.ncbi.nlm.nih.gov/pubmed/17096591.
21. **Laloux G**, **Jacobs-Wagner C**. 2014. How do bacteria localize proteins to the cell pole? Journal of Cell Science. **127**:11-19. https://www.ncbi.nlm.nih.gov/pubmed/24345373.
22. **Doerrler WT**. 2006. Lipid trafficking to the outer membrane of Gram-negative bacteria. Molecular Microbiology. **60**:542-552. https://www.ncbi.nlm.nih.gov/pubmed/16629659.
23. **Doerrler WT**, **Gibbons HS**, **Raetz CRH**. 2004. MsbA-dependent Translocation of Lipids across the Inner Membrane of Escherichia coli. Journal of Biological Chemistry. **279**:45102-45109. http://www.jbc.org/content/279/43/45102.abstract.
24. **Woebking B**, **Reuter G**, **Shilling RA**, **Velamakanni S**, **Shahi S**, **Venter H**, **Balakrishnan L**, **van Veen HW**. 2005. Drug-lipid A interactions on the *Escherichia coli* ABC transporter MsbA. Journal of Bacteriology. **187**:6363-6369. https://www.ncbi.nlm.nih.gov/pubmed/16159769.
25. **Dalebroux ZD**, **Edrozo MB**, **Pfuetzner RA**, **Ressl S**, **Kulasekara BR**, **Blanc MP**, **Miller SI**. 2015. Delivery of cardiolipins to the bacterial outer membrane to promote virulence. Cell Host Microbe. **17**:441-451. https://www.ncbi.nlm.nih.gov/pubmed/25856753.
26. **Copass M**, **Grandi G**, **Rappuoli R**. 1997. Introduction of unmarked mutations in the *Helicobacter pylori vacA* gene with a sucrose sensitivity marker. Infection and Immunity. **65**:1949-1952. https://www.ncbi.nlm.nih.gov/pubmed/9125586.
27. **Henderson JC**, **Herrera CM**, **Trent MS**. **2017**. AlmG, responsible for polymyxin resistance in pandemic *Vibrio cholerae*, is a glycyltransferase distantly related to lipid A late acyltransferases. Journal of Biological Chemistry. **292**:21205-21215. https://www.ncbi.nlm.nih.gov/pubmed/29101229.

28. **Andrews S**. 2010. FastQC: a quality control tool for high throughput sequence data.
29. **Bolger AM**, **Lohse M**, **Usadel B**. 2014. Trimmomatic: a flexible trimmer for Illumina sequence data. *Bioinformatics*. **30**:2114-2120. https://www.ncbi.nlm.nih.gov/pubmed/24695404.
30. **Geis G**, **Suerbaum S**, **Forsthoff B**, **Leying H**, **Opferkuch W**. 1993. Ultrastructure and biochemical studies of the flagellar sheath of *Helicobacter pylori*. Journal of Medical Microbiology. **38**:371-377. https://www.ncbi.nlm.nih.gov/pubmed/?term=8487294.
31. **Johnson JM**, **Church GM**. 1999. Alignment and structure prediction of divergent protein families: periplasmic and outer membrane proteins of bacterial efflux pumps. Journal of Molecular Biology. **287**:695-715. https://www.ncbi.nlm.nih.gov/pubmed/10092468.
32. **Zgurskaya HI**, **Yamada Y**, **Tikhonova EB**, **Ge Q**, **Krishnamoorthy G**. 2009. Structural and functional diversity of bacterial membrane fusion proteins. BBA - Proteins and Proteomics. **1794**:794-807. https://www.ncbi.nlm.nih.gov/pubmed/19041958.
33. **van Amsterdam K**, **Bart A**, **van der Ende A**. 2005. A Helicobacter pylori TolC Efflux Pump Confers Resistance to Metronidazole. Antimicrobial Agents and Chemotherapy. **49**:1477-1482.
34. **Kruse T**, **Bork-Jensen J**, **Gerdes K**. 2005. The morphogenetic MreBCD proteins of *Escherichia coli* form an essential membrane-bound complex. Molecular Microbiology. **55**:78-89. https://www.ncbi.nlm.nih.gov/pubmed/15612918.
35. **Shih YL**, **Rothfield L**. 2006. The bacterial cytoskeleton. Microbiology and Molecular Biology Reviews. **70**:729-754. https://www.ncbi.nlm.nih.gov/pubmed/16959967.
36. **Contreras-Martel C**, **Martins A**, **Ecobichon C**, **Trindade DM**, **Matteï PJ**, **Hicham S**, **Hardouin P**, **Ghachi ME**, **Boneca IG**, **Dessen A**. 2017. Molecular architecture of the PBP2-MreC core bacterial cell wall synthesis complex. Nature Communications. **8**:776. https://www.ncbi.nlm.nih.gov/pubmed/28974686.
37. **Divakaruni AV**, **Loo RR**, **Xie Y**, **Loo JA**, **Gober JW**. 2005. The cell-shape protein MreC interacts with extracytoplasmic proteins including cell wall assembly complexes in *Caulobacter crescentus*. Proceedings of the National Academy of Sciences. **102**:18602-18607. https://www.ncbi.nlm.nih.gov/pubmed/16344480.
38. **El Ghachi M**, **Matteï PJ**, **Ecobichon C**, **Martins A**, **Hoos S**, **Schmitt C**, **Colland F**, **Ebel C**, **Prévost MC**, **Gabel F**, **England P**, **Dessen A**, **Boneca IG**. 2011. Characterization of the elongasome core PBP2:MreC complex of *Helicobacter pylori*. Molecular Microbiology. **82**:68-86. https://www.ncbi.nlm.nih.gov/pubmed/21801243.
39. **Kelley LA**, **Mezulis S**, **Yates CM**, **Wass MN**, **Sternberg MJ**. 2015. The Phyre2 web portal for protein modeling, prediction and analysis. Nature Protocols. **10**:845-858. https://www.ncbi.nlm.nih.gov/pubmed/25950237.
40. **Daleke DL**. 2003. Regulation of transbilayer plasma membrane phospholipid asymmetry. Journal of Lipid Research. **44**:233-242. https://www.ncbi.nlm.nih.gov/pubmed/12576505.
41. **Hrafnsdóttir S**, **Menon AK**. 2000. Reconstitution and partial characterization of phospholipid flippase activity from detergent extracts of the *Bacillus subtilis* cell membrane. Journal of Bacteriology. **182**:4198-4206. https://www.ncbi.nlm.nih.gov/pubmed/10894727.
42. **Pomorski TG**, **Menon AK**. 2016. Lipid somersaults: Uncovering the mechanisms of protein-mediated lipid flipping. Progress in Lipid Research. **64**:69-84. https://www.ncbi.nlm.nih.gov/pubmed/27528189.

43. **Kanonenberg K**, **Schwarz CK**, **Schmitt L**. 2013. Type I secretion systems - a story of appendices. Research in Microbiology. **164**:596-604. https://www.ncbi.nlm.nih.gov/pubmed/23541474.
44. **Wachi M**, **Osaka K**, **Kohama T**, **Sasaki K**, **Ohtsu I**, **Iwai N**, **Takada A**, **Nagai K**. 2006. Transcriptional analysis of the *Escherichia coli mreBCD* genes responsible for morphogenesis and chromosome segregation. Bioscience, Biotechnology, and Biochemistry. **70**:2712-2719. https://www.ncbi.nlm.nih.gov/pubmed/17090951.
45. **Cullen TW**, **Giles DK**, **Wolf LN**, **Ecobichon C**, **Boneca IG**, **Trent MS**. 2011. *Helicobacter pylori* versus the host: remodeling of the bacterial outer membrane is required for survival in the gastric mucosa. PLOS Pathogens. **7**:e1002454. https://www.ncbi.nlm.nih.gov/pubmed/22216004.
46. **Stead CM**, **Zhao J**, **Raetz CR**, **Trent MS**. 2010. Removal of the outer Kdo from *Helicobacter pylori* lipopolysaccharide and its impact on the bacterial surface. Molecular Microbiology. **78**:837-852. https://www.ncbi.nlm.nih.gov/pubmed/20659292.
47. **Doig P**, **Austin JW**, **Trust TJ**. 1993. The *Helicobacter pylori* 19.6-kilodalton protein is an iron-containing protein resembling ferritin. Journal of Bacteriology. **175**:557-560. https://www.ncbi.nlm.nih.gov/pubmed/8419304.
48. **Stähler FN**, **Odenbreit S**, **Haas R**, **Wilrich J**, **Van Vliet AH**, **Kusters JG**, **Kist M**, **Bereswill S**. 2006. The novel *Helicobacter pylori* CznABC metal efflux pump is required for cadmium, zinc, and nickel resistance, urease modulation, and gastric colonization. Infection and Immunity. **74**:3845-3852. https://www.ncbi.nlm.nih.gov/pubmed/16790756.
49. **van Vliet AH**, **Poppelaars SW**, **Davies BJ**, **Stoof J**, **Bereswill S**, **Kist M**, **Penn CW**, **Kuipers EJ**, **Kusters JG**. 2002. NikR mediates nickel-responsive transcriptional induction of urease expression in *Helicobacter pylori*. Infection and Immunity. **70**:2846-2852. https://www.ncbi.nlm.nih.gov/pubmed/12010971.

CHAPTER 4

CONCLUSIONS AND FUTURE DIRECTIONS

Conclusions and Future Directions Related to the Cardiolipin Synthase

Helicobacter pylori colonizes one of the harshest environments in the human body. Classified as a neutrophile, the bacterium must withstand the acidic surroundings while using a tuft of flagella to penetrate a thick mucous layer that lines the stomach epithelium. Once colonization has been established, the flagella are used to maintain a long-term association with the host as the contents of the stomach is periodically emptied and the mucus layer is repeatedly sloughed off. The mechanisms that mediate flagellar biogenesis in other human pathogens like *E. coli* and *Salmonella* do not directly translate to *H. pylori* and other closely related bacteria such as *Campylobacter jejuni* because the regulatory systems that govern expression of the flagellar genes and overall flagellum structure differ significantly. Understanding how *H. pylori* coordinates gene expression and protein assembly may lead to the identification of new therapeutic targets to treat infections and may broadly apply to other related pathogenic bacteria, such as *C. jejuni*.

The work here provides insight into how the glycerophospholipid cardiolipin (CL) influences flagellar synthesis in a *H. pylori* strain-dependent manner. Flagellar biogenesis is a complex process that coordinates the expression of more than fifty structural and regulatory genes with the assembly of the flagellum. The assembly of the flagellum is a highly ordered process in which substrates required in the early stages of flagellar biogenesis are made prior to the substrates needed in the later stages. Glycerophospholipids are known to influence the localization and

activity of proteins, but have yet to be examined for their role in flagellum biosynthesis in *H. pylori*.

H. pylori possesses 2-6 flagella per cell that localizes to a single cell pole, and the goal of my research is to understand the role CL plays in facilitating the assembly of flagellar gene products into the flagellum basal body. Our initial hypothesis proposed the basal body proteins required during the early stages of flagellum assembly would not localize to the cell pole in a strain that is depleted of CL, rendering the strain non-motile. Although disrupting *clsC* in *H. pylori* G27 resulted in loss of motility, the defect in motility was due to failure of the bacterium to synthesize flagella rather than the improper localization of its flagella. Interestingly, the B128 FlgI protein, which polymerizes into the P ring that is anchored in the peptidoglycan layer, was sufficient to overcome the cardiolipin depleted condition in the *H. pylori* G27 *clsC* mutant. Why the FlgI protein from the *H. pylori* B128 strain suppresses the non-motile phenotype of the *H. pylori* G27 *clsC* strain is unclear. There are 5 amino acid differences between the FlgI proteins from *H. pylori* B128 and *H. pylori* G27, but only 3 amino acid substitutions were introduced into the G27 *clsC* mutant in the allelic exchange mutagenesis. Anionic glycerophospholipids have been observed to stimulate enzymatic activities, stabilize protein complexes and promote dimerization of proteins (1-3). One hypothesis is the G27 FlgI protein is not localized to the periplasm in the cardiolipin depleted condition. Alternatively, localization of the G27 FlgI protein to the periplasm occurs properly and the interactions between protein partners are stabilized due to the residue differences with the FlgI protein from the B128 *clsC* strain. To test this, quantifying the amount of G27 FlgI and B128 FlgI protein that is localized to the periplasm in the cardiolipin depleted condition would help to determine if the secretory system is deficient in properly localizing the FlgI protein to the periplasm.

E. coli encodes 3 *cls* genes and each are expressed according to the growth phase and environmental conditions (4-6). We reasoned that *H. pylori* may encode an additional CL synthase. To date, all known bacterial CL synthases possess a conserved $HxKxxxxDx_6GSxN$ motif (HKD motif), which include the *clsC* gene identified in the *H. pylori* B128 and *H. pylori* G27 strains (7). Using a bioinformatic approach, I identified more than 40 proteins that possessed the HKD motif from 4 different *H. pylori* strains (26695, B128, B8 and G27). NucT is a membrane-bound enzyme reported to cleave single-stranded DNA (8). Phylogenetic analysis of the NucT protein sequence indicated this enzyme clustered with other known CL synthases from multiple bacteria, suggesting NucT may be the additional CL synthase responsible for producing the residual CL in the *H. pylori clsC* mutants (9). If *nucT* does encode a second CL synthase, deleting this gene should reduce or eliminate the remaining CL in both mutant strains.

Previous lab members have enriched for motility by passaging the *H. pylori* wild-type strains using soft-agar plates, which resulted in a larger swim halo. I reasoned that the same strategy could be applied to isolate spontaneous mutants using the *H. pylori* G27 *clsC* strain, which might identify additional mutations that suppress the flagellum assembly defect in the *clsC* mutant. Passaging the mutant between soft-agar plates for 4 weeks allowed me to isolate a motile strain that nearly doubled the diameter of the swim halo. The swim halo appeared to be denser when compared to the *H. pylori* G27 wild-type strain, suggesting the strain may be motile, but the chemotaxis system is compromised. I also used a chemical mutagenesis approach to isolate *H. pylori* G27 *clsC* motile variants with stable mutations resulting from exposure of the cells to the mutagen nitrosoguanidine. I placed a crystal of the mutagen in the center of multiple soft-agar plates, and stab-inoculated the *H. pylori* G27 *clsC* mutant at varied distances to simulate a gradient. Following 7 days of incubation, cells were collected from 20 independent swim halos and streaked

for isolation. Isolated colonies were screened for motility using soft-agar plates. The swim halos for the *H. pylori* G27 *clsC* suppressor isolates were dense like the spontaneous mutants previously isolated, indicating both approaches can result in motile variants. Following the isolation of these suppressor candidates, I planned to re-sequence the isolates, but the strains were lost.

Performing the allelic mutagenesis with genomic DNA from the *H. pylori* B128 *clsC* strain as the donor, and the *H. pylori* G27 *clsC* strain as the recipient, resulted in a range of motile variants. The diameter of the swim halo for one of these strains, mv49, was nearly twice the size of those of the other *H. pylori* G27 *clsC* recipients (Fig 2.7A). By analyzing the re-sequencing data, I identified 98 B128 alleles (2492 SNPs) that were unique to the mv49 isolate. I wished to identify additional flagellar genes unique to the mv49 strain. Three of the B128 alleles that were unique to the mv49 isolate were flagellar genes, *flgH* (encodes the L ring), *flgS* (the sensor kinase that is required for RpoN-dependent transcription) and a *flgJ* homolog (predicted to encode a muramidase that allows the rod to penetrate the peptidoglycan layer). One or more of these B128 alleles, together with the *flgI* allele, may account for the enhanced flagellation and motility of the mv49 isolate. Introducing the B128 alleles into the G27 *clsC* mutant would clarify if these genes from the donor can suppress the flagellation and motility defects in a cooperative fashion.

Conclusions and Future Directions Related to the Putative Cardiolipin Efflux Pump

H. pylori assembles a unique cage-like structure that surrounds the flagellar basal body. We identified an operon that encodes a putative cardiolipin efflux pump (HP1486-HP1489) and is preferentially found in *Helicobacter* species that possess a flagellar sheath. The genes encoding HP1486-HP1489 share the organization of a tripartite efflux system found in Gram-negative bacteria. These efflux systems transport a variety of substrates, which includes proteins,

oligosaccharides, small molecules and large cations (10). The components that comprise the efflux systems include an ATP-binding cassette (ABC) transporter that traverses the substrate across the inner membrane (encoded by HP1486 and HP1487), a periplasmic membrane fusion protein (encoded by HP1488; HlyD-like protein) that links the inner and outer membranes, and an outer membrane protein (encoded by HP1489; TolC-like protein) (Fig 3.7) (11, 12). Disrupting the HP1488 homolog in *H. pylori* B128 (Fig. 3.5), as well as deletion of the HP1489 or HP1486/HP1487 homologs in *H. pylori* B128 (our unpublished data), resulted in loss of a region of electron density that corresponds to a portion of the cage-like structure surrounding the flagellar motor.

These above observations raise a couple of interesting questions. For instance, does the efflux system constitute part of the cage-like structure, or is the efflux system required for localization of one or more components of the cage-like structure? If the efflux system forms part of the cage-like structure, what are the other components of this structure? Does the efflux system play a role in flagellar sheath biosynthesis, and if so, what does the efflux system transport?

To address the first two questions, it is imperative to identify protein interaction partners for components of the efflux pump, as well as conduct localization studies for the efflux pump. Based on studies of related efflux systems, we expect the HlyD-like protein to interact with the putative ABC transporter proteins (HP1486-HP1487) and the TolC-like protein (HP1489), while the transporter and TolC-like proteins would not interact with each other (13). To identify additional binding partners for each efflux pump component, chemical crosslinking using formaldehyde followed by a column purification could be performed using tagged (e.g., His-, FLAG- or Myc-tagged) HP1486, HP1487, HP1488 and HP1489. Crosslinked protein complexes could be excised from an SDS-PAGE gel and then sent for mass spectrometry to identify the

protein partners for each component. Localization of the efflux pump could be determined using immunogold-labeling with antibodies directed against the individual components of the efflux pump, or by tagging components of the efflux pump and using commercially available antibodies directed against the protein tag. Alternatively, components of the efflux pump, in particular the ABC transporters, could be tagged with a fluorescent protein for fluorescence microscopy studies. An alternative approach that may prove useful in determining whether the efflux pump forms part of the cage-like structure is to examine the flagellar motor of the highly motile variant ('M') *H. pylori* B128 HP1488:*kan-sacB* mutant by cryo-ET. The 'M' variant has a motility and flagellation pattern that is quite similar to that of wild type (Fig. 3.4). It is possible that the mutation in the 'M' variant suppresses the disruption of HP1488 by rescuing assembly of the cage-like structure, which we could ascertain by examining the flagellar motor of 'M' variant by cryo-ET.

With regard to identifying transport substrates for the efflux system, we hypothesize that the efflux pump transports CL from the inner membrane to the outer membrane where it is incorporated into the flagellar sheath. There are likely additional glycerophospholipid transport systems to distribute glycerophospholipids between the membranes for supporting physiological processes that exclude flagellar biogenesis, and such additional transport systems may make it difficult to demonstrate definitively a function for the efflux system encoded by HP1486-HP1489. An alternative hypothesis is that the efflux pump encoded by HP1486-HP1489 transports a protein required for Using a Sarkosyl treatment, Geis *et al*. separated the inner and outer membranes in a *H. pylori* strain to enrich for flagellar sheaths (14). Using this approach will allow us to analyze the glycerophospholipid and protein content of the inner membrane, outer membrane and flagellar sheath by mass spec.

Finally, it will be of interest to understand the basis for the highly motile 'M' variant of the *H. pylori* B128 HP1488: *kan-sacB* mutant (Fig 3.4). Examining the re-sequenced genomes of a motility impaired 'RM' and highly motile 'M' strains identified a SNP in the *mreC* gene of the highly motile isolate. MreC interacts with the penicillin-binding protein 2 (PBP2) in *H. pylori*, and depletion of MreC or PBP2 leads to a morphological change from spiral rods to coccoidal spheres and eventual cell death (15, 16). Additionally, the MreC protein in *H. pylori* is proposed to be a soluble periplasmic protein, similar to what was identified in *Caulobacter crescentus* (17). The protein partners that interact with MreC or PBP2 have not been defined in *H. pylori*, but studies in other bacteria like *B. subtillis*, *E. coli*, and *C. crescentus* propose RodA, RodZ, MreB and MreD (16). Homologs of RodZ and MreD are not found in the *H. pylori* genome, suggesting MreC may play a more central role in rod-shape maintenance. The SNP identified in the *mreC* gene suggests introducing the *kan-sacB* cassette in the HP1488 gene disrupted the stability of the cell envelope. While no cells were observed to be coccoidal-shaped when examining the cells under TEM, the membrane may have experienced stress that could not be identified by visual inspection. Introducing the *mreC* allele from the 'M' variant into the 'RM' strain and examining motility in the resulting strain would provide strong evidence the amino acid substitution is responsible for suppressing the 'RM' phenotype. Likewise, replacing the *mreC* allele in the 'M' strain with the 'RM' allele should impair the resulting strains ability to swim.

References

1. **Corey RA**, **Pyle E**, **Allen WJ**, **Miroux B**, **Arechaga I**, **Politis A**, **Collinson I**. 2017. Identification and functional analyses of cardiolipin binding sites on the bacterial Sec translocase. bioRxiv.
2. **Corey RA**, **Pyle E**, **Allen WJ**, **Watkins DW**, **Casiraghi M**, **Miroux B**, **Arechaga I**, **Politis A**, **Collinson I**. 2018. Specific cardiolipin-SecY interactions are required for proton-motive force stimulation of protein secretion. Proceedings of the National Academy of Sciences. **115**:7967-7972. https://www.ncbi.nlm.nih.gov/pubmed/30012626.
3. Or E, Navon A, Rapoport T. 2002. Dissociation of the dimeric SecA ATPase during protein translocation across the bacterial membrane. 21.
4. **Tan BK**, **Bogdanov M**, **Zhao J**, **Dowhan W**, **Raetz CR**, **Guan Z**. 2012. Discovery of a cardiolipin synthase utilizing phosphatidylethanolamine and phosphatidylglycerol as substrates. Proceedings of the National Academy of Sciences. **109**:16504-16509. https://www.ncbi.nlm.nih.gov/pubmed/22988102.
5. **Guo D**, **Tropp BE**. 2000. A second *Escherichia coli* protein with CL synthase activity. BBA - Molecular and Cell Biology of Lipids. **1483**:263-274. https://www.ncbi.nlm.nih.gov/pubmed/10634942.
6. **Tropp BE**. 1997. Cardiolipin synthase from *Escherichia coli.* BBA - Lipids and Lipid Metabolism. **1348**:192-200. https://www.ncbi.nlm.nih.gov/pubmed/9370333.
7. **Selvy PE**, **Lavieri RR**, **Lindsley CW**, **Brown HA**. 2011. Phospholipase D - enzymology, functionality, and chemical modulation. Chemical Reviews. **111**:6064-6119. https://www.ncbi.nlm.nih.gov/pubmed/21936578.
8. **O'Rourke EJ**, **Pinto AV**, **Petroni EA**, **Tolmasky ME**, **Ielpi L**. 2004. Evidence for the Active Role of a Novel Nuclease from *Helicobacter pylori* in the Horizontal Transfer of Genetic Information. Journal of Bacteriology. **186**:2586-2593. https://jb.asm.org/content/186/9/2586.
9. **Overbeek R**, **Begley T**, **Butler RM**, **Choudhuri JV**, **Chuang H-Y**, **Cohoon M**, **de Crécy-Lagard V**, **Diaz N**, **Disz T**, **Edwards R**, **Fonstein M**, **Frank ED**, **Gerdes S**, **Glass EM**, **Goesmann A**, **Hanson A**, **Iwata-Reuyl D**, **Jensen R**, **Jamshidi N**, **Krause L**, **Kubal M**, **Larsen N**, **Linke B**, **McHardy AC**, **Meyer F**, **Neuweger H**, **Olsen G**, **Olson R**, **Osterman A**, **Portnoy V**, **Pusch GD**, **Rodionov DA**, **Rückert C**, **Steiner J**, **Stevens R**, **Thiele I**, **Vassieva O**, **Ye Y**, **Zagnitko O**, **Vonstein V**. 2005. The subsystems approach to genome annotation and its use in the project to annotate 1000 genomes. Nucleic acids research. **33**:5691-5702. https://www.ncbi.nlm.nih.gov/pubmed/16214803.
10. **Johnson JM**, **Church GM**. 1999. Alignment and structure prediction of divergent protein families: periplasmic and outer membrane proteins of bacterial efflux pumps. Journal of Molecular Biology. **287**:695-715. https://www.ncbi.nlm.nih.gov/pubmed/10092468.
11. **Nikaido H**, **Takatsuka Y**. 2009. Mechanisms of RND multidrug efflux pumps. BBA - Proteins and Proteomics. **1794**:769-781. https://www.ncbi.nlm.nih.gov/pubmed/19026770.
12. **Symmons MF**, **Marshall RL**, **Bavro VN**. 2015. Architecture and roles of periplasmic adaptor proteins in tripartite efflux assemblies. Frontiers in Microbiology. **6**:513. https://www.ncbi.nlm.nih.gov/pubmed/26074901.

13. **Kanonenberg K**, **Schwarz CK**, **Schmitt L**. 2013. Type I secretion systems - a story of appendices. Research in Microbiology. **164**:596-604. https://www.ncbi.nlm.nih.gov/pubmed/23541474.
14. **Geis G**, **Suerbaum S**, **Forsthoff B**, **Leying H**, **Opferkuch W**. 1993. Ultrastructure and biochemical studies of the flagellar sheath of *Helicobacter pylori.* Journal of Medical Microbiology. **38**:371-377. https://www.ncbi.nlm.nih.gov/pubmed/?term=8487294.
15. **Contreras-Martel C**, **Martins A**, **Ecobichon C**, **Trindade DM**, **Matteï PJ**, **Hicham S**, **Hardouin P**, **Ghachi ME**, **Boneca IG**, **Dessen A**. 2017. Molecular architecture of the PBP2-MreC core bacterial cell wall synthesis complex. Nature Communications. **8**:776. https://www.ncbi.nlm.nih.gov/pubmed/28974686.
16. **El Ghachi M**, **Matteï PJ**, **Ecobichon C**, **Martins A**, **Hoos S**, **Schmitt C**, **Colland F**, **Ebel C**, **Prévost MC**, **Gabel F**, **England P**, **Dessen A**, **Boneca IG**. 2011. Characterization of the elongasome core PBP2:MreC complex of *Helicobacter pylori.* Molecular Microbiology. **82**:68-86. https://www.ncbi.nlm.nih.gov/pubmed/21801243.
17. **Divakaruni AV**, **Loo RR**, **Xie Y**, **Loo JA**, **Gober JW**. 2005. The cell-shape protein MreC interacts with extracytoplasmic proteins including cell wall assembly complexes in *Caulobacter crescentus*. Proceedings of the National Academy of Sciences. **102**:18602-18607. https://www.ncbi.nlm.nih.gov/pubmed/16344480.